EXPLORATORY STUDIES OF CONVECTIVE FLOWS DUE TO ARC TRACKING

by

RICHARD R. MITCHELL

Presented to the Faculty of the Graduate School of

The University of Texas at Arlington in Partial Fulfillment

of the Requirements

for the Degree of

MASTER OF SCIENCE IN AEROSPACE ENGINEERING

THE UNIVERSITY OF TEXAS AT ARLINGTON

August 2007

ACKNOWLEDGEMENTS

I would also like to thank my advisors Dr. Frank Lu, Dr. Don Wilson and Dr. Dereje Agonafer of the Mechanical and Aerospace Engineering Department. Dr. Lu has been extremely helpful (and patient) with his guidance in experimental methods, computational modeling and, most of all, technical writing. Dr. Wilson has been a steady supporter of my graduate work and an insightful and enlightening teacher since my undergraduate days at UTA. Dr. Agonafer set the foundation for my computational fluid dynamics knowledge and encouraged me to begin my graduate education. Thank you all.

I wish to thank my project associate Linda Phonharath for her dedication, hard work and professional attitude. Additionally, thank you to all my colleagues at the ARC for the encouragement, advice and the late night laughs.

I wish to thank Behzad Bigdeli, William Bartloff, Ryan Roth and Terry Leemaster for the opportunity to work with the St. Joseph Technology Center and the Whirlpool Corporation.

I wish to also thank my entire family for being extremely patient with me as I spend my days (and nights) achieving my goals. Without their love and support, this would not have been possible. I am especially thankful to Annahita for her love, patience and encouragement

July 15, 2007

ABSTRACT

EXPLORATORY STUDIES OF CONVECTIVE

FLOWS DUE TO ARC TRACKING

Publication No. _____

Richard R. Mitchell, M.S.

The University of Texas at Arlington, 2007

Supervising Professor: Frank K. Lu

The objective of the research was to develop an understanding of how a flame propagates through an electronic enclosure. FLUENT®, a Navier-Stokes solver, was chosen due to its widespread commercial use, the availability of turbulence models and its ability to handle combustion. The relevance of this study with respect to the aerospace and domestic appliance industry was shown through case reports. Initial observations were made on arc discharges, chemical compounds and their relevance to establishing the flame.

Experimental bench tests highlighted the instigating factors for flame ignition. The first round of bench testing revealed that solder node separation played an important role in establishing an arc discharge. Next, a water/Solventol solution was added to the tests to sustain the arcing of the solder nodes. Once the arc discharge was

sustained, the next round of testing moved into the initiation of the flame on a printed circuit board (PCB). The bench testing showed that a minimum solder node separation of 1mm was necessary to achieve arcing with the water/Solventol solution at 120 VDC. The results also indicated that ignition of the flame was possible after several seconds of arcing occurred on the PCB panel. A method of flame suppression, through expanded metal foil, was suggested.

The control volume was described in detail starting with the computer aided design drawing in Pro/ENGINEER™. The preprocessing software GAMBIT™ was used to further simplify the model and to add a finite volume mesh and initial boundary conditions. The partially-premixed solver was chosen in FLUENT® with a unique incorporation of the non-premixed and premixed combustion chemistry to establish an arc and to track the flame front.

Simulation results indicated a flame front propagation with a spark discharge as the ignition source. Three- and two-dimensional contour plots were used for the flame front visualization and analysis. Additional volume-averaged analysis of the discrete phase model burnout rate, species mole fraction, temperature and progress variables show track the ignition and flame propagation in the control volume. Overall, the results indicate the successful implementation of a hybrid partially-premixed combustion model, to simulate arc tracking and flame propagation in a three-dimensional enclosure.

TABLE OF CONTENTS

LIST OF ILLUSTRATIONS

LIST OF TABLES

CHAPTER 1

INTRODUCTION

1.1 Dramatic Arc Tracking Events

On July 17, 1996: Trans World Airlines Flight 800 crashed off the coast of Long Island, New York. The final National Transportation and Safety Board (NTSB) report concluded that a short circuit and subsequent arcing had ignited the center wing fuel tank of the Boeing 747 killing all 230 people on board [1]. Almost a year later, on July 5, 1997, another incident of arcing occurred on Northwest Airlines Flight 1446, a McDonnell-Douglas DC-9. A position light autotransformer connected to a 3 A circuit breaker shorted out. The high current fused the breaker in the closed position and melted the surrounding insulation which resulted in "smoke billowing" from the center instrument panel. The air crew was forced to put on oxygen masks and the aircraft landed prematurely at Bishop International Airport, Flint, Michigan, without incident [2]. On December 29, 2000, Delta Airlines Flight 219, a Lockheed L-1011 aircraft, in flight from San Francisco, California, to Honolulu, Hawaii, encountered turbulence while flying through a layer of clouds. The crew noted hearing loud popping noises over their communications equipment while flying through the clouds, which is associated with a phenomenon known as Saint Elmo's fire. Soon after the electrical discharges were heard over the radios, sparks, smoke and a strong acidic smell erupted from the co-pilots side of the aircraft. It was determined that the strange aroma was the

result of Kapton®, a common aerospace wire insulator, burning as an arc discharge occurred. Later investigation revealed that a static charge built up on the skin of the plane as it flew through the clouds. The static electricity discharged through some of the cockpit equipment and wiring, damaging the Kapton® coating and causing the smoke [3].

Over four years later, the Canadian submarine HMCS Chicoutimi left Falane, Scotland in the United Kingdom on her maiden voyage destined for Halifax, Nova Scotia, Canada. Three days later, October 5, 2004, the submarine had a substantial amount of water enter through the conning tower. A series of electrical events eventually lead to the arcing of the main power cables and a fire that spread through two decks. Eight injuries and one fatality resulted from the incident [4]. After the fires were contained and outside help arrived, the submarine was towed back to Scotland.

Each of the above examples is a case in which arcing played an important role that resulted in a disaster or near disaster. Usually, the initial arcing phenomenon draws enough current to trip breakers, singe wires or disconnect the circuit from the power supply. However, this "lucky break" is not always so and the results can be catastrophic. As in the previous examples, arcing can inadvertently ignite aircraft fuel, fill a cockpit with smoke or almost sink a submarine.

1.1.1 Previous Research in Arc Tracking

Much of the previous research in arc tracking has been conducted within the aerospace industry including the air and space transportation sectors. The National Aeronautics and Space Administration (NASA) and the Federal Aviation

Administration (FAA) conducted the majority of the arc tracking and mitigation research.

1.1.1.1 NASA Research

In the early 1990s, NASA began presenting reports on arc discharge and arc tracking in a space environment [5-8]. At the time, the Space Station Freedom was in the last stages of design work with a large price tag and a heavier than expected final mass. Polyimide and polyimide-compound wire insulators such as Kapton® appeared to be feasible alternatives to old polymer technology, being well suited for the extreme temperatures of space. The compounds also helped to reduce the mass of the space station. Kapton® insulation was a common wire covering that had been used for years; however, studies showed that degradation of the polyimide insulation could be significant for space applications [9]. The NASA report reflected the known properties, benefits and risks with using polyimide [9]. Figures 1.1 and 1.2 illustrate some of the testing conducted by NASA on potential arc tracking damage.

Figure 1.1. Space station insulation damaged by arc track [5].

Figure 1.2. Damage to Kapton® coated wire by arc tracking [5].

Requirements for space applications are the most stringent because of the strict guidelines that must be followed for selecting insulation. Among the general requirements, the wire insulation must not be flammable, not release toxic gases, not release aromatic gases, be resistant to inside environment especially moisture and be resistant to the outside environment (radiation, cold, vacuum) [10]. All of these requirements are an effort that collectively alleviate, but do not eliminate, the potential risk of fires in space. "In the space environment, the cables and wires considered to be critical parts in flammability and toxicity have to meet a large number of operational, functional, safety and reliability requirements with the supplementary limitations of space and weight" [10]

Increased understanding of the destructive behavior of Kapton® pyrolysis, arc tracking and propagation phenomenon were crucial for deploying the new space station. Some of the initial reports concentrated on the Flexible Current Carrier (FCC) that ran from the photovoltaic panels to the Space Station Freedom (SSF) [8]. Later reports focused on arc tracking inside spacecraft with the possibility of flame propagation [6]. One of these reports concluded that wire insulators being used at the time were not flame retardant after arc tracking occurred [7].

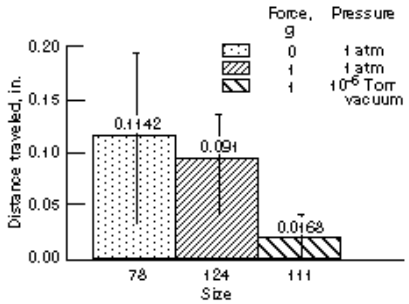

Figure 1.3. Arc tracking propagation in a low pressure and gravity environment [7].

1.1.1.2 FAA Research

Reports filed by the National Transportation and Safety Board (NTSB) are primarily to state the cause of aircraft incidents. Some examples of these reports were mentioned earlier [1-3]. Continuing the research to understand the foundation of an aviation safety problem, such as arc tracking, however was deemed the responsibility the Federal Aviation Administration (FAA).

Congress passed the Aviation Safety Research Act of 1988 after an explosive decompression of a Boeing 737 in service with Aloha Airlines [11]. The Act enlarged the FAA mission to include research into the causes, effects and mitigation of fatigue and environmental degradation of aircraft structures. The FAA later created the Arc Fault Evaluation Laboratory (AFEL) to investigate electrical ignition of materials and mitigation techniques [12]. The FAA, with the help of companies such as Eaton Aerospace, Texas Instruments, Letromechanical Design Company and others, have conducted multiple investigations on dry arc tracking, arc fault ignition and mitigation, aircraft material fire testing and interconnection electrical systems [13].

1.1.1.3 Whirlpool Corporation

The Whirlpool St. Joseph Technology Center, located in St. Joseph, Michigan, was tasked with researching arc discharges and their potential risk in household appliances. General inspection of these household appliances does not occur as in routine maintenance schedules of the airlines and in the aerospace industry. However, much like the airline and aerospace industries, many appliances are kept in homes and businesses in working order for tens of years. Everyday use can easily result in the

appliance suffering progressive housing damage while the mechanical and electronic components remain in working condition. The circuitry of the appliance may be exposed to contamination and further damage. Contaminants, especially organic compounds such as those found in cleaning chemicals, can increase the arcing potential on printed circuit boards (PCBs).

The inclement nature of arc tracking in domestic appliances recently became more evident when Maytag® and Jenn-Air® recalled approximately 2.3 million dishwashers under the advisement of the U.S. Consumer Product Safety Commission [14]. By February 1, 2007, when the recall was issued, 135 reports of fires that resulted in property damage and personal injury were filed. The hazard that initiated the recalled was determined to be a leak in the liquid rinse-aid dispenser. In some cases, liquid came into contact with the dishwashers' internal wiring causing arcing and igniting internal components.

1.1.2 Definitions of Arc, Arc Discharge and Arc Tracking

According to [10], the definition of an arc discharge is a continuous, luminous discharge of electric current crossing a gap or an insulating surface between two conductors. The same steady luminous phenomenon is also deemed a glow discharge [15]. This type of electrical fault does not necessarily draw a large enough current to trip a breaker or melt a wire, but can create enough Joule heating to damage surrounding wiring and other components. A simple example of this is a wire with cracked or missing insulation. Once the exposed wire is energized, it can short to other electrical or mechanical components (e.g. hydraulic lines).

An arc discharge is described as a high current discharge that occurs when two electrodes are shorted and then separated [15]. High current flow will allow an arc discharge to occur over a relatively large gap, connecting the electrode or exposed wire to another grounding source. High current draw of this nature usually trips breakers or melt components, cutting off the power supply. However, in some cases the arc and arc discharge can melt components in the closed, or continuous current flow, position allowing the discharge to continue for extended periods of time [2].

If the arc and/or arc discharges continue, damage will occur to the surrounding area. This is the phenomenon of arc tracking. According to [10], arc tracking is an arc between two or more wires that will sustain itself through a conductive path provided by the degradation of the insulation. An example of this was described earlier in the case of the Lockheed L-1011 flying from San Francisco to Honolulu [3]. The strong aroma smelled by the pilots was a result of the Kapton® wiring being pyrolized, or heat treated, and releasing the aromatic molecules from the polyimide compound.

1.1.3 Polyimide and Polyimide Compounds

Wiring commonly used in aerospace and other industrial applications contains a variety and combination of many different polymers. Some such polymer insulations include polyimide (i.e Kapton ®), tetrafluoroethylene (TFE), and cross-linked ethylene tetrafluroethylene (PTFE). These polymers also contain some of the same chemical constituents that were chosen for the FLUENT® simulation model. The polyimide Kapton®, for example, includes a central nitrogen atom that is essentially surrounded by carbon atoms and two double bonded oxygen atoms (Figure 1.4).

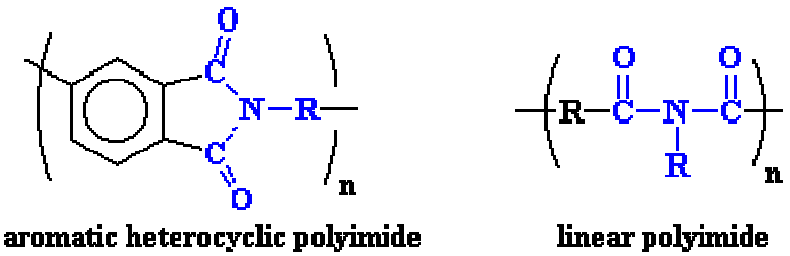

Figure 1.4. Polyimide compound structure [16].

It is assumed that initial arcing produces enough energy to break the bonds of the fluorine, nitrogen and oxygen atoms, thus leaving a pyrolized carbon substance behind. These carbon atoms have two effects. First, the carbon provides a conductive path, thereby enabling repeated arcing. Second, the carbon also provides fuel to feed the electrical fire and create a flame front.

1.2 Arcing Phenomenon in Electronic Circuits

While an arc is defined as a high current discharge that occurs when two electrodes are shorted and then separated [15], this description is not necessarily what occurs in electronic packaging. Current investigations by the Air Force and FAA are examining damaged wire insulation and the effects of arcing on surrounding material [12,17] The Materials Directorate of the Air Force Research Labs concluded that arc discharges can occur from four main sources: chemical contamination, mechanical failure, thermal effects and electrical disruptions [12]. Alone, arc tracking in an aircraft can be severely damaging to an aircraft. As seen in Figure 1.5, arc tracking inside an aircraft lead to the rupture of a high pressure hydraulic line. The fluid in the line ignited when it was exposed to subsequent arc discharges. The crew was able to successfully

land without further incident and the damage was confined to the internal wiring components.

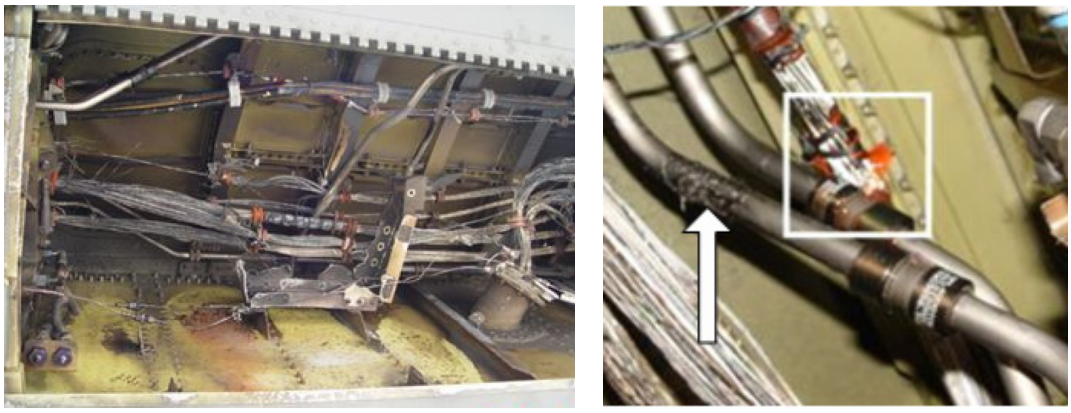

(a) (b)

Figure 1.5. (a) Location of fire and internal damage, (b) arc discharge location (box) and hydraulic damage (arrow) [18].

Similarly, contamination of an electronic package can come from many sources. Dust collection, being one of the most common, is not usually as hazardous or degrading to protective coatings on electronic components. However, other contaminants such as moisture can cause particles to stick to electric components and connections, such as the solder nodes. In some cases, the moisture may contain other secondary contaminants such as chemical reagents in the form of cleaning compounds and detergents. These types of reagents contain organic compounds that can chemically wear down a PCB's protective coating and pose an additional arcing threat [19].

In addition to environmental contaminants, another factor in the arcing process is the high current draw from the shorting of the circuit. When the arc is established the resistance approaches zero and the high power consumption chars the surrounding material. Charred polymers can act as either fuel, for an electrical fire, or hazardous connectors that continue the arcing process. The process by which arcing chars and

melts the surroundings is called joule heating, which is also referred to as ohmic or resistance heating. From Ohm's law, the power dissipated as heat by the electronics is proportional to the square of the current. The data from [20] shows that the current can briefly exceed 80 A in a high-power electronic circuit, which exceeds a typical draw of about 20 A. Thus, the heating can momentarily increase sixteen times. When the power surge occurs, the electrodes that were once spaced properly are now too close.

1.3 Objectives of the Present Study

The primary focus of the FLUENT® simulation was in creating an initially non-reactive carbon-rich environment. A medium-volatile coal model, described in later sections, was used for this purpose. The exact chemistry of the flow will not be the primary purpose of this study; however, by monitoring the carbon content of the model, the flame propagation could be followed

The objectives of the study is to (i) localize the cause of arc tracking and ignition source of the flame and (ii) simulate the same type of ignition and flame front propagation in an electronic closure by means of a Navier-Stokes solver. Chapter 2 highlights a series of benchtop experiments that isolated the cause of arcing and arc tracking on a PCB. The spacing and contamination is related to the operating environment of the PCB as part of a control panel in a dishwasher. The results were summarized to explain the cause and effect of the arc tracking.

Chapter 3 begins with the creation of a computer-aid design drawing of a dishwasher control panel. The simplification of the model in Pro/ENGINEER™ is described, followed by the meshing and application of the initial boundary conditions in

GAMBIT™. The choice of combustion models is described, followed by the choice of the solver to create a hybrid arc tracking simulation. The results are summarized in Chapter 4 with a series 2-D and 3-D of transient contours plots. Chapter 5 is an in depth analysis of the results. The transient analysis is given more detail and additional interpretation of the flame front propagation was explored.

CHAPTER 2

EXPERIMENTAL BENCH TESTS

2.1 Whirlpool Beginnings

Arcing is obviously an undesirable electrical phenomenon that, as highlighted in Chapter 1, can occur in domestic appliances [14]. In most cases, arcing causes power disruption by failure of the electrical components. However, in some isolated cases, the power remains intact, resulting in continuous arcing following by arc tracking and possibly fire.

The Whirlpool Corporation is an international manufacturer of domestic appliances with millions being produced annually. Even though the chances of arc tracking are slim, the Whirlpool Corporation expressed interest in arc tracking research and mitigation techniques with the University of Texas at Arlington (UTA).

During the fall of 2005, a trip was made to the Whirlpool Corporation Saint Joseph Technology Center to observe arc tracking tests of a dishwasher. The experimental work was conducted at a near by facility, nicknamed "The Campus," located in Benton Harbor, Michigan. While at the Benton Harbor facilities, the UTA team was able to take notes, pictures and videos of procedures, equipment used for the experiment and examine arc tracking first hand (Figures 2.1 and 2.2). All materials were used as guidelines for the continued work at UTA.

Figure 2.1. Generic door panel before testing (note injection tubes top right; courtesy: St. Joseph Technology Center).

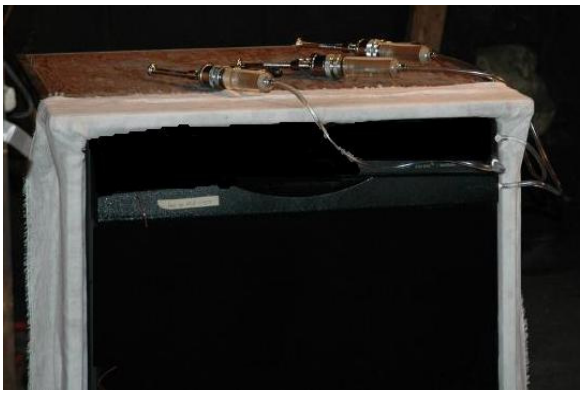

Figure 2.2. Door panel ready for testing (note injection tubes are connected to syringes; courtesy: St. Joseph Technology Center).

After all the testing was complete, two sample PCBs, like the ones seen in the dishwasher panel (Figure 2.3) were provided to UTA. One PCB, a complete control board, had not been exposed to any testing (Figure 2.4). The other PCB had previously been tested and had experienced arc tracking (Figure 2.5). These boards were used to determine the next phase of testing to be completed at UTA.

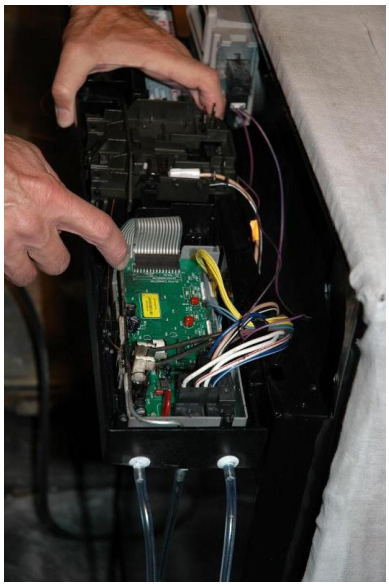

Figure 2.3. PCB located inside door panel assembly - Note injection ports tubes located at bottom of picture (courtesy: St. Joseph Technology Center).

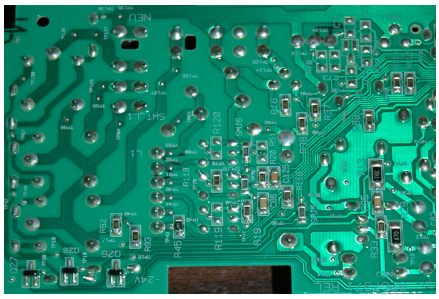

Figure 2.4. PCB before arc tracking (courtesy: St. Joseph Technology Center).

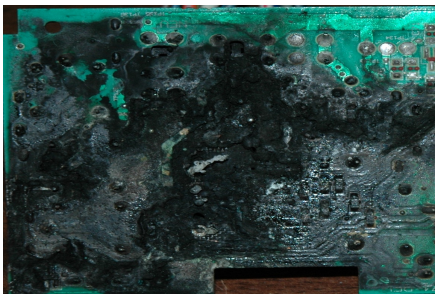

Figure 2.5. PCB after arc tracking (courtesy: St. Joseph Technology Center).

2.2 UTA Benchtop Experiments

Soon after the visit to the Whirlpool Saint Joseph Technology Center, the Aerodynamics Research Center (ARC) at UTA began bench tests to evaluate the effects of contamination. This work was reported in [20].

2.2.1 Separated Node Bench Tests

The original tests conducted at Benton Harbor by Whirlpool were given a pass/fail grade with respect only to fire prevention. Arc tracking was considered a consequence of the testing and was not studied in depth. The UTA tests were aimed at understanding the effects of contamination of the PCB solder nodes on arc tracking. A benchtop setup was constructed to simulate just the solder nodes, without the PCB or other potential sources of arcing (Figure 2.6). A solution of one part Solventol (Rooto Corporation of Howell, Michigan 48843), a commercial cleaner, with four parts distilled water was mixed to represent household dishwasher contaminant. The experimental setup was as follows. The on/off switch at the top left corner of Figure 2.6 was used simply as a safety measure. Variable power for the arrangement was supplied by the autotransformer, second from the left. The autotransformer was equipped with

an 80A fuse. A multimeter, third from the left, was used to measure the voltage output from the autotransformer. Power output from the autotransformer went into the power strip located on the far right. The multimeter was plugged into the power strip and read to determine the output voltage delivered to the nodes (located at the bottom).

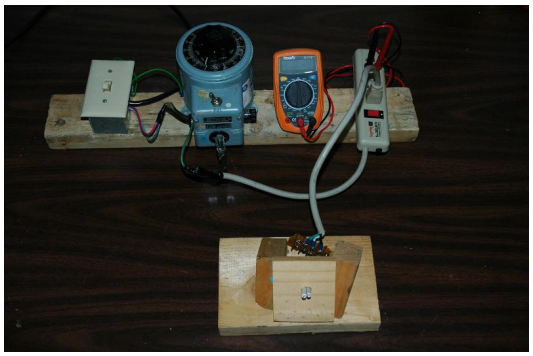

(a)

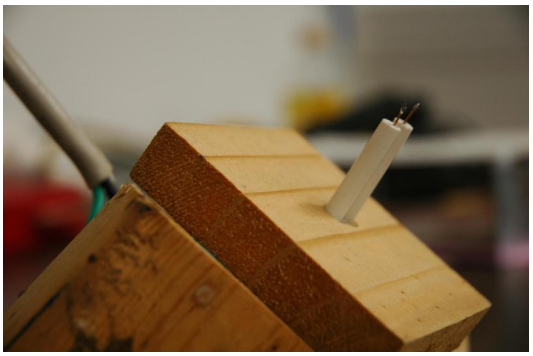

(b)

Figure 2.6. (a) Equipment used for benchtop test and (b) solder nodes placed inside ceramic holders.

Initial tests placed the solder nodes inclined at a 60 degree angle with two different spacings of 3.175 mm (1/8 inch) and 1 mm apart. These dry runs were conducted with no distilled water or no solvent at a maximum supply of 120V DC. No arcing or unusual phenomenon occurred for any of the dry tests. The results show that the spacing of the nodes without the influence of any contamination is acceptable.

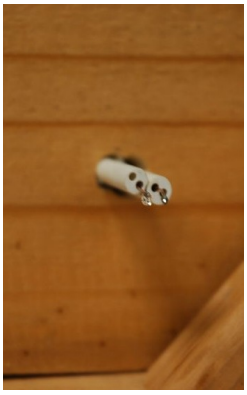

Figure 2.7. View of initial testing with solder 1/8 in. apart at angle of 90 deg.

Figure 2.8. View of initial testing with solder 1 mm apart at angle of 90 deg.

Next, the nodes were placed parallel to each other and perpendicular to the bench. The nodes were sprayed with distilled water. Again, there was no reaction for the nodes spaced 3.175mm (1/8 inch) apart. However, the nodes spaced at 1 mm began to fizzle and experienced a "vapor explosion" at 100 VDC. Further tests concluded that solder contamination from solder flux was the probable cause of explosion.

During the final testing, the nodes were sprayed with the Solventol solution [19]. Once again, the 1/8 in. spaced nodes did not show any visible arcing. The 1 mm spaced notes did however begin to arc at 110 VDC, following by smoke and violent arcing that burst off the soldering nodes from the wiring.

The conclusion from theses tests attributed two factors that can cause arcing: the distance of the base of the solder nodes and the mixture (or contamination) that the nodes are exposed to when power is supplied.

2.2.2 Mounted Node Bench Tests

Following the bench test with successful arcing of isolated solder nodes, the next set of bench tests was to mount the node on a PCB (Radio Shack), with similar spacing and wire configuration. A two-node configuration demonstrated a simple circuit of voltage supply and return Figure 2.9. A four-node configuration demonstrated a configuration similar to control panels that contained four current driven nodes Figure 2.10.

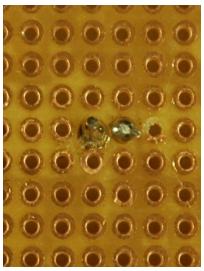

Figure 2.9. Two node test configuration.

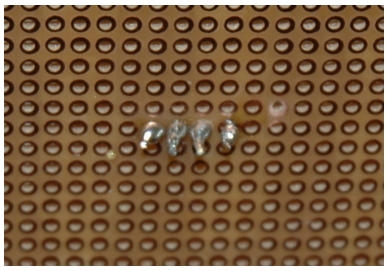

Figure 2.10. Four node test configuration.

Testing protocol called for the power to be increased in 10 VDC increments. After each voltage increase, the solder nodes were sprayed with the Solventol solution and allowed to soak for one minute. The results summarized in Table 2.1 show that fizzing of the Solventol solution between the nodes began at voltages as low a 30 VDC and brief arcing occurred as low as 50 VDC. Continual arcing and smoking occurred for voltages from 90 to 110 VDC. When 120 VDC was applied, the arcing and flame persisted for 20 s when the nodes blew off.

Table 2.1. Two node experimental test results.

Volts (V)	Arcing (Y/N)	Observations
10	N	
20	N	
30	Y	Fizzing
40	Y	Fizzing plus arcing
50	Y	Brief arcing, then stop
60	Y	Brief arcing, build up of Solventol
70	Y	Brief arcing, smoke
80	Y	Brief arcing
90	Y	Arcing, smoke
100	Y	Arcing, slight flame
110	Y	Arcing, slight flame
120	Y	Arcing, then slight flame, 20 seconds later, explosion

The two-node, PCB mounted test concluded with continual arcing, smoke and a slight flame located at the node pairs. It was assumed that a four-node configuration, will also present these features.

Two different tests were performed using the same type of PCB with four solder nodes. The same procedure was used for each test. The results are summarized in Table 2. For the first test, slight fizzing of the electrodes began at a low voltage of 20 VDC, followed by bubbling at the nodes at 30 VDC. The solder nodes were relatively inert until 70 VDC was reached, when a sudden burst occurred followed by sparking and flickering at the nodes. It was noted that the loud burst sounded very similar to the popping heard and recorded in the Benton Harbor, Michigan tests. When the voltage was increased to 80 VDC, the sparking continued until 90 VDC when a small flame erupted from the board. The second test was less active. A slight blackening at the base of the solder nodes occurred at 20 VDC. No activity was recorded until 60 VDC when the nodes smoked slightly. At 70 VDC the nodes smoked again, followed by a bursting of the nodes and the subsequent end of the test.

Table 2.2. Four node experimental test results.

	Test 1		Test 2	
Volts (VDC)	**Arcing (Y/N)**	**Observations**		
10	N		N	
20	N	Slight bubbling from Solventol mixture	N	Blackening of base
30	N	Bubbling	N	
40	N		N	
50	N		N	
60	N		N	Slight smoke
70	Y	Burst, Flame, sparking and flickering	N	Smoking, nodes burst
80	Y	Sparking, arcing, flame	NA	
90	Y	Flame, continuous sparks	NA	
100	NA	NA	NA	
110	NA	NA	NA	
120	NA	NA	NA	

Overall, arcing was successfully achieved, followed by unstable flames for test one. Test two yielded only smoke and the bursting of nodes. However, no continuous

flame was experienced even with the four-node arrangement. Upon examining the PCBs purchased from Radio Shack, it was noted that a protective, fire retardant coating was applied to the board. The original tests conducted by Whirlpool used production line PCBs that were not coated with the same type of fire retardant film.

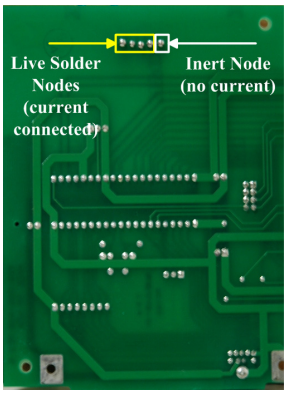

Figure 2.11. Five node configuration on computer PCB.

Next, a PCB was removed from an obsolete computer, which did not have a flame retardant coating, and used for mounting solder nodes. This time, five electrodes were mounted on the board and the same test protocol was used. The results are summarized in Table 3.

Table 2.3. Five solder node experimental PCB test results.

Volts (VDC)	Arcing (Y/N)	Observations
40	N	
50	N	
60	Y	Evaporation, arcing from rear
70	Y	Arcing, steady smoking
80	Y	Arcing, smoking, increase, smoking from back
90	Y	Persistent arcing, smoke
100	Y	Smoking, arcing
110	Y	Smoking, arcing
120	Y	Initial flame, arcing
110 (8 min. exposure)	Y	Initial flame, arcing, flame left side, smoking
120 (10 min. exposure)	Y	Smoking, slight flame, sparking, loss one node, flame right side

The tests of the five-node arrangement did not yield any activity from 10 – 50 VDC. At 60 VDC arcing began to occur on the reverse side of the board. The arcing persisted with increasing smoke as the voltage was increased and solution was added. The voltage was increased to 120 VDC without the nodes bursting off the board, so an extended run was conducted. After the board was sprayed with the solution and run for eight minutes at 110 VDC a slight flame was achieved. When the voltage was increase to 120 VDC, sprayed again and run for ten minutes, a slight flame was maintained (Figure 2.12a), followed by a stronger flame (Figure 2.12b). The flame was extinguished when the power was removed.

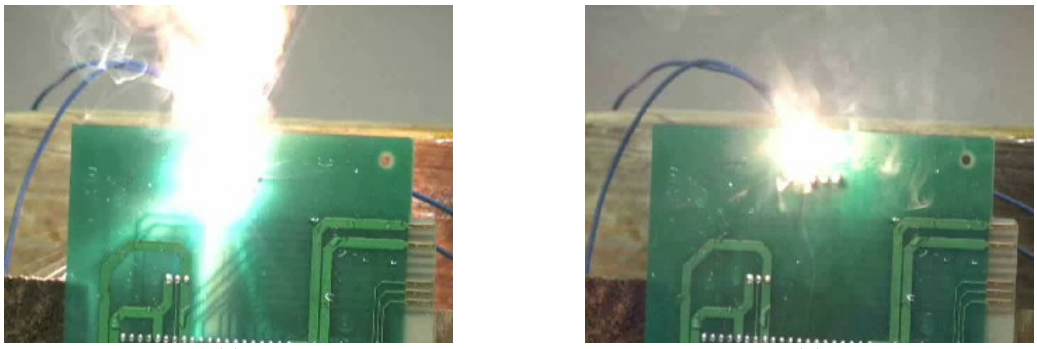

(a) **(b)**

Figure 2.12. (a) Short initial flame located at PCB solder nodes at 120 VDC, (b) longer secondary flame located at PCB solder nodes at 120 VDC.

2.2.3 Flame Suppression Tests

As part of the series of tests, an attempt at flame suppression was made with the use of a different PCB board. No solder nodes or voltages were applied during the test. The main objective was to explore the effectiveness of an expanded metal network in flame suppression. A clear Plexiglas enclosure was constructed to fit around the PCB as seen in Figure 2.13. The Plexiglas enclosure simulated the close panel that surrounds the dishwasher control panel and allowed the flame to be seen.

A flame accelerant was utilized to ensure the continued combustion. The accelerant was a mixture of a 1/2 tablespoon of gasoline, a 1/2 tablespoon of two-cycle engine oil and 55 ounces of polystyrene (Styrofoam™). This was all combined and stirred occasionally for a period of five hours, when all the foam dissolved. The mixture was applied to the PCB in a 0.04 in. thick layer, 1 in. by 1 in. square.

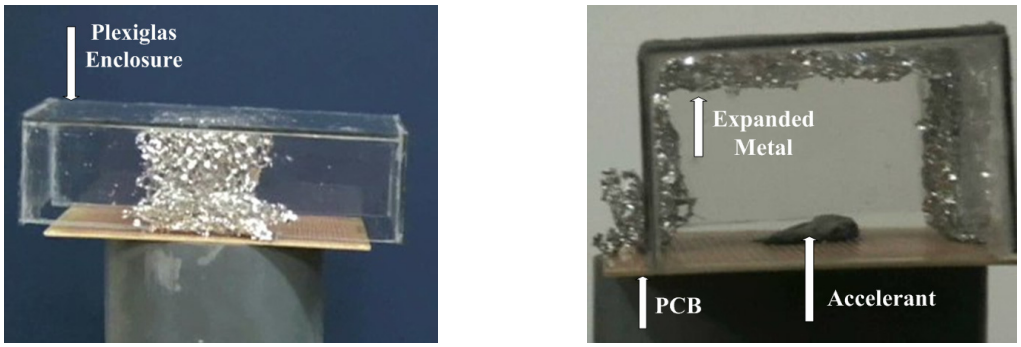

(a) (b)

Figure 2.13. (a) Side view of Plexiglas container, PCB and expanded metal foil, (b) front view of same flame suppression testing configuration.

Initial testing of expanded metal did not utilize the plastic enclosure. Instead, a series of tests placed multiple layers of expanded metal, measuring 6 in. by 2 in. approximately 2 in. above the ignited PCB to simulate the distance to the enclosure.

Examining Figures 2.14–2.17, it can be seen that one layer of expanded metal foil did not suppress the flame (Figure 2.14). Two layers of material were more effective, but a flame can still be seen above the mesh (Figure 2.15). Three layers were highly effective, but slight flames were still seen through the mesh (Figure 2.16). The last test used four layers of expanded metal foil and, as seen in Figure 2.17, was effective in stopping the flame.

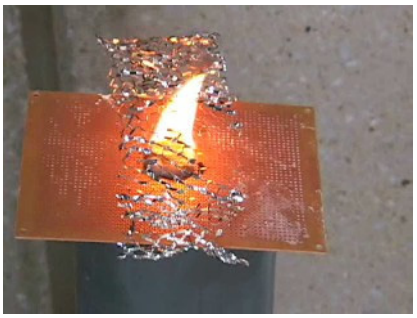

Figure 2.14. One layer of expanded metal foil with flame.

Figure 2.15. Two layers of expanded metal foil with flame.

Figure 2.16. Three layers of expanded metal foil with flame.

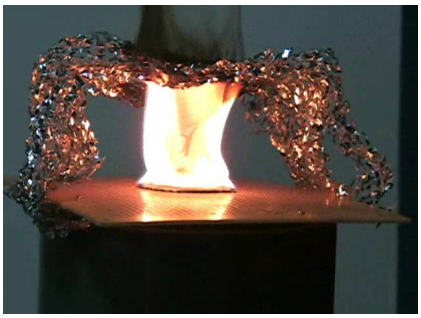

Figure 2.17. Four layers of expanded metal foil with flame.

2.2.4 Bench Test Observations

Experiments were performed to isolate the cause of arc tracking between solder nodes on a PCB when subjected to a Solventol/water solution. The preliminary results indicate that a minimum spacing of 1mm is susceptible to arc tracking and an initiation of a flame. The results also indicate a spacing of approximately 3.2 mm (1/8 of an inch) is adequate in preventing arc tracking.

If arc tracking does occur and a flame is ignited, a unique solution of flame suppression shown through the use of expanded metal networks. As Figures 2.14–2.17 indicate, the more layers of network, the more effective suppression. One minute tests show a quenching of the flame with no resulting damage to the enclosure (Figure 2.18).

(a) (b)

Figure 2.18. (a)One minute flame test with four layers of expanded metal foil, (b) enclosure after one minute test, black residue with no visible damage.

The use of expanded metal foils is recommended for flame suppression in small enclosures. Further investigations and testing should be conducted in full-scale domestic applications to ensure a more realistic environment.

CHAPTER 3

ESTABLISHING THE COMPUTATIONAL MODEL

3.1 Creating the Model

The first step to starting the simulation in FLUENT® was to create a computer-aided design (CAD) model of a generic dishwasher door panel. The experiments observed at both the Saint Joseph Technology Center and the Aerodynamics Research Center were key to isolating the relevant components for the simulation. Basic geometry was created in Pro/ENGINEER™, exported to GAMBIT™ for meshing and run in FLUENT®.

After the successful generation of the CAD model, the governing equations for the computational model were explored in detail. The partially premixed combustion model was chosen from the available reaction models in FLUENT®. In particular, a unique combination of the non-premixed and partially premixed combustion solvers is detailed, followed by the construction of the chemical constituents. Background into the basic transport equations of the models are discussed in second section.

3.1.1 Pro/ENGINEER™ Model

A generic CAD model of a dishwasher door panel was obtained from the Saint Joseph Technology Center. The front and back views (Figure 3.1) show the full door panel assembly with all of the mechanical parts. Electrical components such as the wiring, printed circuit board and electrical switches were not included in the model.

Even though the model was fairly basic and generic, it contained too many details for the computational model.

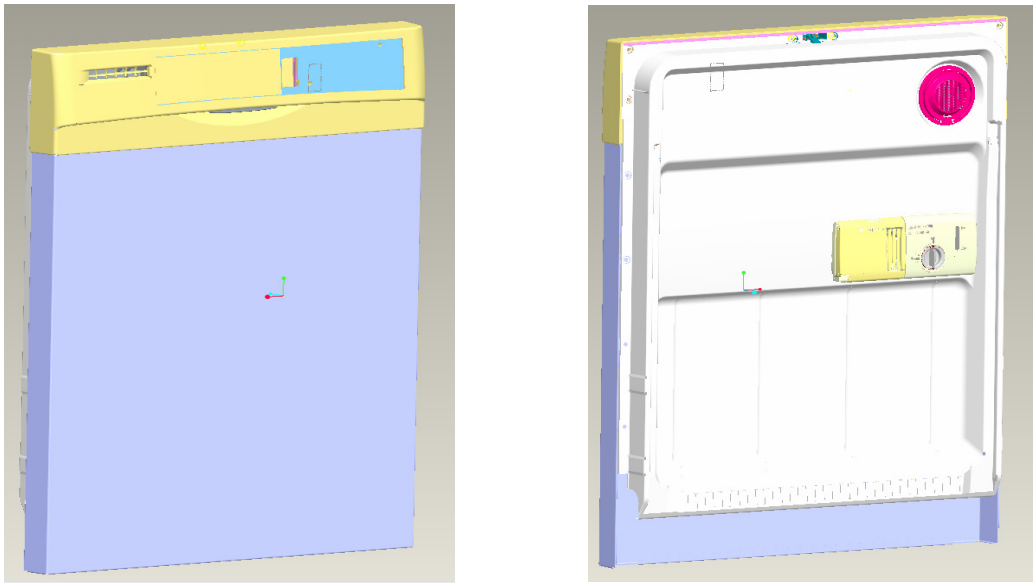

(a) (b)

Figure 3.1. Generic door panel assembly (a) front side and (b) back side.

Disassembly of the door panel began with the back inside cover. Behind the panel was the control panel holder (Figure 3.2, circled) with additional parts like the door handle and a separate vent that were not needed.

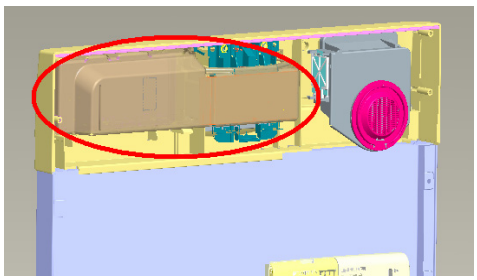

Figure 3.2. Location the control panel holder (circled).

Additional geometry was removed to further simplify the model. Figure 3.3 shows the close-up perspective of the control panel holder. The main interest is the

outer cover (brown) in Figure 3.3a and highlighted (in red) in Figure 3.3b. This later became the outer control volume boundary for the computational model.

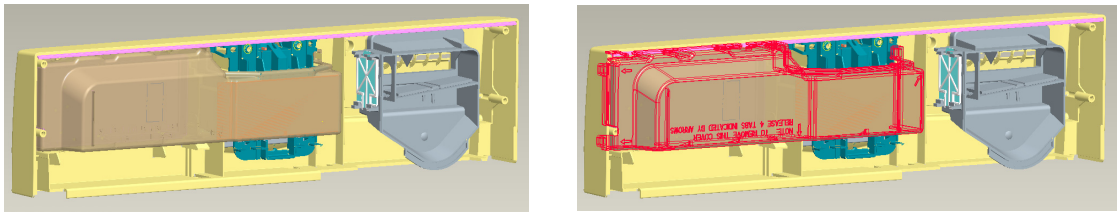

(a) (b)

Figure 3.3.(a) Magnified image of top panel and (b) control volume highlighted.

Various electrical components lie inside the assembly. The control panel cover was removed to show the inside components. The PCB holder, seen in Figures 3.4a and 3.4b on the far left in purple, was other volume used from the Pro/ENGINEER™ model. The handle assembly, seen in Figure 3.4a, was removed and replaced with a rectangular flow blockage. The handle had a gap around the edge that was modeled as a vent (Figure 3.4b).

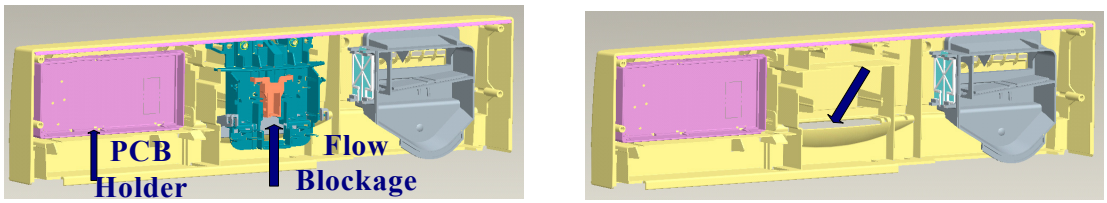

(a) (b)

Figure 3.4. (a) Location of PCB holder and flow blockage, (b) flow blockage removed to show vent.

The final simplified model, as seen in Figure 3.5, comprised of two volumes with many of the geometry assembly line details removed. The flow blockage and additional vents were added later in GAMBIT™. The approximate dimensions were 9.03 in. in the *x* direction, 2.36 in. the *y* direction and 1.7 in. in the *z* direction. Additional simplifications were performed in GAMBIT™.

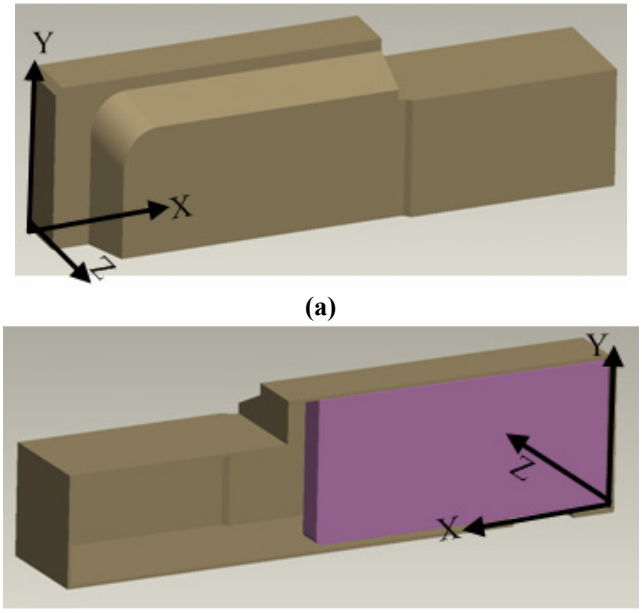

Figure 3.5. (a) Front and (b) back isometric views of final simplified model, ready for export.

3.1.2 GAMBIT™ Model

GAMBIT™ is a preprocessing application that was used for its three-dimensional mesh capabilities and to also apply the initial boundary conditions to the geometry. Some of the Pre/ENGINEER geometry was subtracted and replace with walls to simulate the flow blockage from the dishwasher handle. Two outlets were also added. One outlet was already designed on the control panel holder, as seen in red in the bottom left-hand portion of Figure 3.8a and bottom right-hand portion of Figure 3.8b. The other outlet was added to simulate the gap between the door handle and top door panel.

A solid panel, 0.2 in. thick, that measured 4 in. long by 2 in. tall was created. This panel, the PCB, was positioned inside the PCB holder approximately 0.2 in. from the holder wall. The PCB was partitioned, or mutually joined, with the PCB holder to

get rid of extraneous volumes that would otherwise exist in between the solid geometries and which can create skew elements in the model. The connection of the two volumes eliminated the gaps between the PCB and the PCB holder, similar to the way that the board is actually secured. The PCB was also partitioned from the air volume to establish flow continuity.

The partitioning process is important to ensure that no skew elements are created between any interfaces. Partitioning also creates a connection between adjacent volumes for the purposes of solid/solid, solid/fluid or fluid/fluid interactions. Examples of this include conduction heat transfer between two solids, convection heat transfer between a fluid and solid or radiation heat transfer between fluids.

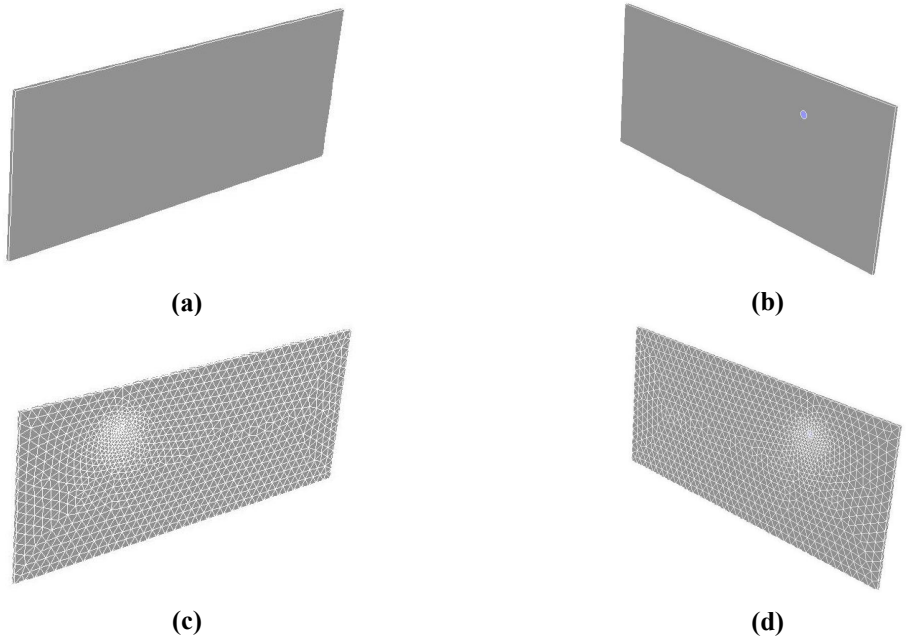

Figure 3.6. (a) Front and (b) back isometric views before meshing PCB panel, (c)front and (d) back isometric views after meshing PCB panel.

As seen in Figures 3.6c and 3.6d, a non-uniform tetrahedral volume mesh was used on the PCB to create a concentration of elements around the fuel inlet site. Since a

3-D volume mesh was used, the element spacing becomes smaller on both sides of the board, even though the fuel was injected on one side. The injection site can be seen in Figures 3.6b and 3.6d.

The PCB holder was meshed next. Since the PCB panel was located inside the PCB holder, approximately 0.2 in. from the inside wall, a partitioning of the two volumes was required. This created a solid/solid boundary condition to connect the two volumes and recreate the seal between the panel and holder. In addition, the PCB holder had to be partitioned from the control volume to create a solid/fluid boundary condition. Three-dimensional tetrahedral volume elements were used to mesh the PCB holder.

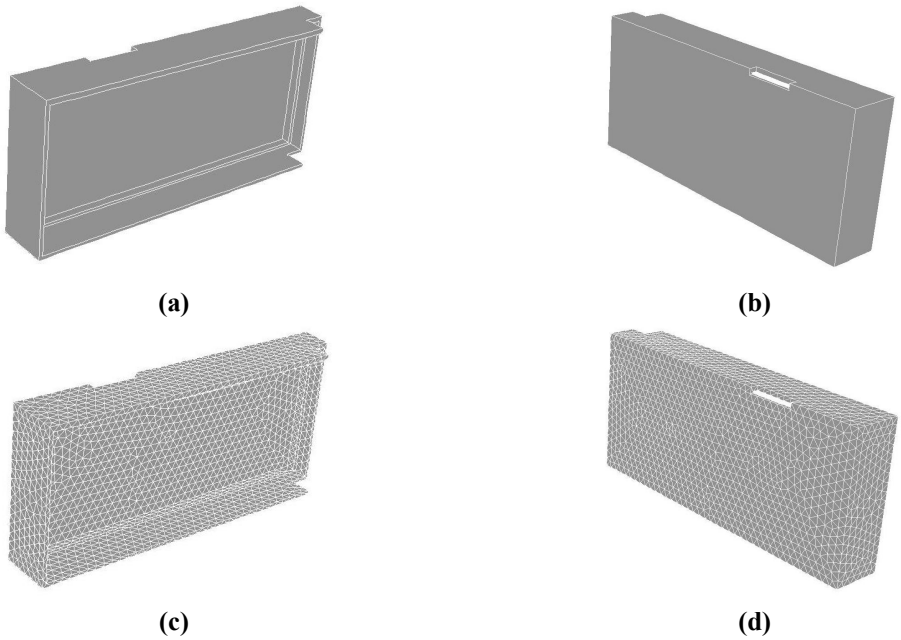

Figure 3.7. (a) Front and (b) back isometric views before meshing PCB holder, (c)front and (d) back isometric views after meshing PCB holder.

The previous steps established separate entities, or partitioned the inner volumes, from the surrounding control volume. The control volume, for this case, is

where the combustion and flame front phenomena will take place. The outer walls, as seen in Figure 3.8a, were meshed with the rest of inner control volumes such as the PCB panel and the PCB holder.

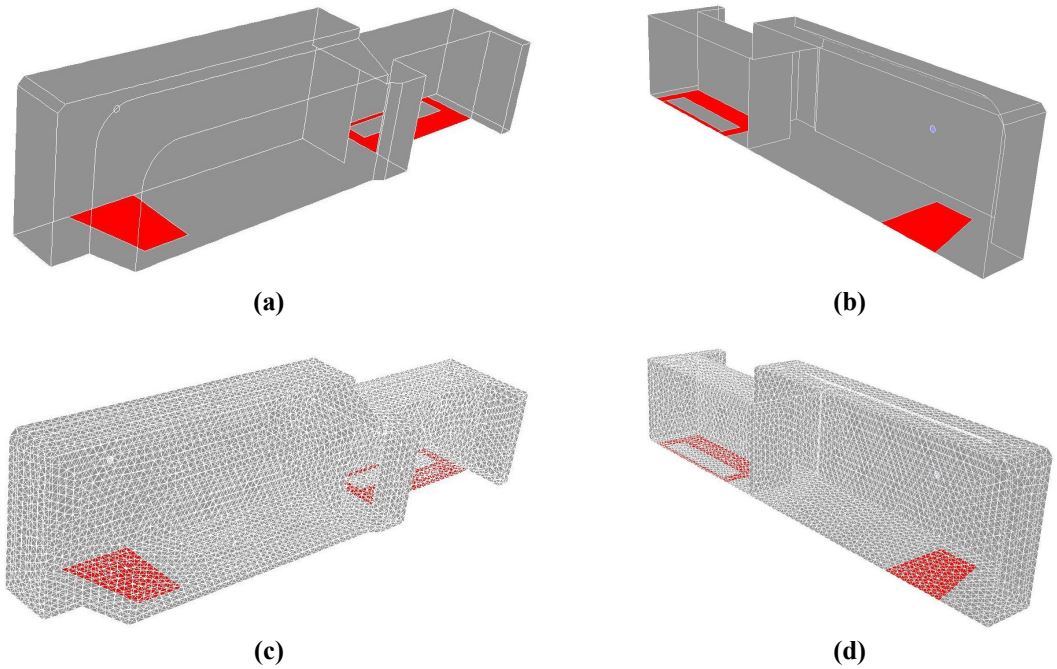

Figure 3.8. (a) Front and (b) back isometric view before meshing control volume, (c)front and (d) back isometric view after meshing control volume.

3.1.2.1 Mesh Generation and Preprocessing

The approximate dimensions of the model were 9.03 in. in the *x* direction, 2.36 in. in the *y* direction and 1.70 in. in the *z* direction (Figure 3.9).

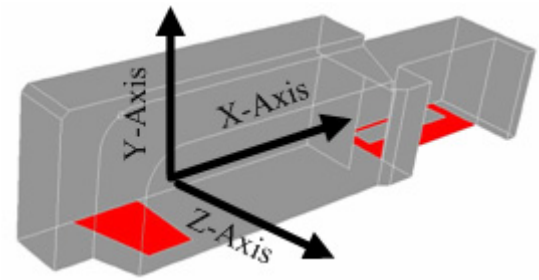

Figure 3.9. Control volume with axes for dimensioning.

The model was non-symmetric and had two inner volumes that were partitioned from the outer control volume. Smaller spaces between inner volumes such as the inner wall of the PCB panel (Figure 3.6b) and the inside wall of the PCB holder (Figure 3.7a) were only a fraction of an inch in separation. Larger gaps between areas such as the outer control volume walls were, in some cases, over two inches. The large gradients caused by the differences in the gaps and volume sizes created a problem for most grid generators. A tetrahedral/hybrid mesh was chosen because it contained the most the most flexible mesh generator scheme. The Tet/Hybrid, as it is labeled in GAMBIT™, had the ability to create a mesh compromised of tetrahedral, hexahedral, pyramidal and wedge elements (Figure 3.10). The TGrid™ option was also selected to create a volume mesh compromised of mostly tetrahedral elements.

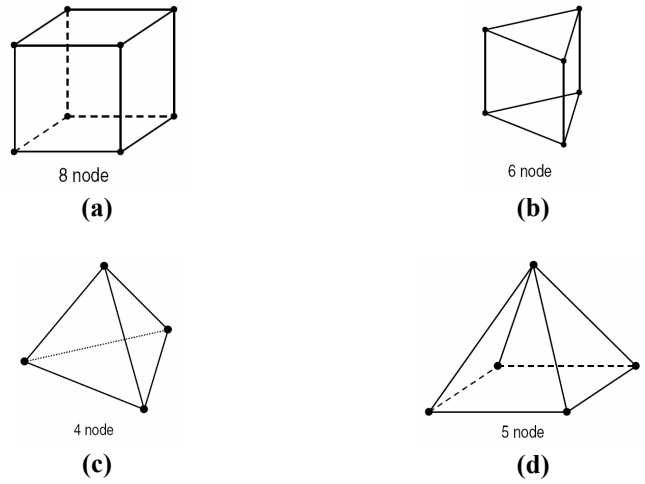

Figure 3.10. Examples of basic volume elements in GAMBIT™: (a) hexahedron, (b) wedge, (c) tetrahedron, and (d) pyramid [21].

Some initial meshes were generated with the Tet/Hybrid TGrid™ scheme using a fixed spacing assumption. In essence, the generator determined the smallest gap between any two edges or surfaces and began the mesh based on that length scale.

These meshes were unsuccessful as each one generated more than the maximum number of elements allowed in GAMBIT™. The result was an incomplete mesh and an error message.

To overcome this error, the edge line nodal points were arbitrarily moved to create self-imposed meshing gradients. In addition to the aforementioned benefits, the tetrahedral mesh generator also allowed for the most flexible movement of the edge line nodal points. These nodal points are located along the outer edges of the geometry and are the points from which the center volume mesh is generated. By moving these nodal points, the overall number of elements was reduced, thereby generating a complete mesh.

The final unmodified mesh contained 89,355 tetrahedral cells in 2 zones, with 191,933 triangular wall faces and 21,206 nodes. The final preprocessing in GAMBIT™ included adding boundary conditions such as the walls, the outlets and one inlet. A mesh file was created for the export of the model to FLUENT®.

3.2 FLUENT® Reaction Model

Five reaction models are provided in FLUENT® for species transport and chemical reactions. These are: (i) generalized finite-rate model, (ii) non-premixed combustion, (iii) premixed combustion, (iv) partially premixed combustion and (v) the composition probability density function (PDF) transport model. Of these five, the partially premixed combustion was chosen because it appears best suited, for reasons later described, to model the problem of a propagating flame front in an electronic enclosure with partially premixed reactants.

According to FLUENT®, the non-premixed combustion model is primarily used for coal combustion whereas the premixed and partially premixed models are used for gaseous combustion (e.g. methane with air). The non-premixed model is ideal for systems that are particle laden with multiple fuel streams and char particles. The premixed combustion model is ideal for characterizing the flame propagation, but it does not have the capability to use a PDF to predict discrete-phase (volatile and char) composition of a flow field.

A unique solution is hereby proposed by using a hybrid of these two systems with the partially premixed combustion solver. In brief, the non-premixed combustion model allows for an injection of discrete-phase particles and also allows for a premixed inlet at the same site. However, the model will not track a flame front propagation whereas the premixed combustion model will track a flame front propagation, but will not calculate volatile evolution of the fuel constituents. The hybrid approach of the combustion scheme used the discrete-phase particles, a fuel/oxidizer premixed inlet, and the progress variable to track the flame through the partially premixed solver.

The series of events that were modeled in FLUENT® are as follows:

(i) As seen in the previous experimental investigations, an arc was sustained for a period of time before a flame ignited. During this time it is assumed that potentially combustible gases are released (i.e., the premixed fuel injection).

(ii) An increase in voltage brought on more vigorous arcing that ejected char particles from the board (i.e. the discrete-phase injection).

(iii) Continued arcing at higher voltage ignited the mixture resulting in a small, unsustained flame.

According to [22], the partially premixed solver is a combination of the non-premixed and premixed models. A brief description of the solver is provided in [22], but no details were given about the coupling of the two models. The transport equations for the non-premixed and premixed combustion models are presented as found in [22] and are used to substantiate the hybrid partially-premixed model.

3.2.1 Species Transport and Non-Premixed Combustion

In order to fundamentally understand the partially premixed combustion model, the governing transport equations must be examined. These are the continuity, momentum and energy equations, with equations of state and constitutive relations. These will not be reviewed for brevity except for the species transport equation. The species transport equation that solves the conservation equations for the local mass fraction of each species, Y_i.

$$\frac{\partial}{\partial t}\left(\rho Y_i\right)+\nabla\cdot\left(\rho\vec{v}Y_i\right)=-\nabla\cdot\vec{J}_i+R_i+S_i \tag{3.1}$$

The typical assumption of the same diffusivities for the various species equal reduces the multiple species transport equations to one equation. The new transport equation becomes a function of the mixture fraction, *f*.

The mixture fraction, the basis of the non-premixed combustion model, simply determines the instantaneous thermal and chemical state of the fluid. The equation for *f* is written in terms of the atomic mass fractions [22] as

$$f = \frac{Z_i - Z_{i,ox}}{Z_{i,fuel} - Z_{i,ox}} \tag{3.2}$$

The subscripts *ox* and *fuel* denote the oxidizer and fuel mass fractions of the *i*th species.

Assuming equal diffusivities, the species transport equation is rewritten as a function of the mixture fraction. Equation 3.3 is thus the Favre-averaged, mixture fraction Navier-Stokes equation

$$\frac{\partial}{\partial t}\left(\rho \overline{f}\right) + \nabla \cdot \left(\rho \vec{v} \overline{f}\right) = \nabla \cdot \left(\frac{\mu_t}{\sigma_t} \nabla \overline{f}\right) + S_m + S_{user} \tag{3.3}$$

where $\overline{f}$ is the mixture fraction scalar, S_m is the source term due to mass transfer; S_{user} is an optional user-defined source term that is not used in the present study. The mixture fraction is the one of the variables used in the generation of the PDF table.

In addition to the Equation (3.3), the mixture fraction variance, $\overline{f'^2}$, is used to solve for turbulent chemical interactions. The mixture fraction variance plays an important role in generating the probability function density (PDF) table, scribed later in chapter.

$$\frac{\partial}{\partial t}\left(\rho \overline{f'^2}\right) + \nabla \cdot \left(\rho \vec{v} \overline{f'^2}\right) = \nabla \cdot \left(\frac{\mu_t}{\sigma_t} \nabla \overline{f'^2}\right) + C_g \mu_t \left(\nabla \overline{f}\right)^2 + C_d \rho_k \frac{\varepsilon}{k} \overline{f'^2} + S_{user} \tag{3.4}$$

where $f' = f - \overline{f}$; C_g, C_d , and σ_t are predefined constants in FLUENT® and S_{user}, is once again a user-defined source term that is not used.

The equivalence ratio ϕ is defined as the local fuel/air mixture to the stoichiometric fuel/air mixture

$$\phi = \frac{\left(fuel/air\right)_{actual}}{\left(fuel/air\right)_{stoichiometric}} \tag{3.5}$$

Consider a combustion system that include a fuel stream (F), an oxidant stream (O) and a product stream (P). A simple stoichiometric representation can be written as:

$$\mathrm{F} + r\,\mathrm{O} \rightarrow \left(1 + r\right)\mathrm{P} \tag{3.6}$$

where r is the air-to-fuel mass ratio. Equation (3.5) is used to rewrite Equation (3.6), yielding

$$\phi\,\mathrm{F} + r\,\mathrm{O} \rightarrow \left(\phi + r\right)\mathrm{P} \tag{3.7}$$

Deducing from the left side of the equation, the mixture fraction can be written in terms of the equivalence ratio. Equation (3.8) allows for the computation of the mixture fraction for all conditions from fuel-lean to stoichiometric to fuel-lean conditions.

$$f = \frac{\phi}{\phi + r} \tag{3.8}$$

Assuming chemical equilibrium, the thermal and chemical scalar properties of temperature, density and species fraction are now related to the mixture fraction. In general, the equation for a non-adiabatic system can be described as:

$$\phi_i = \phi_i\left(f, H\right) \tag{3.9}$$

where H is the instantaneous total enthalpy based on the mass fraction of each species:

$$H = \sum_j Y_j H_j \tag{3.10}$$

Equations (3.9) and (3.10) describe the relationships between the mixture fraction and the resulting scalar quantities of temperature, species fractions and density. Again, these are calculated assuming a full equilibrium model.

The probability density function (PDF) $p(f)$ is a representation of the fraction of time that the fluid spends in the state *f*. Figure 3.11 is a graphical description of a PDF, showing the time trace of the mixture fraction at a point (right plot) and the probability density function of *f* (left plot).

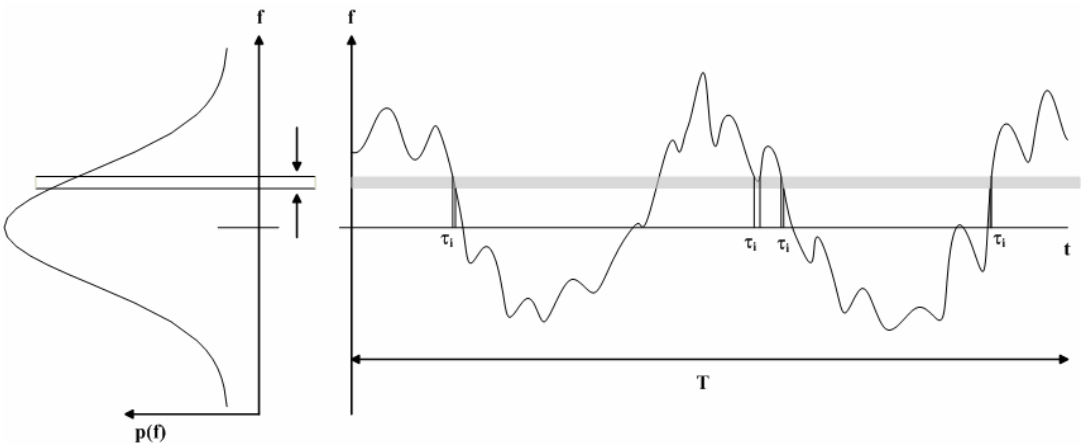

Figure 3.11. Graphical representation of PDF [22].

The equation describing the PDF is:

$$p(f)\Delta f = \lim_{T\to\infty} \frac{1}{T} \sum_i \tau_i \tag{3.11}$$

where *T* is the period and τ_I is the amount of time that *f* spends in the band of Δf. The shape of the probability density function, $p(f)$, depends on the turbulent fluctuation of

the state of the fluid (f). Actual PDFs depend on experimental observations to determine the shape of the function.

The PDF describes the state of the fluid at the individual time steps. This can be used to calculate average scalar values like temperature, density and mass fractions. For an adiabatic system the mean density-weighted mass fraction and temperature is computed as a function of the PDF and the instantaneous mass fraction.

$$\overline{\phi_i} = \int_0^1 p(f)\phi_i(f)df \tag{3.12}$$

The time-averaged density of the fluid can also be calculated from the shape of the PDF.

$$\frac{1}{\overline{\rho}} = \int_0^1 \frac{p(f)}{\rho(f)}df \tag{3.13}$$

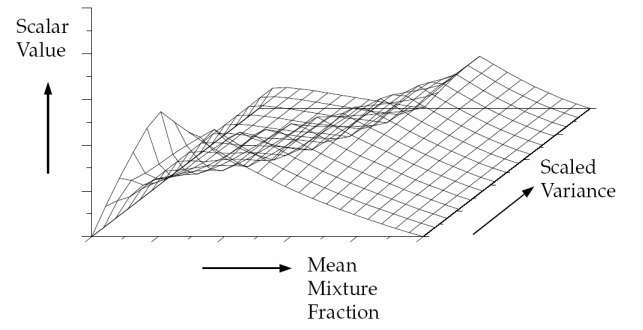

Figure 3.12. Visual representation of an adiabatic, single mixture PDF [22].

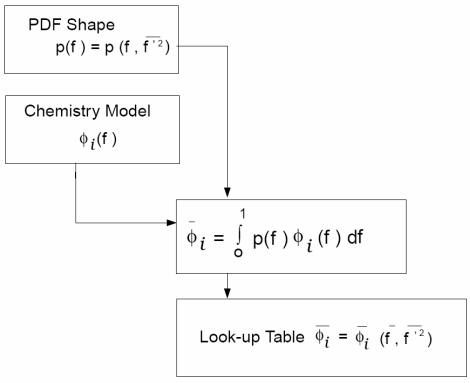

Figure 3.13. Logic dependence of an adiabatic system [22].

Reacting flows have local, time-dependent thermochemical properties. The previous relations show the PDF only calculated as a function of the local state f.

However, non-adiabatic systems, such as particle-laden system (e.g. coal combustion) that includes heat transfer in the flow, need an additional term because turbulent fluctuations cause heat loss or gain in the fluid. The enthalpy *H* is used for this purpose. A series of joint PDFs are calculated to find the normalized heat loss of the fluid at the discrete time and location in the fluid, see Figures 3.14 and 3.15.

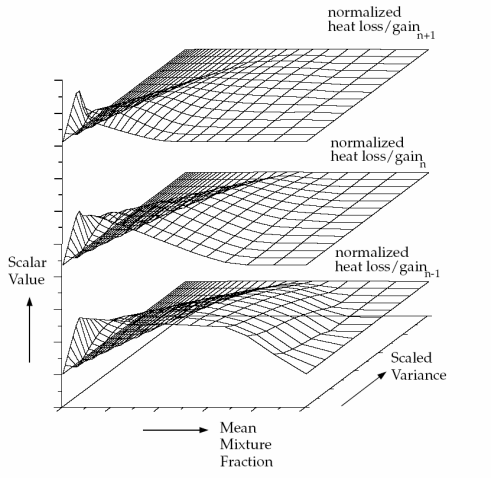

Figure 3.14. Visual representation of a non-adiabatic, single mixture PDF [22].

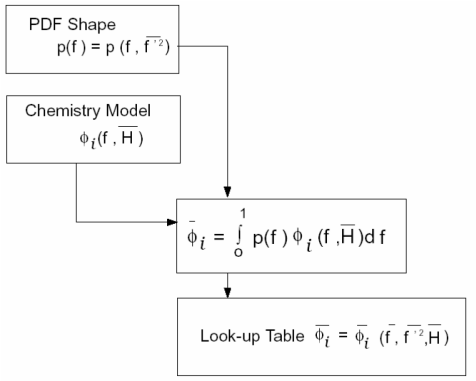

Figure 3.15. Logic dependence of a non-adiabatic system [22].

The previous transport equation has to be altered to include the terms for enthalpy change as follows:

$$\frac{\partial}{\partial t}\left(\rho\overline{H}\right)+\nabla\cdot\left(\rho\vec{v}\overline{H}\right)=\nabla\cdot\left(\frac{k_t}{c_p}\nabla\overline{H}\right)+S_h \tag{3.14}$$

where S_h accounts for the source terms due to radiative heat transfer with dispersed phase.

3.2.2 *Premixed Combustion*

The next step is to add the premixed combustion theory to achieve a partially-premixed model. Another transport equation is added to track the flame front propagation:

$$\frac{\partial}{\partial t}(\rho c)+\nabla\cdot(\rho\vec{v}c)=\nabla\cdot\left(\frac{\mu_t}{Sc_t}\nabla c\right)+\rho S_c \tag{3.15}$$

where c is the mean reaction progress variable, Sc_t is the turbulent Schmidt number and S_c is the reaction progress source term.

$$\frac{\partial}{\partial t}(\rho c)+\nabla\cdot(\rho\vec{v}c)=\nabla\cdot\left(\frac{\mu_t}{Sc_t}\nabla c\right)+\rho S_c \tag{3.16}$$

The transport equation is solved in terms of ρS_c

$$\rho S_c = AG\rho_u I\left[\frac{\tau_t}{\tau_c(\lambda_{lp})}\right]^{1/4}|\nabla c| \tag{3.17}$$

where A is a constant of the solver, G the flame stretch factor, τ_t is a turbulent time scale, τ_c is the combustion time scale, λ_{lp} is the preferential diffusion (heat based) and c is the reaction progress variable.

Premixed combustion also uses a non-adiabatic temperature calculation

$$\frac{\partial}{\partial t}(\rho h)+\nabla\cdot(\rho\vec{v}h)=\nabla\cdot\left(\frac{k+k_t}{c_p}\nabla h\right)+S_{h,chem}+S_{h,rad} \tag{3.18}$$

where h is the enthalpy, $S_{h,rad}$ is the losses due to radiation and $S_{h,chem}$ is the gains due to chemical reactions. This is based on:

$$S_{h,chem} = \rho S_c H_{comb} Y_{fuel} \tag{3.19}$$

where Y_{fuel} is the fuel mass fraction, H_{comb} is the heat of combustion for 1 kg of fuel (defined by user) and S_c is the normalized average rate of product formation.

3.2.3 Partially Premixed Combustion

According to [22], the partially premixed solver is a combination of the previously described non-premixed and premixed combustion models. The premixed reaction variable c indicates the flame front position. Ahead of the flame front, $c = 0$ and the unburnt mixture is calculated from mass fractions, temperature and density. Behind the flame front, $c = 1$ and the burnt mixture is calculated by an equilibrium mixture fraction.

The partially premixed model solves a transport equation for a mean reaction progress variable $\bar{c}$ in addition to solving the mixture fraction $\overline{f}$ and the mixture fraction variance $\overline{f'^2}$. Then, density mean scalars, such as mixture fraction and temperature, are calculated from the PDFs of f and c.

$$\overline{\phi} = \int_0^1 \int_0^1 \phi(f,c) p(f,c) df\, dc \tag{3.20}$$

Assuming a thin flame, unburnt reactants and burnt products exist, the mean scalars are determined from:

$$\bar{\phi} = \bar{c}\int_0^1 \phi_b(f)p(f)df + (1-\bar{c})\int_0^1 \phi_u(f)p(f)df \tag{3.21}$$

The partially premixed model is initialized by the progress variable.

To reiterate, the non-premixed model allows the user to input either a gaseous, liquid or solid fuel to mix with an oxidizer within a control volume (Figure 3-16a). In some cases, such as a furnace coal bed, an oxidizer may be injected at high temperatures over a discrete phase model (DPM) solid fuel (Figure 3-16b). The non-premixed model allows for either full rich ($f = 1$) or full lean inlets ($f = 0$). No other combination of fuel and oxidizer ($0 < f < 1$) is allowed in FLUENT®.

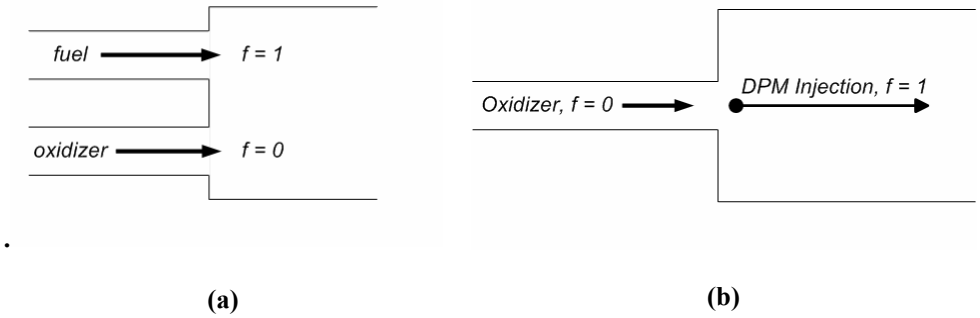

Figure 3.16. Illustrations of non-premixed systems for (a) separate fuel and oxidizer inlets and (b) hot oxidizer blowing over DPM injection.

A premixed model allows the user to combine a fuel and oxidizer at the inlet, but only in a fully premixed ($f = 1$) condition (Figure 3.17). The DPM is not allowed for premixed systems. The premixed combustion model is most commonly used for gaseous fuel/oxidizer simulations such as methane/air or propane/air. The user can define a fully burnt ($c = 1$) or fully unburnt ($c = 0$) mixture at the inlet.

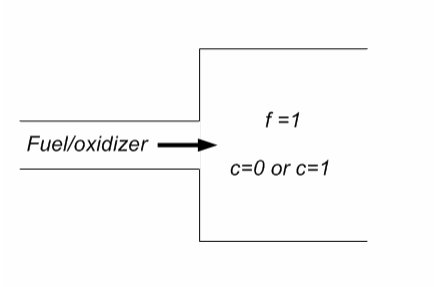

Figure 3.17. Illustration of a premixed system.

The partially-premixed model allows the user to combine the non-premixed and premixed systems. In most cases, the partially premixed is again used for gaseous combustion [22]. A non-uniform mixture is used at the inlet and injected into a lean, or oxidizer rich, atmosphere.

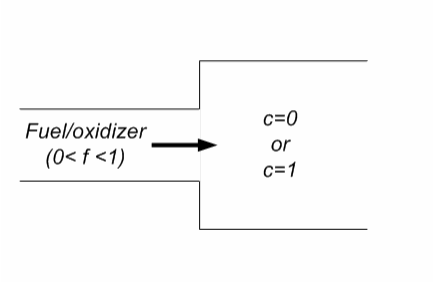

Figure 3.18. Illustration of a partially-premixed system.

A unique approach is proposed here to simulate the partially premixed combustion inside the appliance control panel. A fully premixed inlet ($f = 1$), consisting of gaseous coal volatiles and air, was injected with a secondary medium-volatile DPM solid fuel (Figure 3.19). Both fuels contained the same chemical species, enabling two discrete fuels to be calculated from a single fuel stream PDF. By avoiding the secondary fuel stream calculations, the computational time can be drastically reduced [22].

The premixed inlet had a mass flow rate 0.008 kg/s of gaseous reactants at an injection speed of 0.2 m/s. This gaseous fuel was used to simulate the outgassing of the PCB panel when continual arcing pyrolizes the surrounding material. The DPM model also had the same mass and velocity rates and was used to simulate the injection of solid fuel by violent bursting caused by arc tracking. The mass injection rates were calculated on a scaled basis from [24]. The velocity was assumed to be at or below the laminar burning velocity [23].

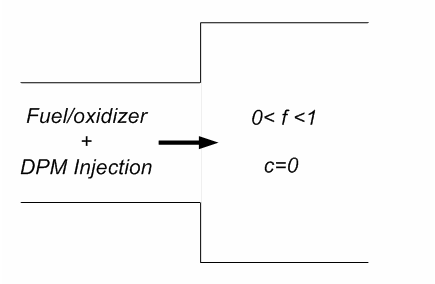

Figure 3.19. Illustration of the hybrid partially-premixed system.

As seen from the experimental results in Chapter 2, a flame may not ignite even though arcing occurs. For the purpose of the computational model, it was assumed that during this time the surrounding material was being pyrolized, or thermally broken down, and the electrical components were releasing gaseous fuel. The benchtop experiments also showed bursting, or strong arc discharges, at the nodes that did not always ignite a flame. Additionally, it was assumed that during this time the bursting caused solid particles of carbonized material to be ejected from the PCB. This material was simulated by the medium-volatile DPM injection.

3.2.4 Injection Site and Discrete Phase Model

The injection site has to be treated with special consideration. A combusting solid particle injection will undergo devolatilization or char combustion. In addition to solving the transport equations, FLUENT® offers the discrete phase model (DPM). The DPM can be used to simulate injected particles, of a spherical nature, that are dispersed into the continuous phase. Once the particles are introduced, the trajectories and the heat and mass transfer of the particles must be calculated. Specifically for this simulation, the DPM is used to calculate the volatile evolution and char rate of the medium-volatile coal model.

An injection site was overlaid on the surface of the inlet, as seen in Figure 3.19, for the mass injection. The injected fuel is described as "combusting particles" that are reacted with oxygen [24]. In addition, the injection site is giving an "escaped" boundary condition, allowing the all combusting particles to be freely emitted. The adjacent walls of the PCB panel and PCB holder are set to the "reflecting" boundary condition, so all of the DPM particles will rebound off the walls.

3.2.5 Chemical Constituents for Combusting Particles

When coal is modeled by a single mixture fraction, the fuel stream composition can be input using the conventional approach or an empirical fuel approach [24]. For the present case the fuel consists of 30.4% volatiles and 69.6% char. References [23,24] suggest similar chemical constituents. The ultimate analysis, to define the coal composition, char and volatiles content, is derived as follows.

Convert the standard coal mole percentages to a dry-ash-free (DAF) model as shown in Table 3.1.

Table 3.1. Approximated weight percentage of volatiles and char particles in coal [24].

Proximate Analysis	Wt% (dry)	Wt% (DAF)
Volatiles	28	30.4
Char [c(s)]	64	69.6
Ash	8	-

The ultimate analysis for the DAF model is shown in Table 3.2.

Table 3.2. Weight percentage of coal chemical constituents [24].

Element	Wt% (DAF)
C	89.3
H	5.0
O	3.4
N	1.5
S	0.8

The sulfur content of the coal can be combined into the nitrogen mass fraction, to further simplify the model, as listed in Table 3.3.

Table 3.3. Simplified weight percentage of coal chemical constituents [24].

Element	Wt% (DAF)
C	89.3
H	5.0
O	3.4
N	2.3
S	-

Combine the approximate and ultimate analysis data to yield the following elemental composition of the volatile stream (Table 3.4).

Table 3.4. Mole fraction of coal chemical constituents [24].

Element	Wt%	Moles	Mole Fraction
C	89.3	7.44	0.581
H	5.0	5	0.390
O	3.4	0.21	0.016
N	2.3	0.16	0.013
Total	100	12.81	1.0

3.2.6 Spark Ignition Model

Spark ignition is commonly used to initiate combustion at a desired time and location in a computational model. A physical spark is accomplished by sending a high voltage across the gap between two electrodes. The spark is relatively quick and its energy can be several orders of magnitude less than the chemical energy released by the reaction. The true physical nature of the spark is complicated to describe, so the modeling is simplified. The governing transport equation is modeled from the premixed theory. The spark region is set to a burned state $(c = 1)$ and the density and temperature quantities are calculated afterwards via

$$\frac{\partial}{\partial t}(\rho c) + \nabla \cdot (\rho \vec{v} c) = \nabla \cdot (D_t \nabla c) + \rho_u U_t |\nabla c| \tag{3.22}$$

where D_t is the turbulent diffusivity, ρ_u is the density of the unburnt mixture and U_t is the turbulent flame speed. The spark size is very small compared to the grid size, so the Zimont model is used to simplify the turbulent diffusivity to laminar [24].

$$\frac{\partial}{\partial t}(\rho c) + \nabla \cdot (\rho \vec{v} c) = \nabla \cdot [(\kappa + D_t) \nabla c] + \rho_u U_t |\nabla c| \tag{3.23}$$

This effectively creates a spark with a decaying exponential characteristic and propagation behavior.

The spark theory can be used for any combustion model, but it is most compatible with the premixed and partially premixed combustion models. In some cases, the spark will only increase the temperature of the immediate area of discharge,

but will not initiate combustion. This non-trivial matter can be attributed to issues such as the chemical mixture at the node, spark size and the diffusion rate of the spark. Simply the flow did not receive enough energy from the spark to initiate combustion even though $c = 1$ is imposed at that node.

3.3 Boundary Conditions

In addition to applying the hybrid combustion model, boundary conditions must be applied. The main solver is a three-dimensional, double precision and segregated model. The double precision solver was used to alleviate errors associated with the high aspect-ratio grid. The turbulence was computed using the standard κ–ε model in FLUENT®. An unsteady or transient solver was chosen to capture the initiation of the combustion and track the flame front propagation. Additional details and more comprehensive set up of the boundary conditions are supplied in Appendix C.

The solution was initialized with two patches. The (i) progress variable was set to zero and (ii) the temperature was set to 350 K. Both patches were imposed on the entire control volume. These patches were only initial boundary conditions of the solution and did not have an effect on transient solver. Each time step was determined and monitored by the solver with an adaptive time step scheme.

Two simulations were run. Each solution started at $t = 0$ seconds with the hybrid model comprising a fully premixed injection and a DPM injection. The DPM injection was modeled with a medium-volatile coal that contained 69.6% solid char and 30.4% volatiles. For the first transient analysis, a 220 J spark occurred at 1 ms for a duration of 1 ms. The delay of the spark allowed for the gaseous fuel to propagate

through the control volume, simulating the volatile release due to arc tracking. The contour plots do not show the entire simulation because the flame front propagation decays after 1.01E-3 seconds. The control volume chemistry begins to refill with combustible particles and contours look vague.

The second simulation initiated combustion also with a 220 J spark but at $t = 10$ ms and also for a duration of 1 ms. The contour plots are shown at 10 ms and 10.01 ms for comparison with the first transient analysis.

CHAPTER 4

RESULTS

4.1 Description of Contour Plots

The results from the combustion modeling are mostly displayed as two-dimensional (2-D) cuts or isometric views. In order to properly show the flame front propagation, two isometric views are shown with complementing 2-D plane cuts. The 2-D plane cut show one top view (*x*-*z* plane), one back view (*x*-*y* plane) and four lengthwise views (*y*-*z* planes). All eight views are grouped together to make one figure for each time step. Since a large number of figures are needed to highlight the flow characteristics, only two time steps are chosen for brevity.

The 3-D isometric views located at the top of each time step figure show the outline and features of the PCB panel, PCB holder and control volume. The 2-D plane cuts are also seen in the isometric views to give an approximate location of each of the planes. The 2-D top view or *x*-*z* 01 is a plane cut intersecting the fuel/oxidizer and spark ignition site. The PCB panel is seen in the 2-D top view as a thick, white line located at the bottom, right portion of the view. The 2-D back view or *x*-*y* 01 is another plane cut that also intersects the fuel/oxidizer and spark ignition location and is placed between the PCB panel and PCB holder. The next set 2-D plane cuts are located along the *x*-axis of the geometry. The first cut labeled *y*-*z* 01, is also located at the fuel/oxidizer and spark ignition site. Additionally, this plane is perpendicular to an

outlet and that seen as a red outline at the bottom of the view. The next plane cut *y-z* 02 is arbitrarily placed half-way from the first plane and the third plane cut. The third plane cut, *y-z* 03 is placed at a contraction of the geometry where an inside wall is located. This wall is part of the handle assembly and created a potential area of interest. The last plane cut, *y-z* 04 is arbitrary located perpendicular to the gaps in the handle assembly that were modeled as outlets and are seen as red outlines..

4.2 Description of First Transient Analysis

A spark was initiated at 1 ms for the first transient analysis. The data shown at 1 ms do not indicate any chemical changes because the spark and associated reactions did not propagate until the next time step of 10 μs. Proliferation of the chemical reactions was tracked by the DPM burnout rate, and carbon monoxide, carbon dioxide and carbon mole fractions. Additionally, flame front verification was monitored by the temperature and progress variable contours.

4.2.1 Discrete Phase Model Char Burnout Rates (First Simulation).

According to the non-premixed combustion theory in [24], the DPM char burnout rate is an indication that the solid char particles are oxidizing. An example characteristic equation is seen below.

$$char(s) + S_{b,ox}(g) \rightarrow products(g) \tag{4.1}$$

The following contour plots for the DPM burnout rate show a relatively diminutive amount of activity, but did still offer visible results. This was mainly attributed to the small amount of solid fuel that was present when the ignition spark occurred. The most notable contour change is seen in the 3-D isometric back view and the 2-D back view (*x*-*y* 01). The range of results for both sets of contours is indicated from 0 – 4E-12 kg/s for the DPM burnouts rate.

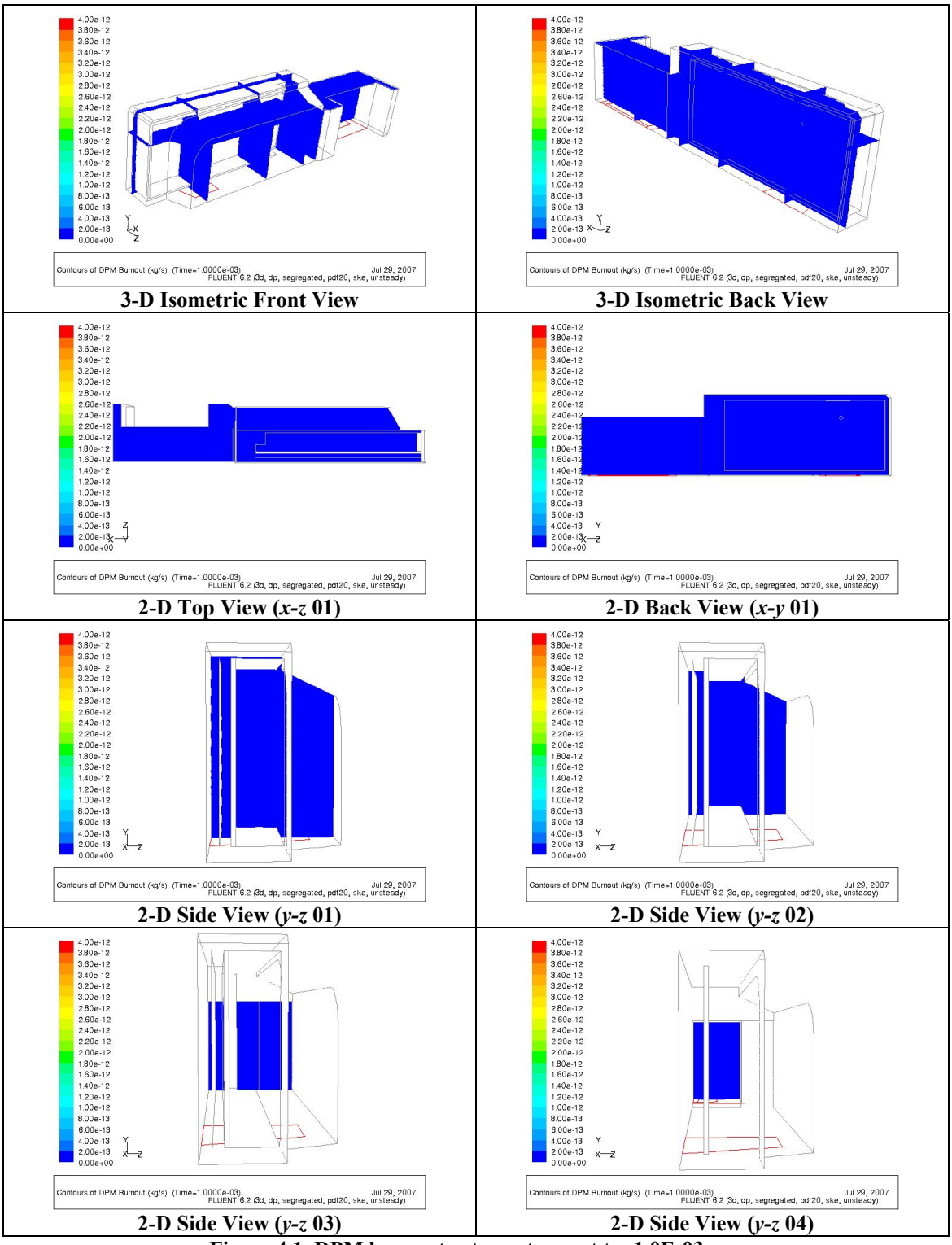

Figure 4.1. DPM burnout rate contours at t = 1.0E-03 sec.

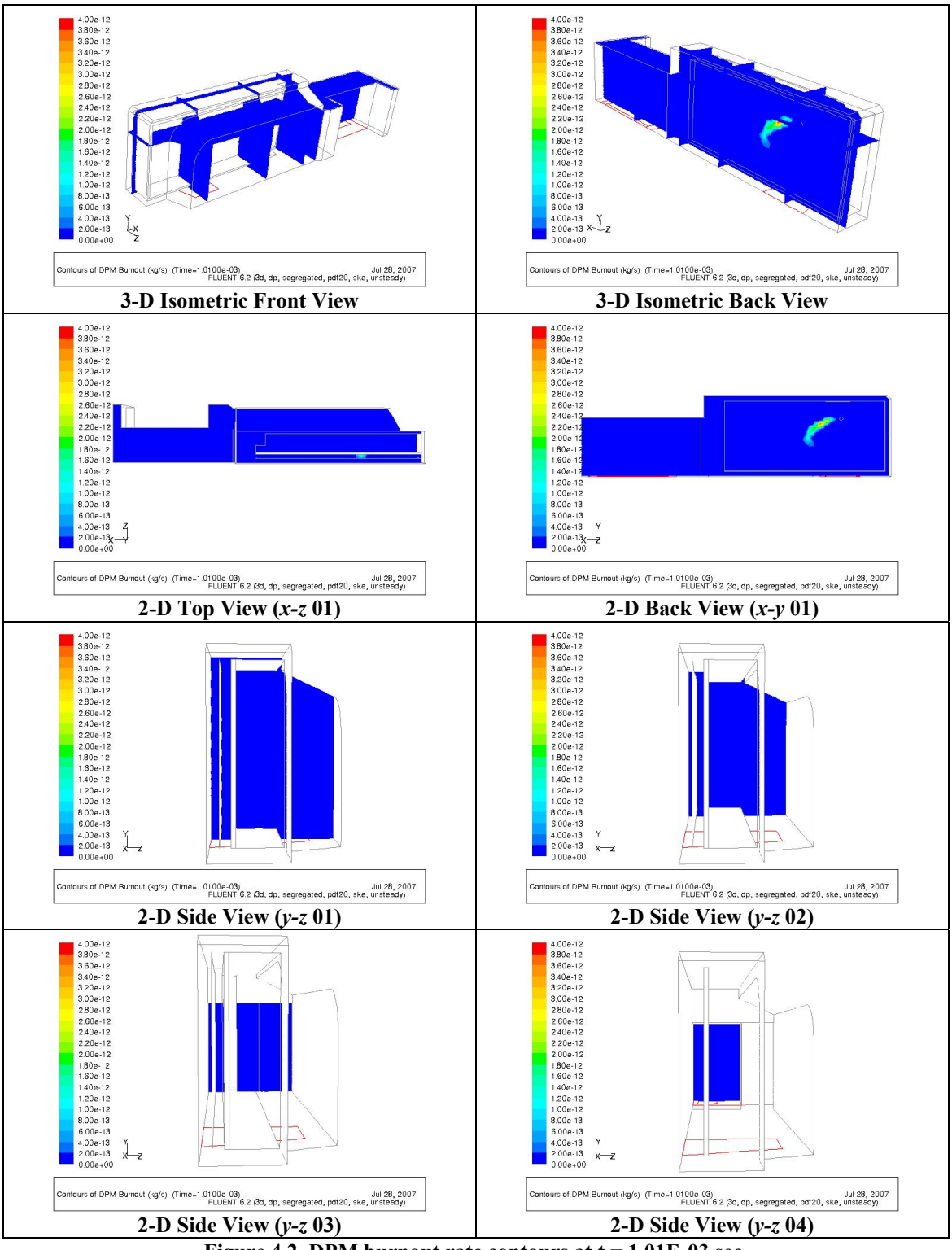

3-D Isometric Front View

3-D Isometric Back View

2-D Top View (*x-z* 01)

2-D Back View (*x-y* 01)

2-D Side View (*y-z* 01)

2-D Side View (*y-z* 02)

2-D Side View (*y-z* 03)

2-D Side View (*y-z* 04)

Figure 4.2. DPM burnout rate contours at t = 1.01E-03 sec.

4.2.2 Mole Fractions of Carbon Monoxide (First Simulation)

For hydrocarbon reactions, such as coal, Equation (4.1) can yield two primary products. One of the products, carbon monoxide, is more commonly associated with the char-oxidizer interaction and is shown in the next set of contours [23]. Section 4.2.3 will highlight the evolution of the other primary product, carbon dioxide.

The first set of contour views are at 1 ms and indicates no production of carbon monoxide. The second set of contour views are 10 μs after the spark ignition. The range of results for both sets of contours is indicated from 0 – 1E-9 for the mole fraction of carbon monoxide.

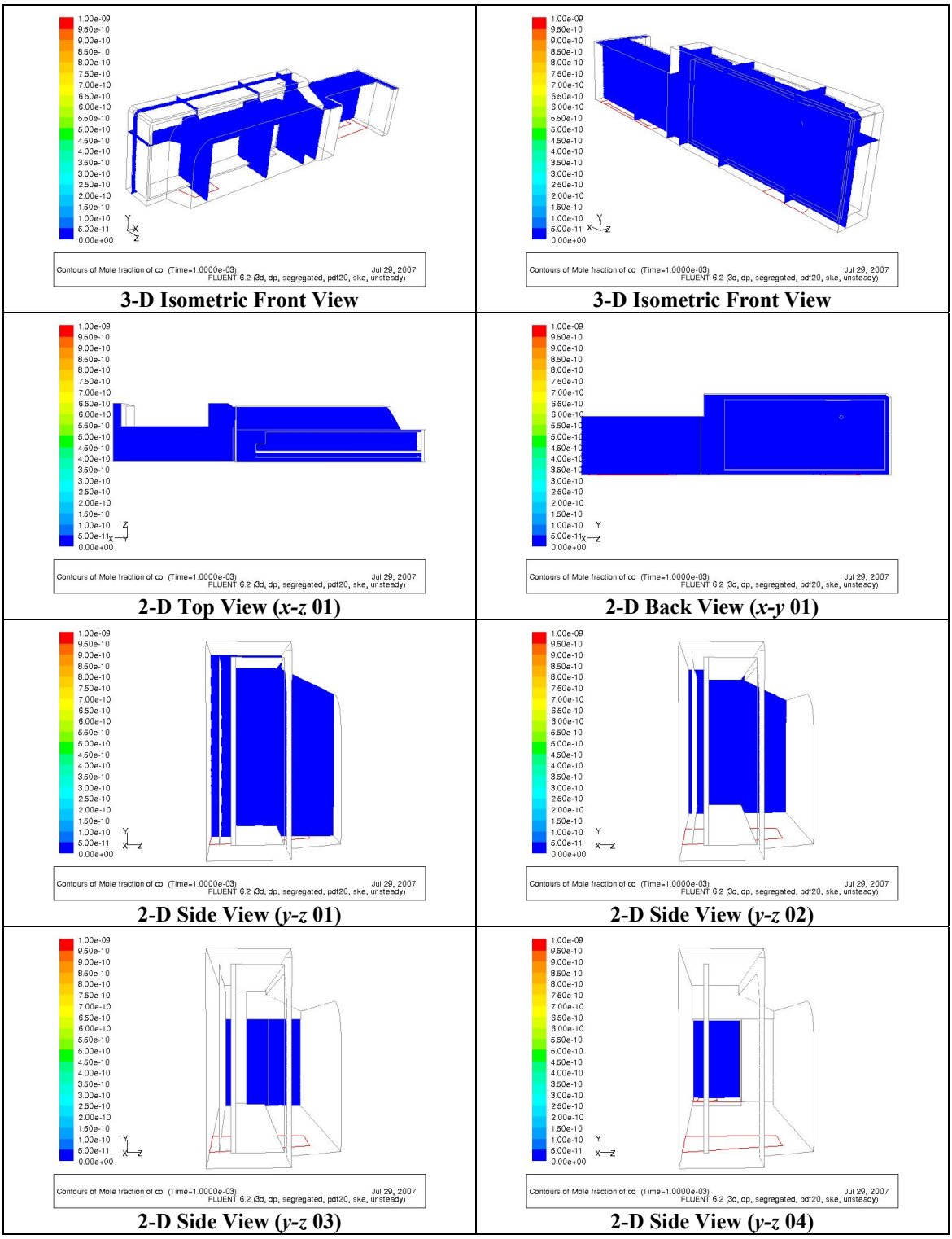

3-D Isometric Front View | **3-D Isometric Front View**

2-D Top View (*x-z* 01) | **2-D Back View (*x-y* 01)**

2-D Side View (*y-z* 01) | **2-D Side View (*y-z* 02)**

2-D Side View (*y-z* 03) | **2-D Side View (*y-z* 04)**

Figure 4.3. Mole fraction contours of carbon monoxide at t = 1.0E-03 sec.

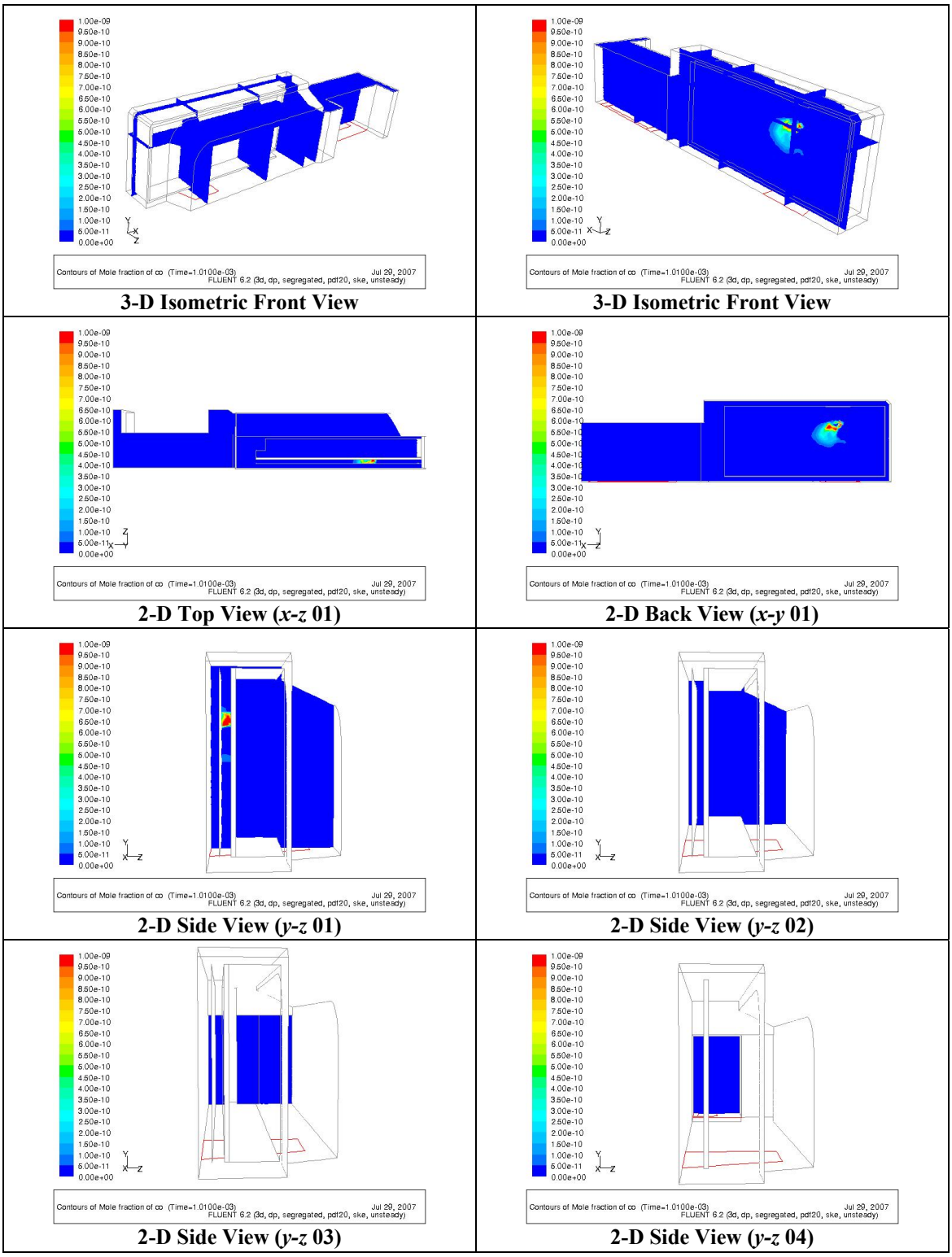

3-D Isometric Front View | 3-D Isometric Front View

2-D Top View (*x-z* 01) | 2-D Back View (*x-y* 01)

2-D Side View (*y-z* 01) | 2-D Side View (*y-z* 02)

2-D Side View (*y-z* 03) | 2-D Side View (*y-z* 04)

Figure 4.4. Mole fraction contours of carbon monoxide at t = 1.01E-03 sec

4.2.3 Mole Fractions of Carbon Dioxide (First Simulation)

As previously stated, the char-oxidizer yields two primary products. The second product, carbon dioxide was examined and showed higher mole fraction concentrations. The first set of contour views were taken at 1 ms and indicated no production of carbon dioxide. The second set of contour views were taken 10 ms after the spark ignition. The range of results for both sets of contours is indicated from 0 – 1E-6 for the mole fraction of carbon dioxide.

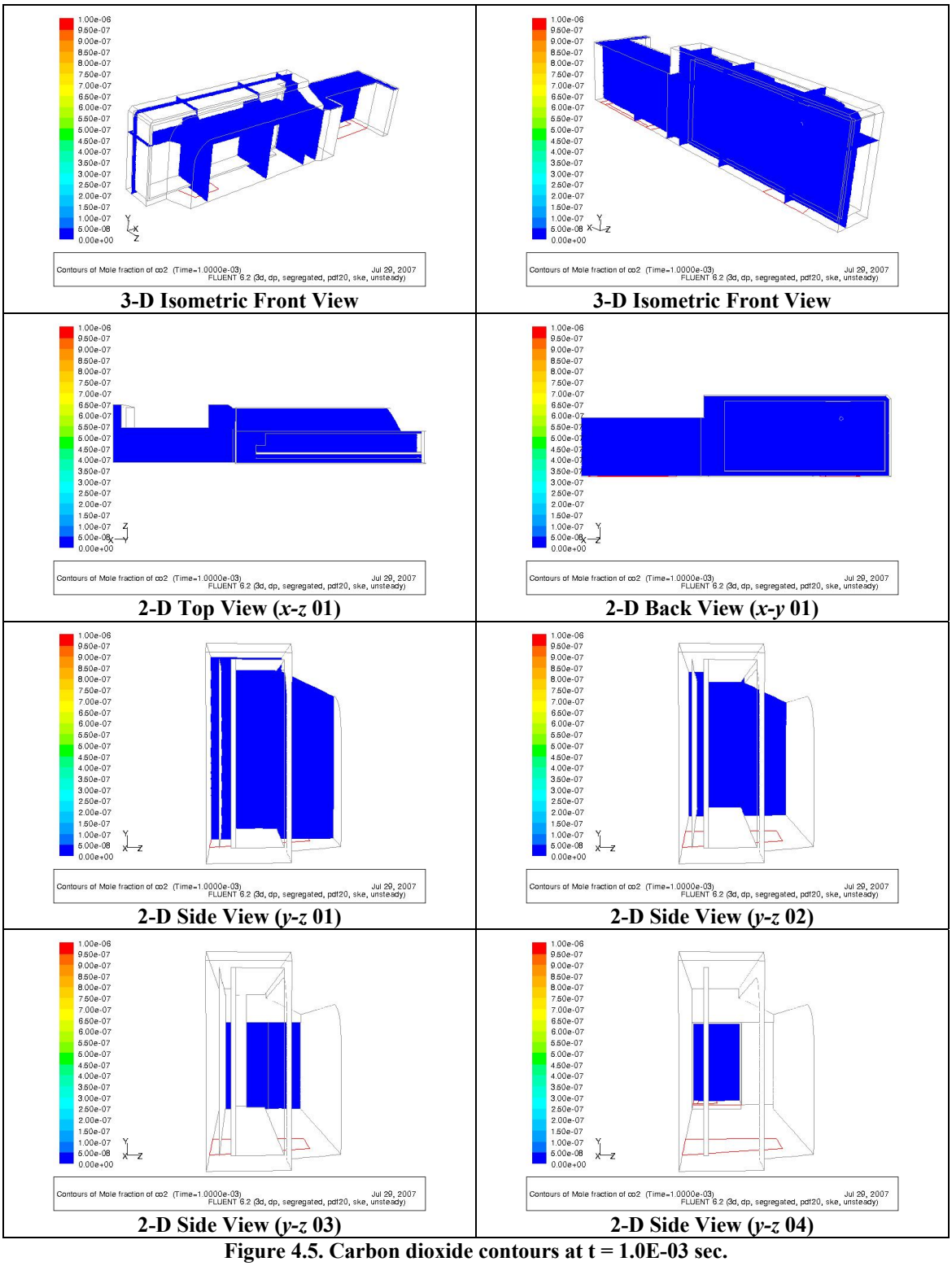

Figure 4.5. Carbon dioxide contours at t = 1.0E-03 sec.

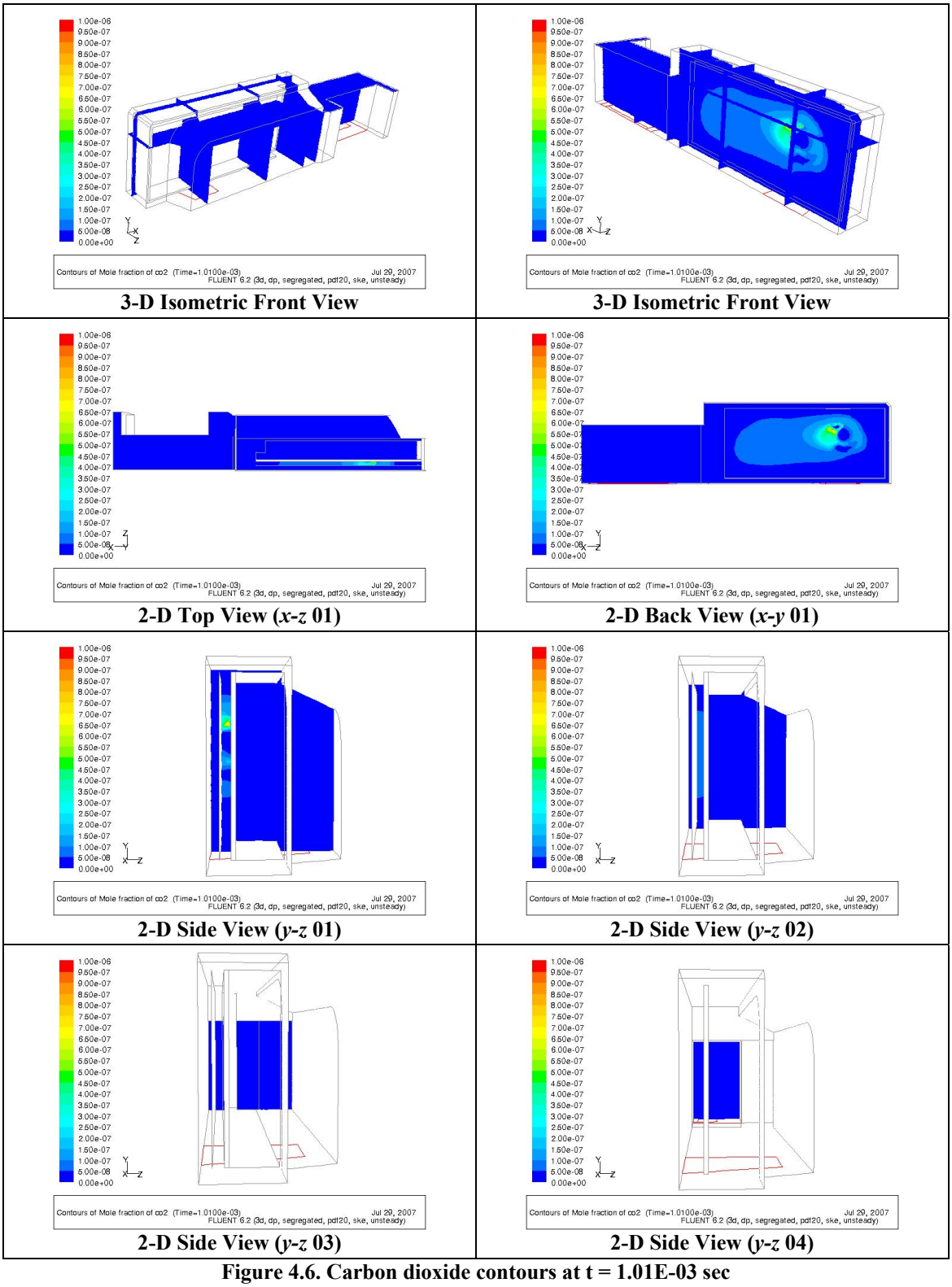

3-D Isometric Front View | 3-D Isometric Front View

2-D Top View (*x-z* 01) | 2-D Back View (*x-y* 01)

2-D Side View (*y-z* 01) | 2-D Side View (*y-z* 02)

2-D Side View (*y-z* 03) | 2-D Side View (*y-z* 04)

Figure 4.6. Carbon dioxide contours at t = 1.01E-03 sec

4.2.4 Mole Fractions of Carbon (First Simulation)

Most analysis contained in the literature [23-25], assumes solid char is the predominate reactant available for the oxidation process. However, the differences between DPM burnout rate and mole fraction contours indicate the solid carbon is not primary reactant. It was therefore assumed the gaseous carbon was the main source of fuel for the oxidization process.

As shown from the previous DPM burnout rate and mole fraction contours, a reaction does occur. The carbon contours are shown for visual reference of the dispersion of the gaseous volatiles within the control volume. The first set of contour views were taken at 1 ms and indicated a uniform dispersion of carbon that was concentrated between the PCB panel and PCB holder. The second set of contour views was taken at 10 μs after the spark ignition. The contour levels changed and showed the propagation of flame front away from the ignition source. This ignition point is most visible in the second set of contours views, on the 2-D back view (*x*-*y* 01) as a dark blue spot. The range of results for both sets of contours is indicated from 0 – 1E-5 for the mole fraction of carbon.

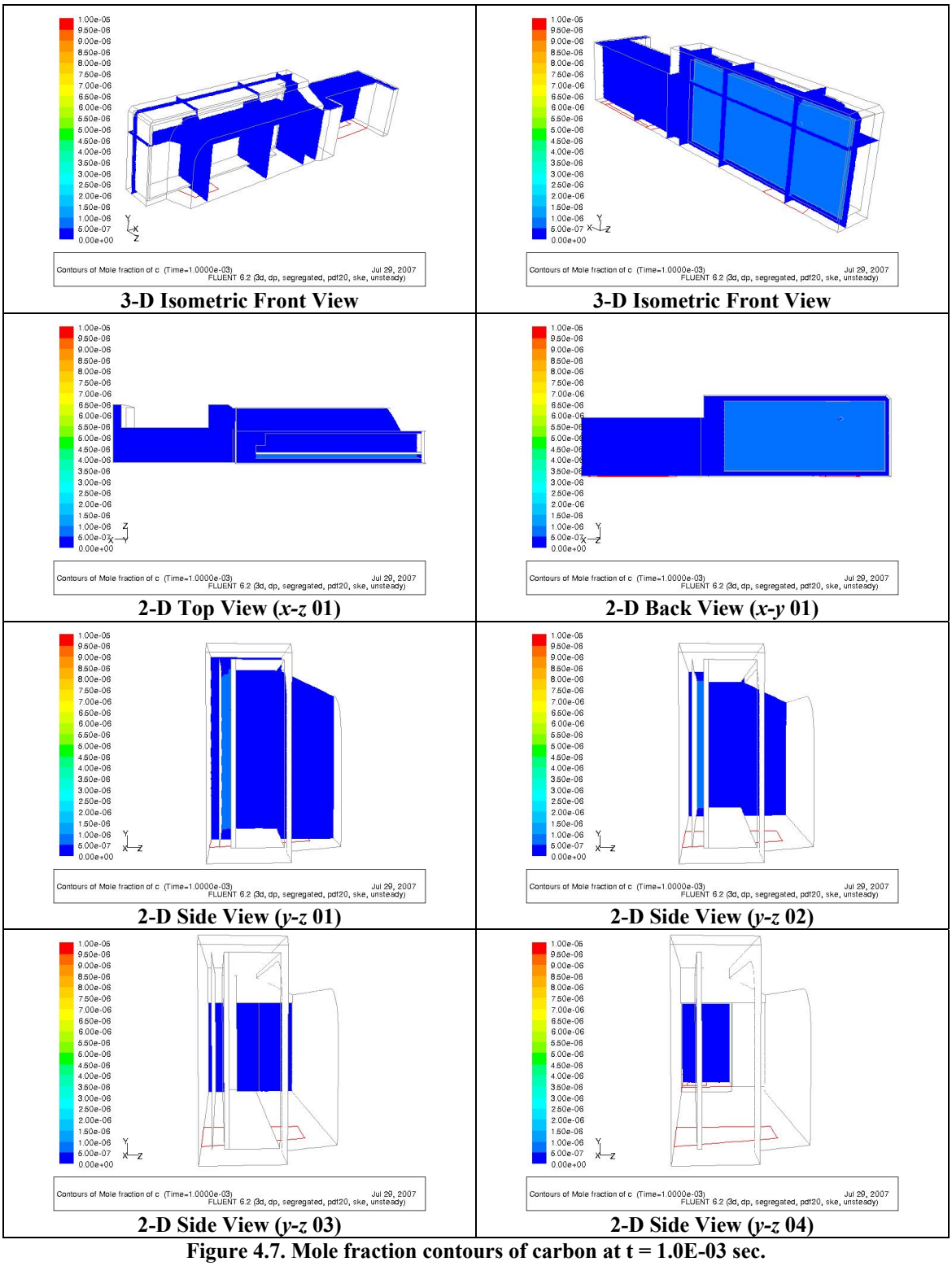

Figure 4.7. Mole fraction contours of carbon at t = 1.0E-03 sec.

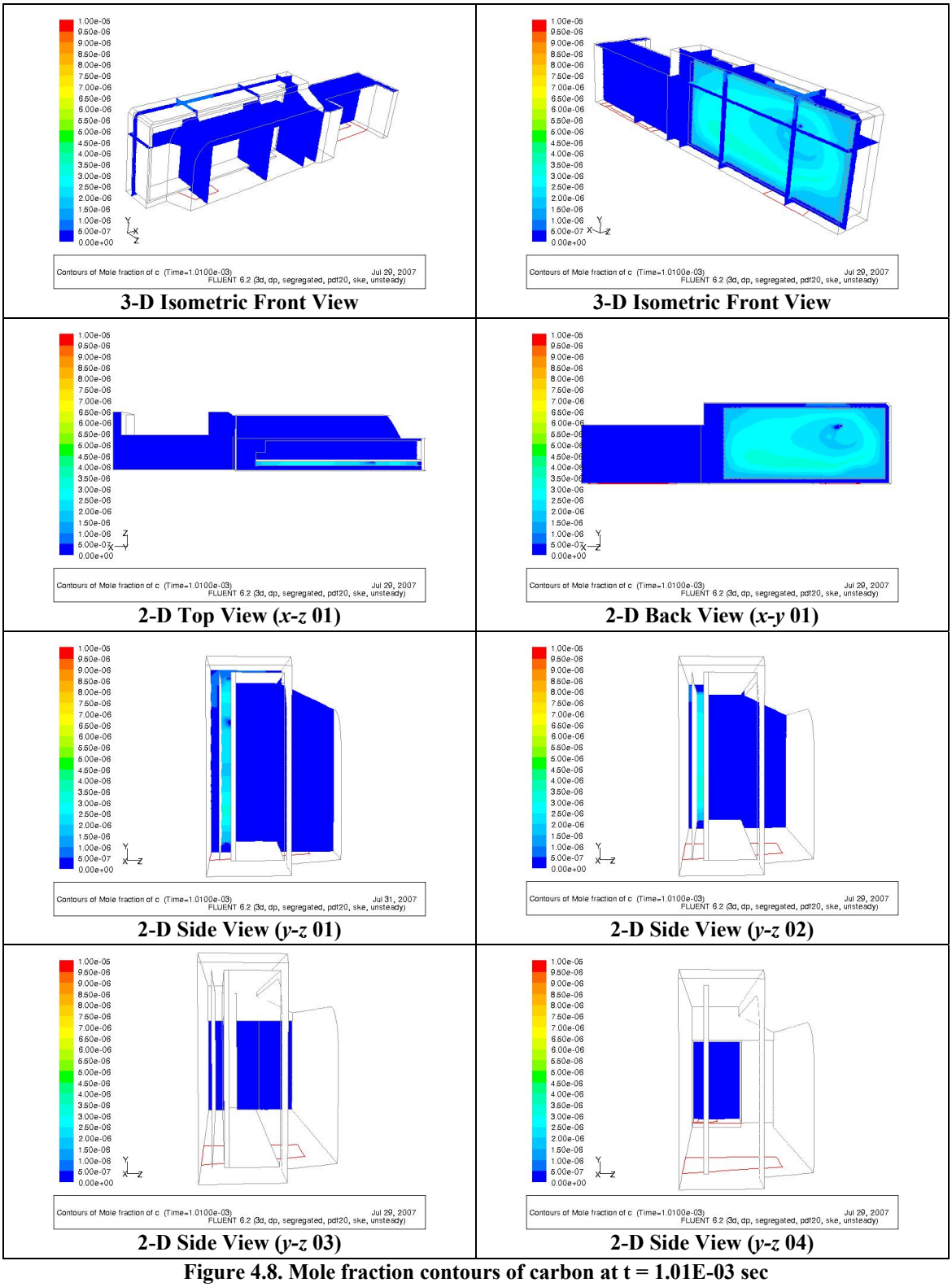

Figure 4.8. Mole fraction contours of carbon at t = 1.01E-03 sec

4.2.5 Temperature Profiles (First Simulation)

According to [23], solid coal char can ignite at 410 $^{\circ}$C (683K) and coal volatiles can ignite at 350 $^{\circ}$C (623K). Therefore, temperature profiles are used in conjunction with the progress variable, DPM burnout rate and mole fractions to determine the location of the flame. If the temperature is above the injection temperature of 350 K, has a progress variable greater than zero, and it producing CO or CO_2 then it is probable to assume a flame front. The first set of contour views was taken at 1 ms and indicated a uniform temperature of 350 K through entire control volume. The second set of contour views were taken at 10 μs after the spark ignition. The contour levels indicated a temperature spike at the ignition source with little or no propagation. The range of results for both sets of temperature contours is indicated from 350 – 700 K.

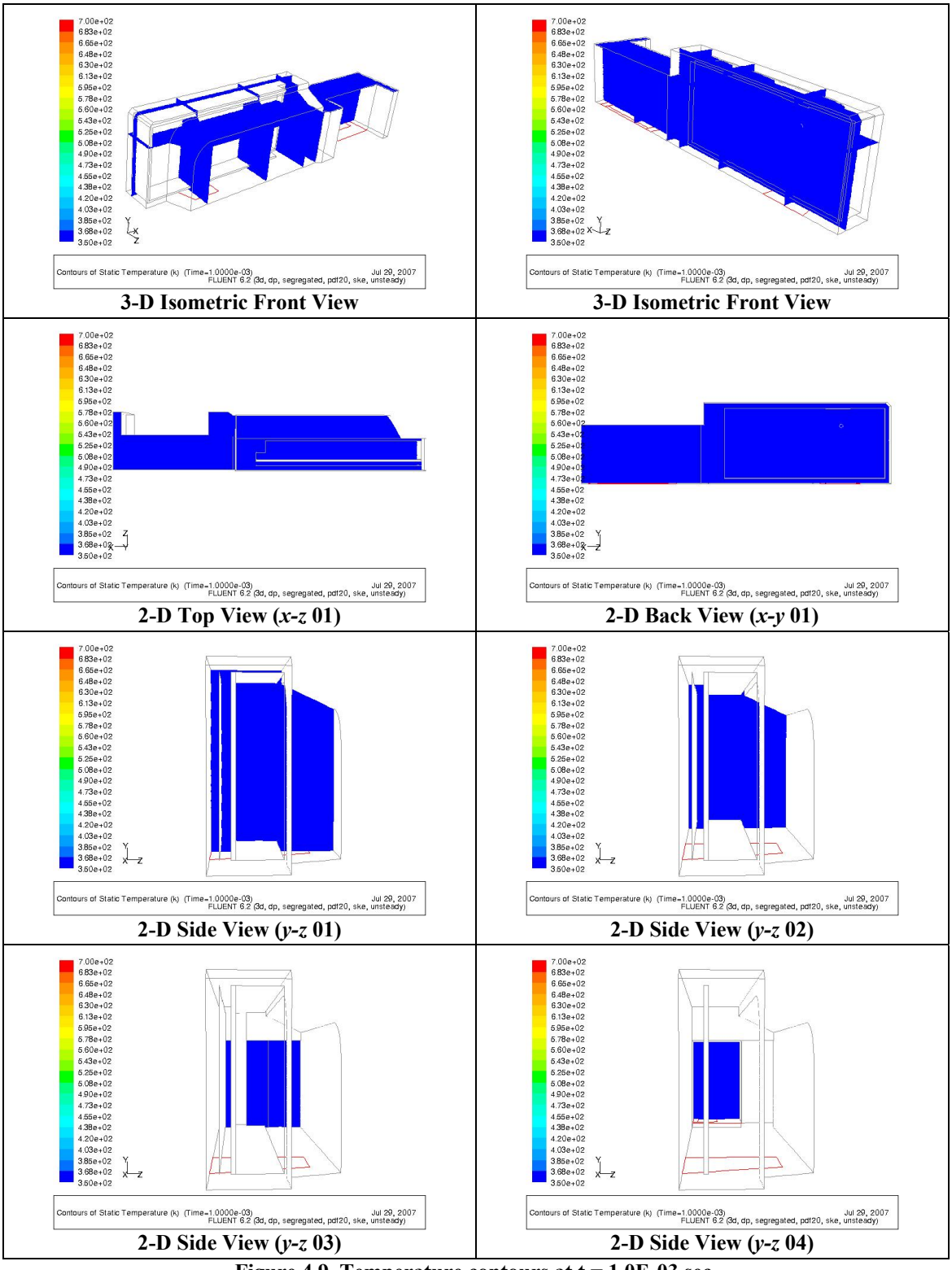

Figure 4.9. Temperature contours at t = 1.0E-03 sec.

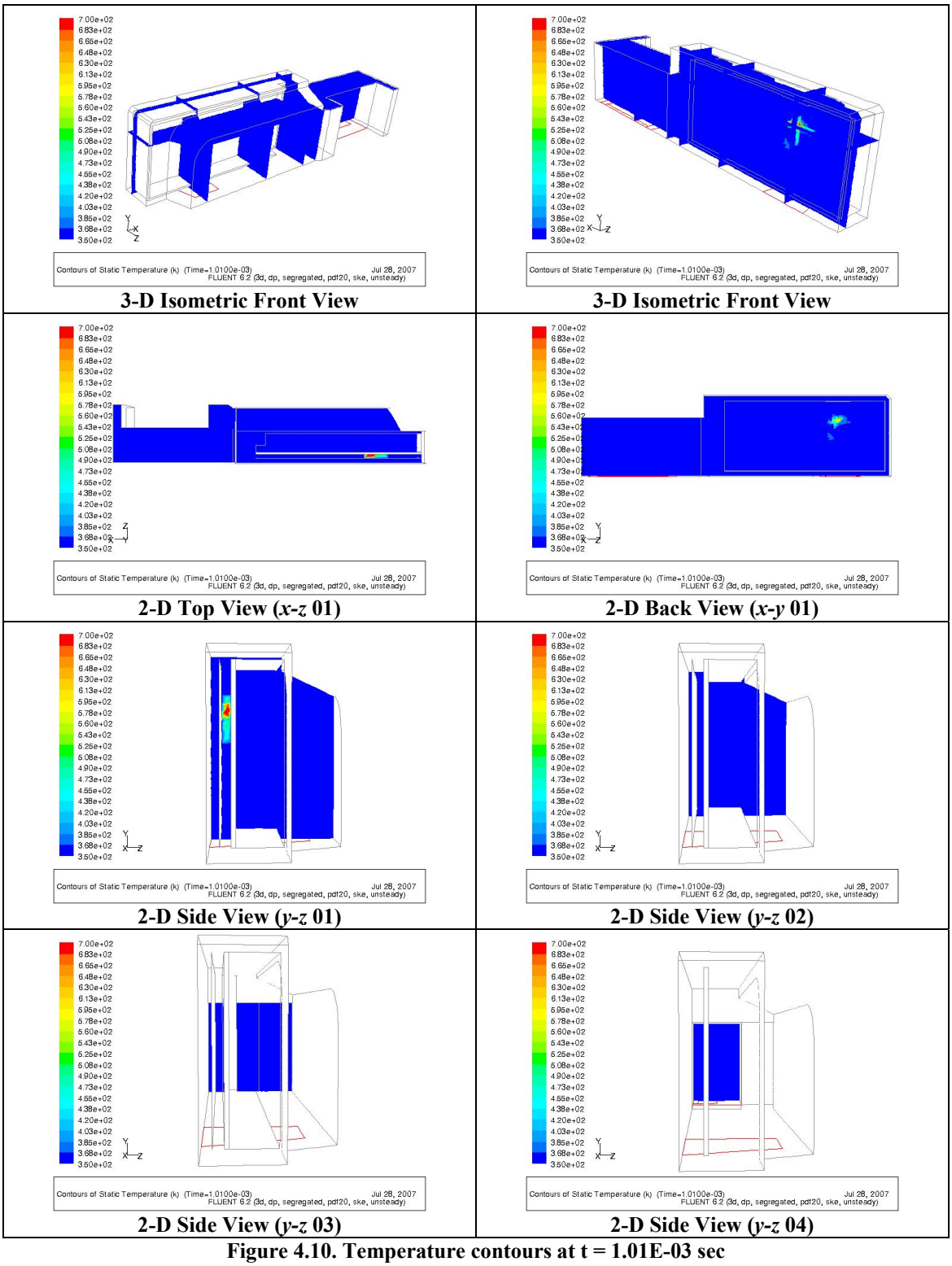

Figure 4.10. Temperature contours at t = 1.01E-03 sec

4.2.6 Reaction Progress Variable Contours (First Simulation)

The progress variable contour plots are a method of tracking the flame front propagation by the premixed transport equation (Equation 3.15). The variable ranges from 0 to 1 ($0 \le c \le 1$) depending on the burnt or unburnt species combination. When $c = 0$ the chemical reactions are inert and when $c = 1$ the reactions have gone to full completion. The products of a completely reacted system are calculated by the PDF function. The first set of contour views were taken 1 ms and indicated no reaction. The second set of contour views were taken at 10 μs after the spark ignition. The contour levels changed and showed the propagation of flame front away from the ignition source. The second set of contour views indicate the reaction between the gaseous constituents dominate the flow chemistry. The range of results for both sets of contours is indicated from 0 – 1 for the reaction progress variable.

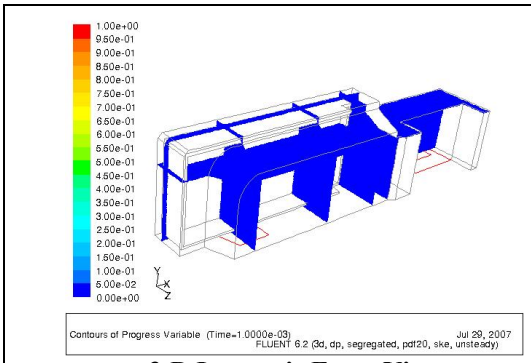

3-D Isometric Front View

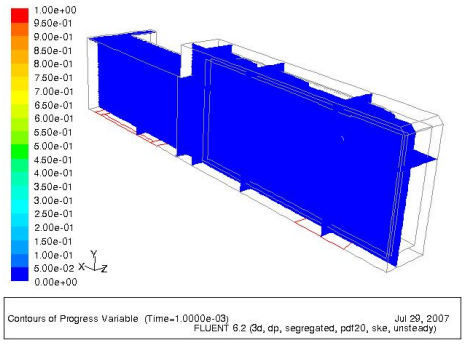

3-D Isometric Back View

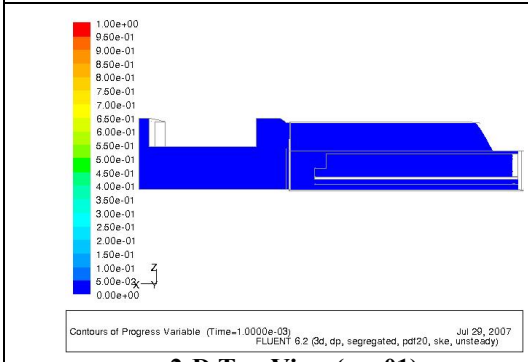

2-D Top View (*x-z* 01)

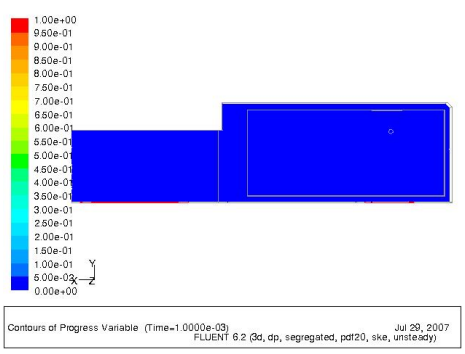

2-D Back View (*x-y* 01)

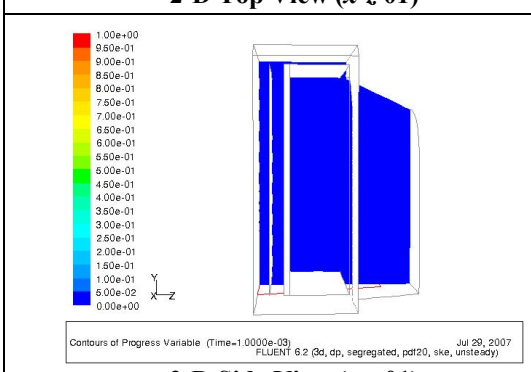

2-D Side View (*y-z* 01)

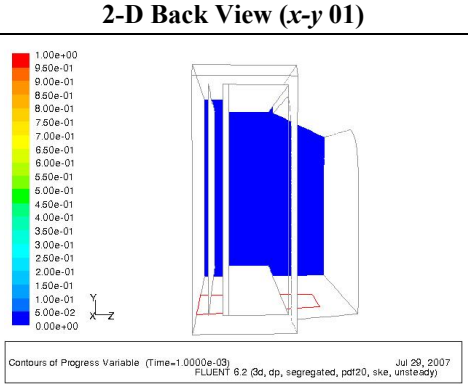

2-D Side View (*y-z* 02)

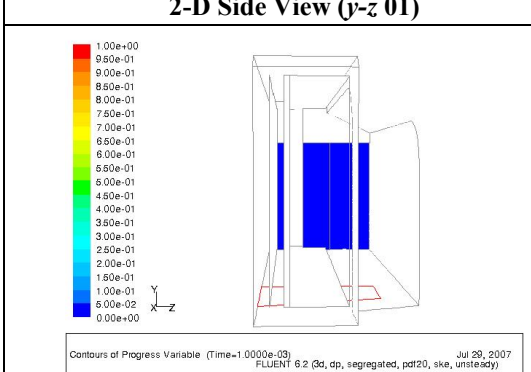

2-D Side View (*y-z* 03)

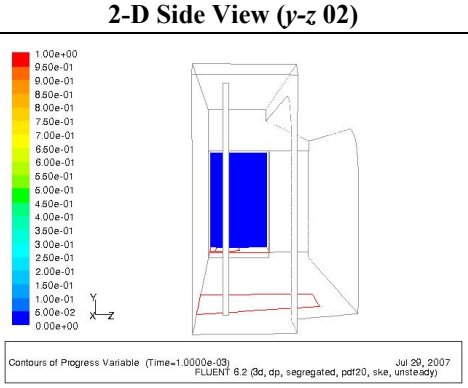

2-D Side View (*y-z* 04)

Figure 4.11. Reaction progress variable contours at t = 1.0E-03 sec.

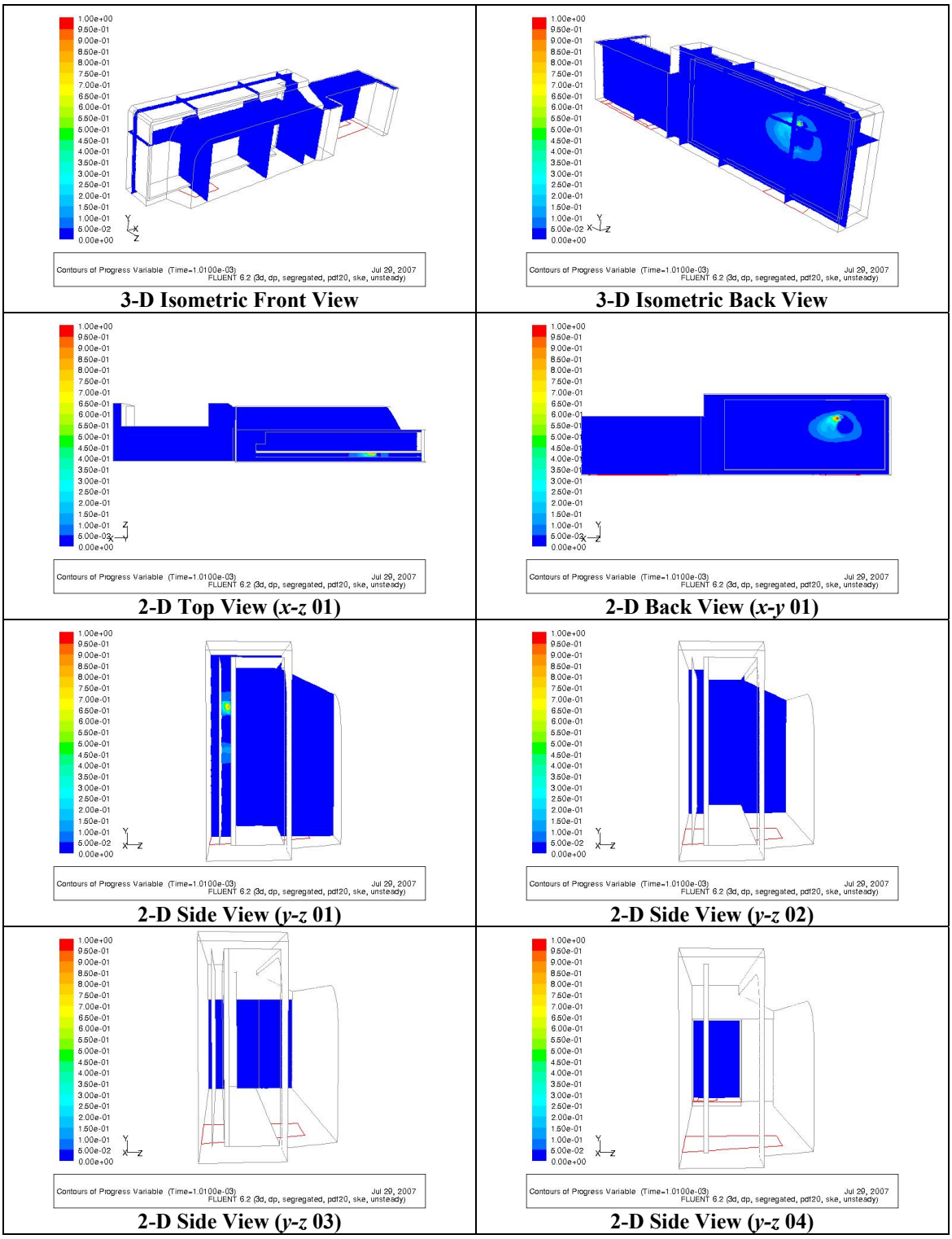

Figure 4.12. Reaction progress variable contours at t = 1.01E-03 sec

4.3 Description of Second Transient Analysis

The contours from the first transient analysis indicated that the numerical modeling was viable, but further analysis was needed to show more prominent results. The next simulation contained all of the same boundary conditions but the spark discharge was delayed until 10 ms which allowed for larger concentrations of fuel to be injected.

The following results are planar and isometric views of the second transient analysis. The same contour plots, view point and plane cuts were made for the second analysis as were for the first. Again, all eight contour plots represent one time step and only two time steps are shown for brevity. The second set of contour data were examined at the same time step after the spark (10 μs) as the first transient analysis.

4.3.1 Discrete Phase Model Char Burnout Rates (Second Simulation)

As previously stated in section 4.2.1, the DPM char burnout rate is an indication the solid char particles oxidizing. The following contour plots for the DPM burnout rate showed relatively more activity when compared to the first transient analysis. These differences are most notable around the ignition source. As with the first analysis, this was mainly attributed to the small amount of solid fuel that was present when the ignition spark occurred. The most notable contour changes are seen in the 3-D isometric back view and the 2-D top view (*x*-*z* 01), back view (*x*-*y* 01) and side view (*y*-*z* 01). The contour plot legend indicates a range of 0 – 4E-12 kg/s for the DPM burnouts rate.

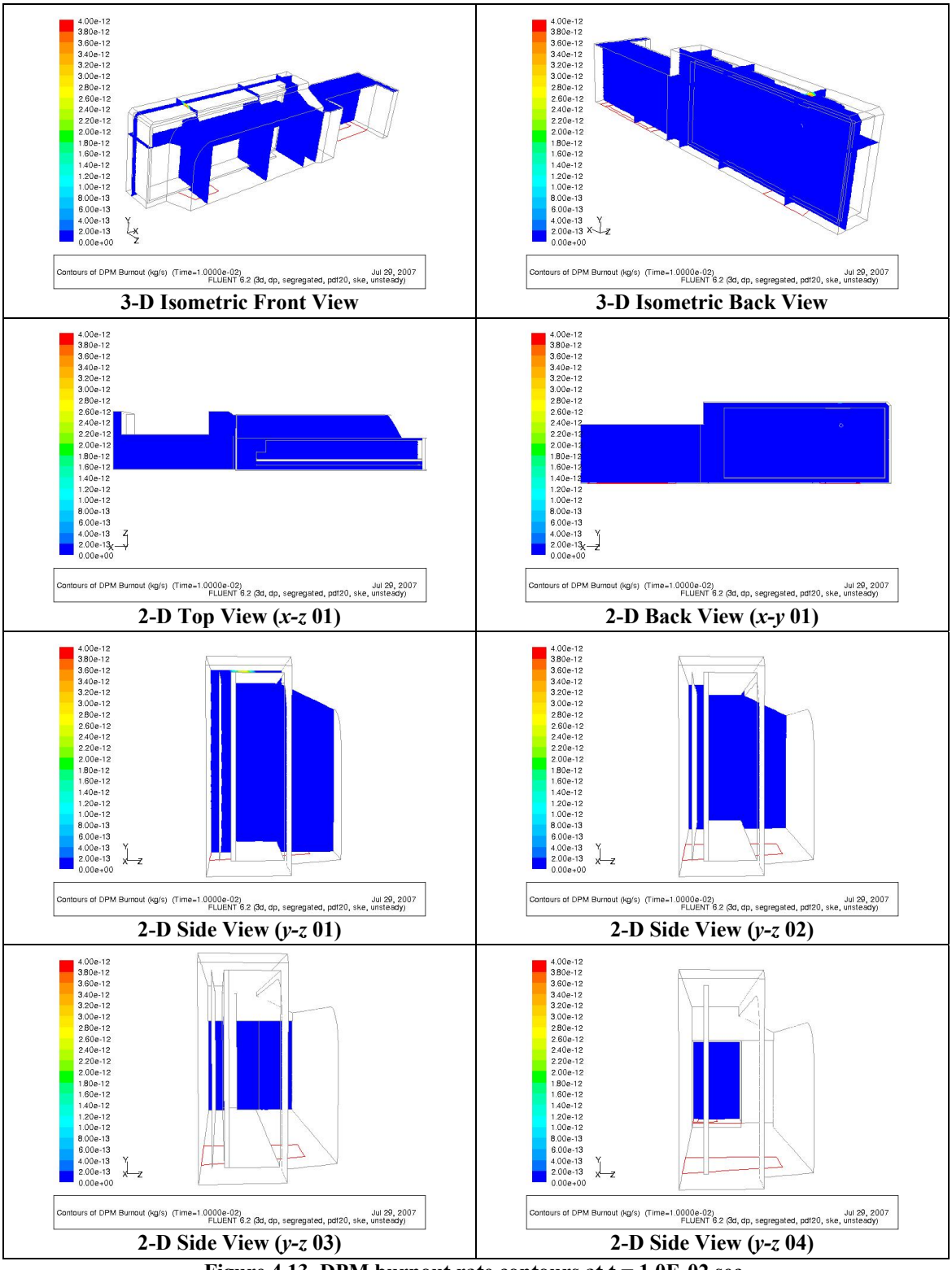

3-D Isometric Front View

3-D Isometric Back View

2-D Top View (*x-z* 01)

2-D Back View (*x-y* 01)

2-D Side View (*y-z* 01)

2-D Side View (*y-z* 02)

2-D Side View (*y-z* 03)

2-D Side View (*y-z* 04)

Figure 4.13. DPM burnout rate contours at t = 1.0E-02 sec.

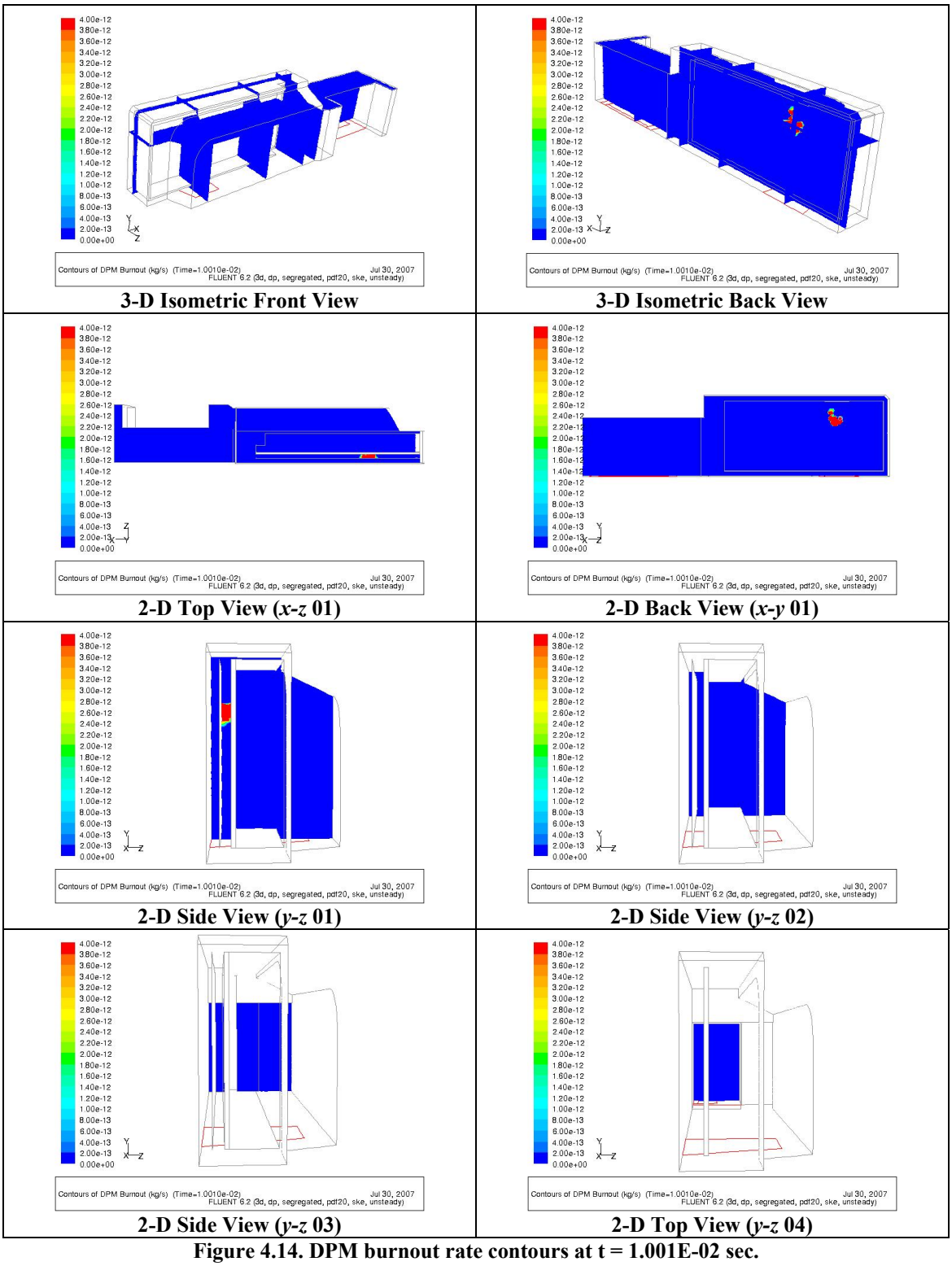

Figure 4.14. DPM burnout rate contours at t = 1.001E-02 sec.

4.3.2 Mole Fractions of Carbon Monoxide (Second Simulation)

As previously stated in section 4.2.2, hydrocarbon reactions, such as coal can yield two primary products. The carbon monoxide, more commonly associated with the char-oxidizer interaction, is shown in the next set of contours. Section 4.3.3 will highlight the evolution of the other primary product carbon dioxide.

The first set of contour views were taken at 10 ms and indicated no production of carbon monoxide. The second set of contour views were taken at 10 μs after the spark ignition. The range of results for both sets of contours is indicated from 0 – 1E-9 for the mole fraction of carbon monoxide

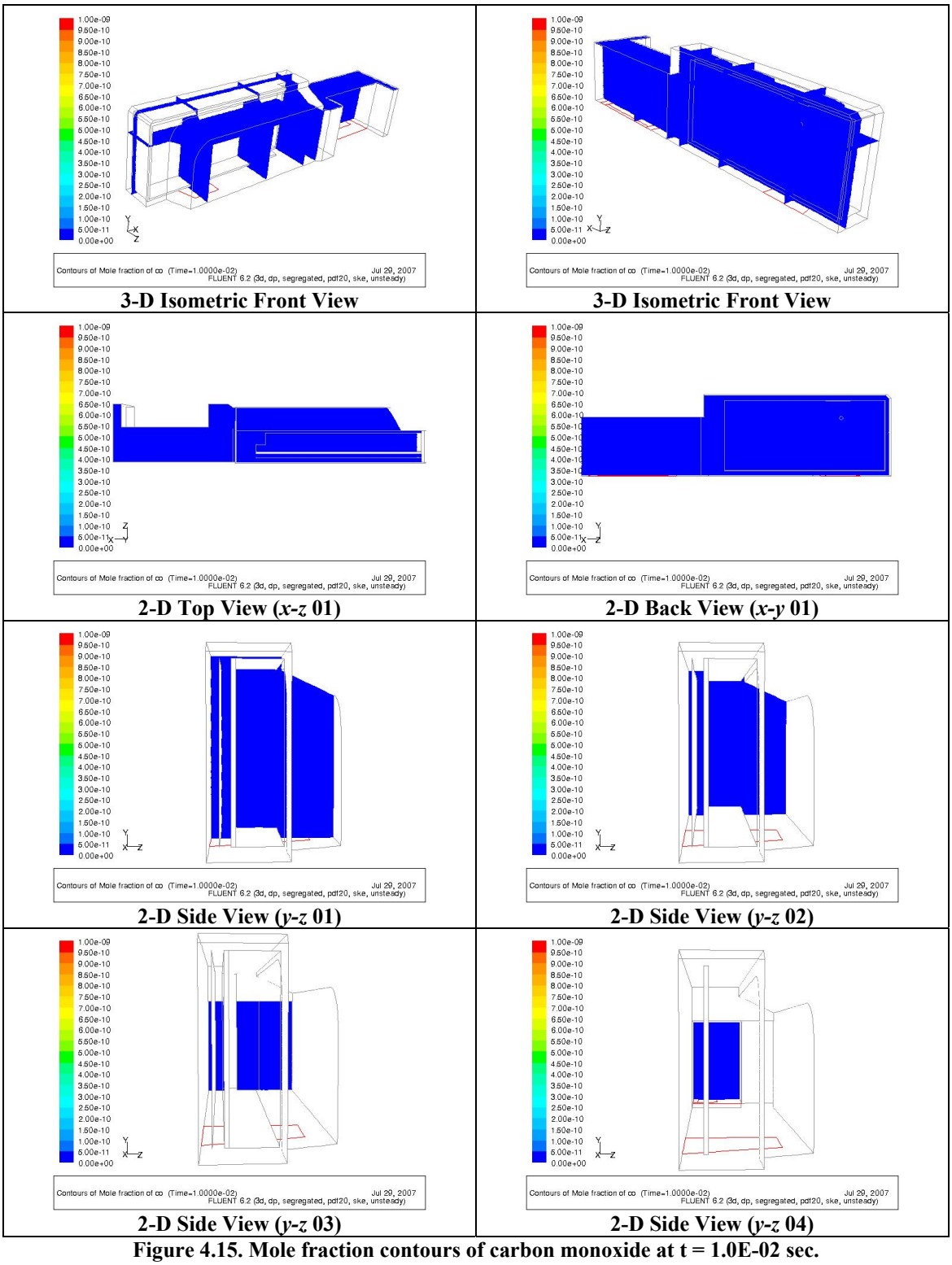

3-D Isometric Front View

3-D Isometric Front View

2-D Top View (*x-z* 01)

2-D Back View (*x-y* 01)

2-D Side View (*y-z* 01)

2-D Side View (*y-z* 02)

2-D Side View (*y-z* 03)

2-D Side View (*y-z* 04)

Figure 4.15. Mole fraction contours of carbon monoxide at t = 1.0E-02 sec.

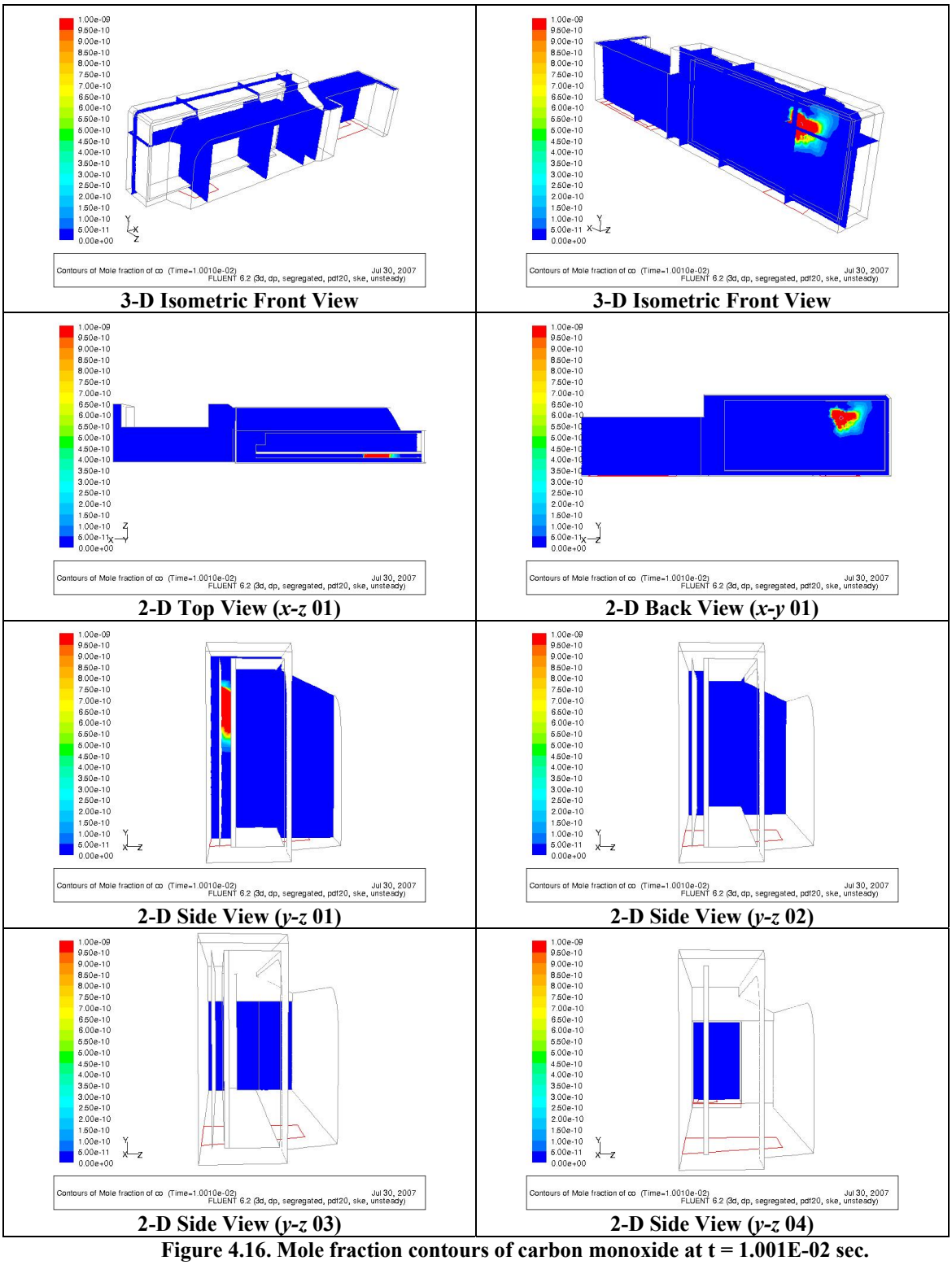

3-D Isometric Front View

3-D Isometric Front View

2-D Top View (*x-z* 01)

2-D Back View (*x-y* 01)

2-D Side View (*y-z* 01)

2-D Side View (*y-z* 02)

2-D Side View (*y-z* 03)

2-D Side View (*y-z* 04)

Figure 4.16. Mole fraction contours of carbon monoxide at t = 1.001E-02 sec.

4.3.3. Mole Fraction of Carbon Dioxide (Second Simulation)

As previously stated, the char-oxidizer yields two primary products. The second product, carbon dioxide was examined and showed higher mole fraction concentrations. The first set of contour views were taken at 10 ms and indicated no production of carbon dioxide. The second set of contour views were taken at 10 μs after the spark ignition. The range of results for both sets of contours is indicated from 0 – 1E-6 for the mole fraction of carbon dioxide.

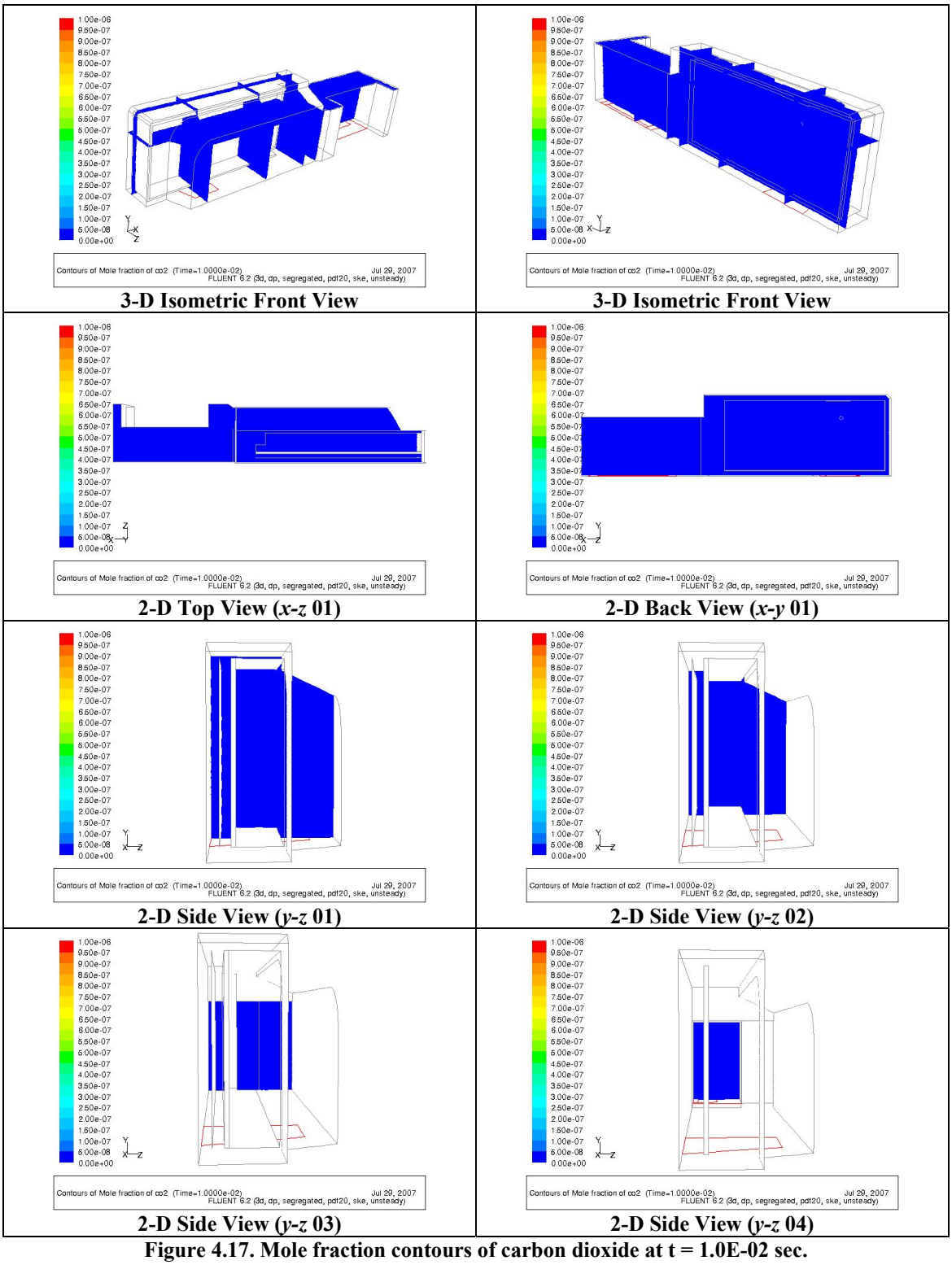

3-D Isometric Front View | 3-D Isometric Front View

2-D Top View (*x-z* 01) | 2-D Back View (*x-y* 01)

2-D Side View (*y-z* 01) | 2-D Side View (*y-z* 02)

2-D Side View (*y-z* 03) | 2-D Side View (*y-z* 04)

Figure 4.17. Mole fraction contours of carbon dioxide at t = 1.0E-02 sec.

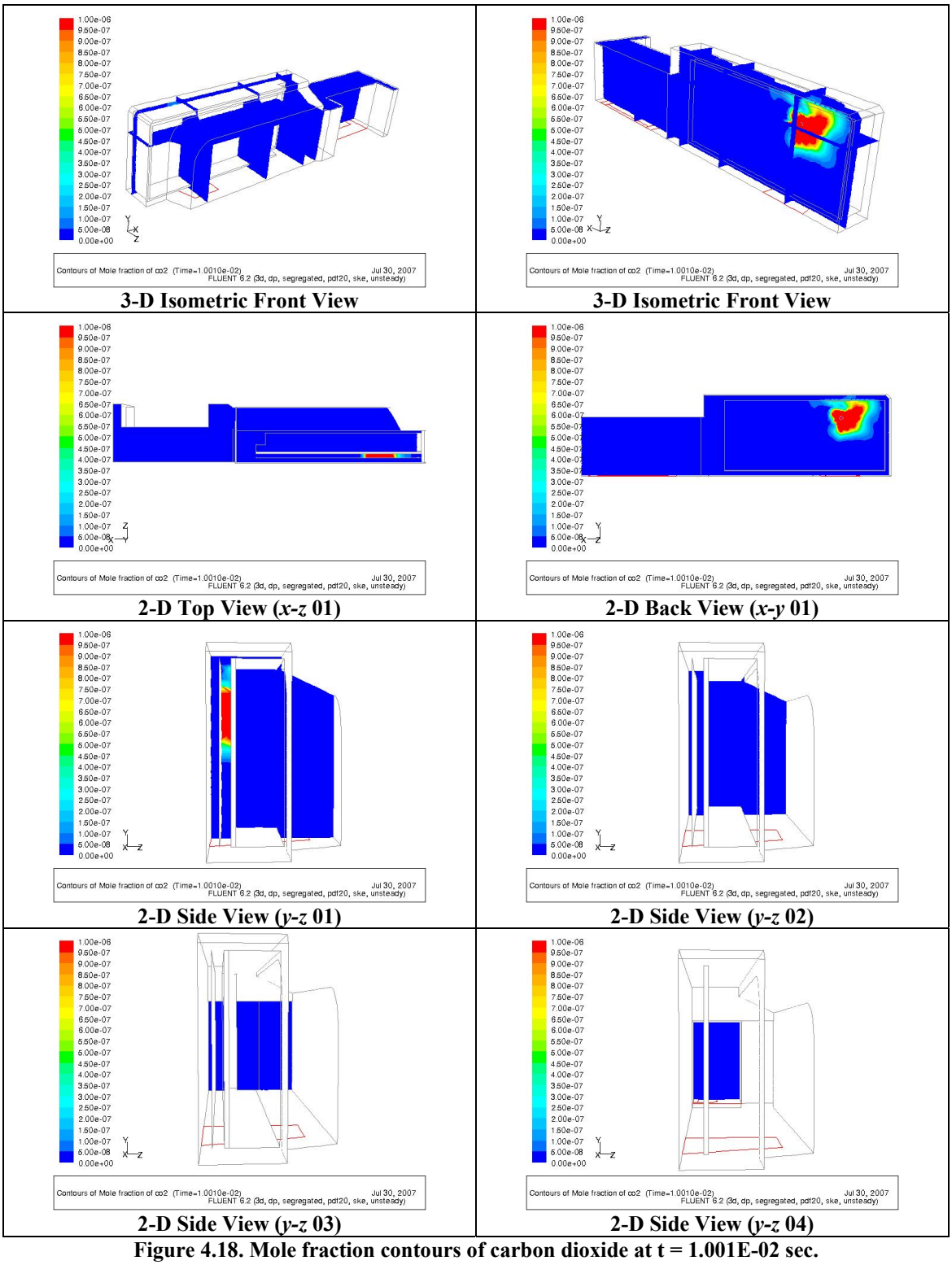

3-D Isometric Front View | **3-D Isometric Front View**

2-D Top View (*x-z* 01) | **2-D Back View (*x-y* 01)**

2-D Side View (*y-z* 01) | **2-D Side View (*y-z* 02)**

2-D Side View (*y-z* 03) | **2-D Side View (*y-z* 04)**

Figure 4.18. Mole fraction contours of carbon dioxide at t = 1.001E-02 sec.

4.3.4 Mole Fractions of Carbon (Second Simulation)

Even though more solid fuel was injected for the second transient analysis, the DPM burnout rate and mole fraction contours indicated the oxidization of solid carbon was not the prominent reaction. As shown from the above DPM burnout rate and mole fraction contours for the second transient analysis, a reaction does occur. It was therefore assumed the gaseous carbon was the main source of fuel for the oxidization process.

The carbon contours are shown for visual reference of the dispersion of the gaseous volatiles within the control volume. The first set of contour views were taken at 10 ms and indicated carbon was dispersed throughout much more of the control volume than the first transient analysis. The second set of contour views were taken at 10 μs after the spark ignition. Similar to the first analysis, the dark blue spot located at the ignition point indicates the oxidization of carbon. The range of results for both sets of contours is indicated from 0 – 1E-5 for the mole fraction of carbon

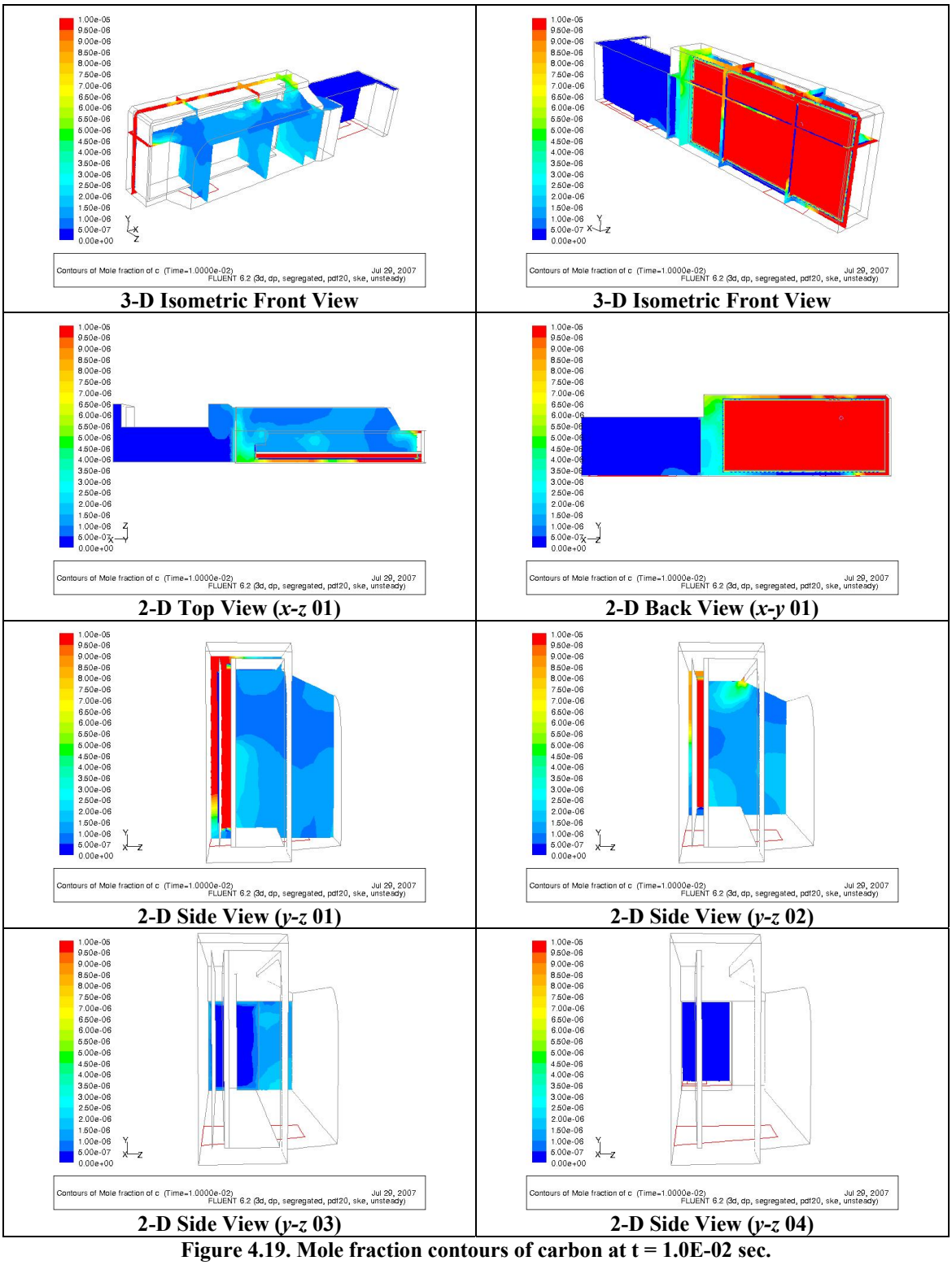

Figure 4.19. Mole fraction contours of carbon at t = 1.0E-02 sec.

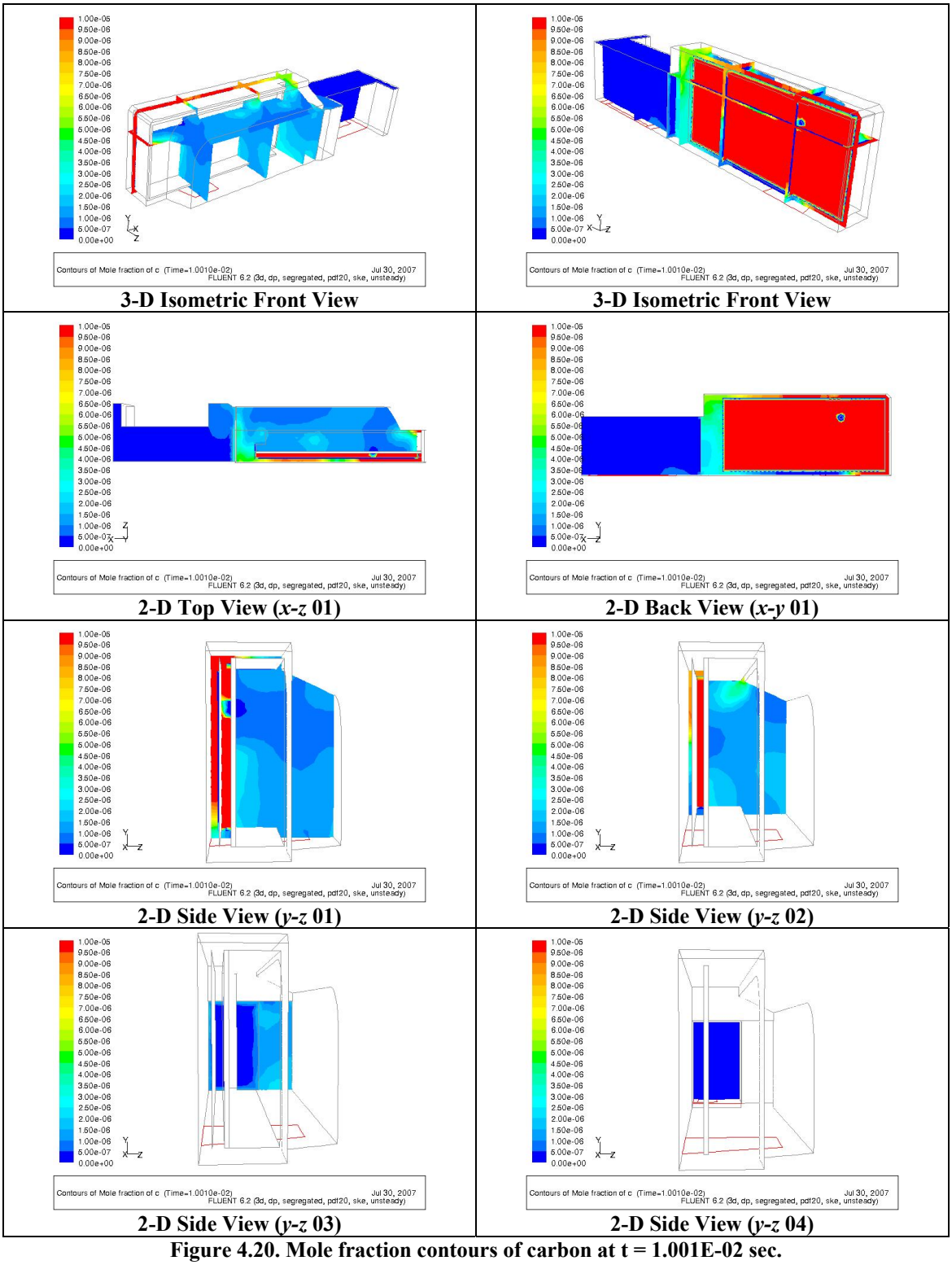

Figure 4.20. Mole fraction contours of carbon at t = 1.001E-02 sec.

4.3.5 Temperature Profiles (Second Simulation)

As previously stated in section 4.2.5, solid coal char can ignite at 410 $^{\circ}$C (683K) and coal volatiles can ignite at 350 $^{\circ}$C (623K). Therefore, temperature profiles are used in conjunction with the progress variable, DPM burnout rate and mole fractions to determine the location of the flame. If the temperature is above the injection temperature (350 K), has a progress variable greater than zero, and it producing CO or CO_2 then it is probable to assume a flame front. The first set of contour views was taken at 10 ms and indicated a uniform temperature of 350 K through entire control volume. The second set of contour views were taken at 10 μs after the spark ignition. The contour levels show a temperature spike at the ignition source. However, the propagation appears to be on both sides of the PCB panel. It was assumed that a large enough molar concentration of carbon is present on both side of the board to cause a reaction. Additionally, the spark energy was transmitted to the flow through conjugate heat transfer (a coupling of conduction and convection heat transfer) to initiate combustion on the reverse side. The range of results for both sets of temperature contours is indicated from 350 –700 K.

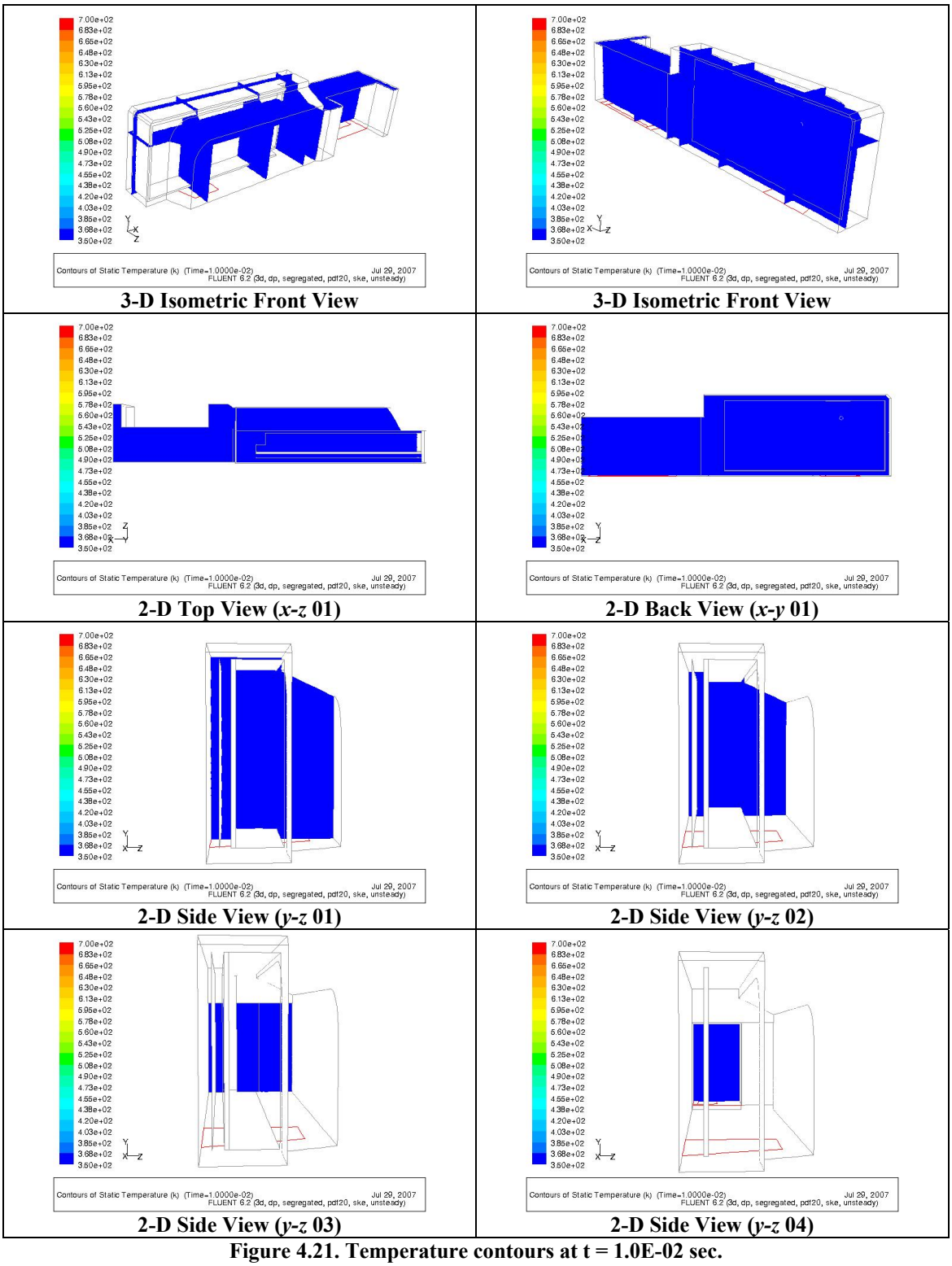

Figure 4.21. Temperature contours at t = 1.0E-02 sec.

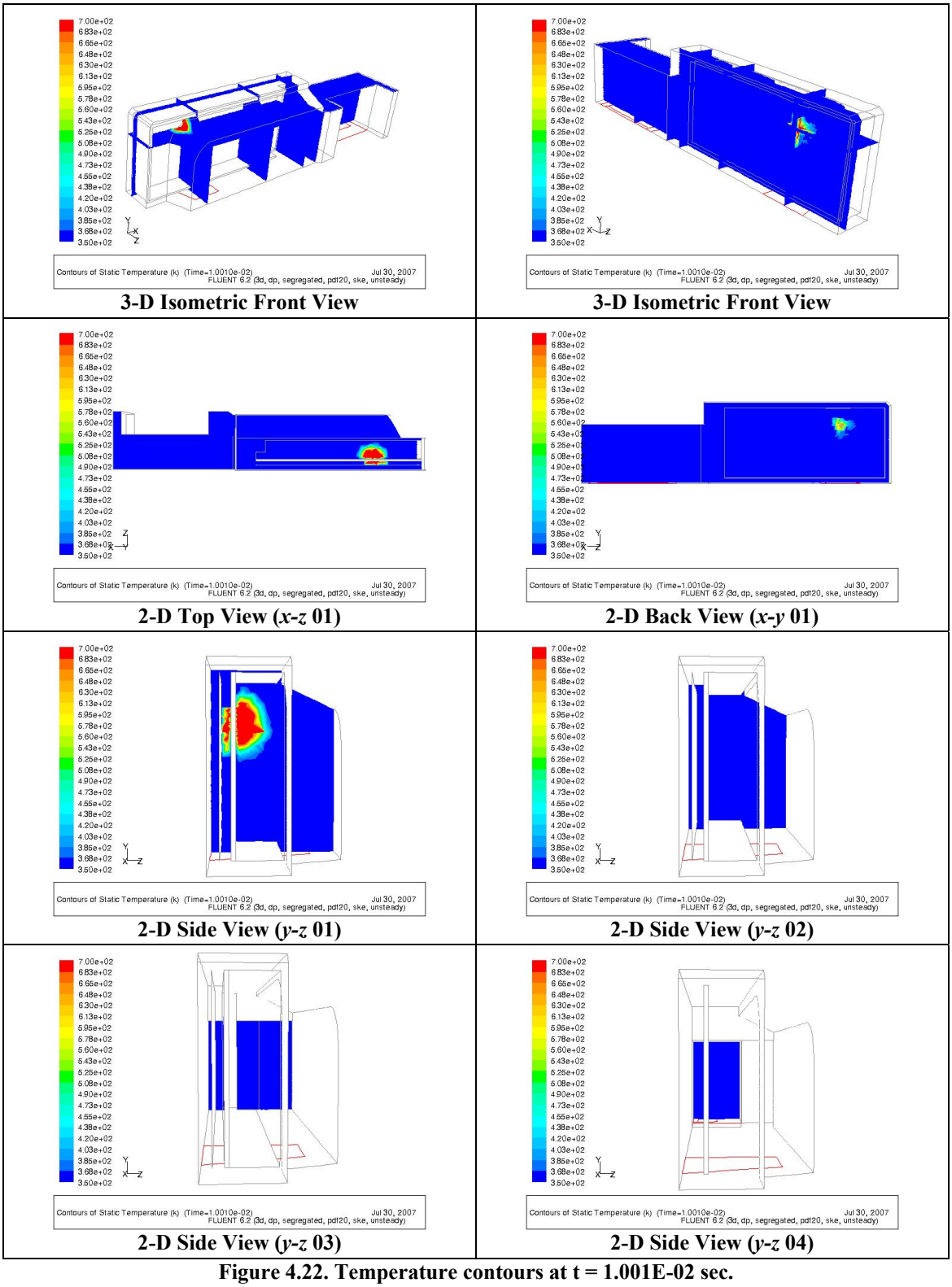

Figure 4.22. Temperature contours at t = 1.001E-02 sec.

4.3.6 Reaction Progress Variable Contours (Second Simulation)

As previously described in section 4.2.6, the progress variable contour plots are a method of tracking the flame front propagation by the premixed transport equation (Equation 3.15). The variable ranges from 0 to 1 ($0 \le c \le 1$) depending on the burnt or unburnt species combination. When $c = 0$ the chemical reactions are inert and when $c = 1$ the reactions have gone to full completion. The products of a completely reacted system are calculated by the PDF function. The first set of contour views were taken at 10 ms and indicated no reaction through the control volume. The second set of contour views were taken at 10 μs after the spark ignition. When compared to the first transient analysis, the contour levels indicate a much stronger reaction by the greater concentration of burnt species around the ignition source. Similarly, the contours also indicate the gaseous fuel dominate the reactions. The range of results for both sets of contours is indicated from 0 – 1 for the progress variable.

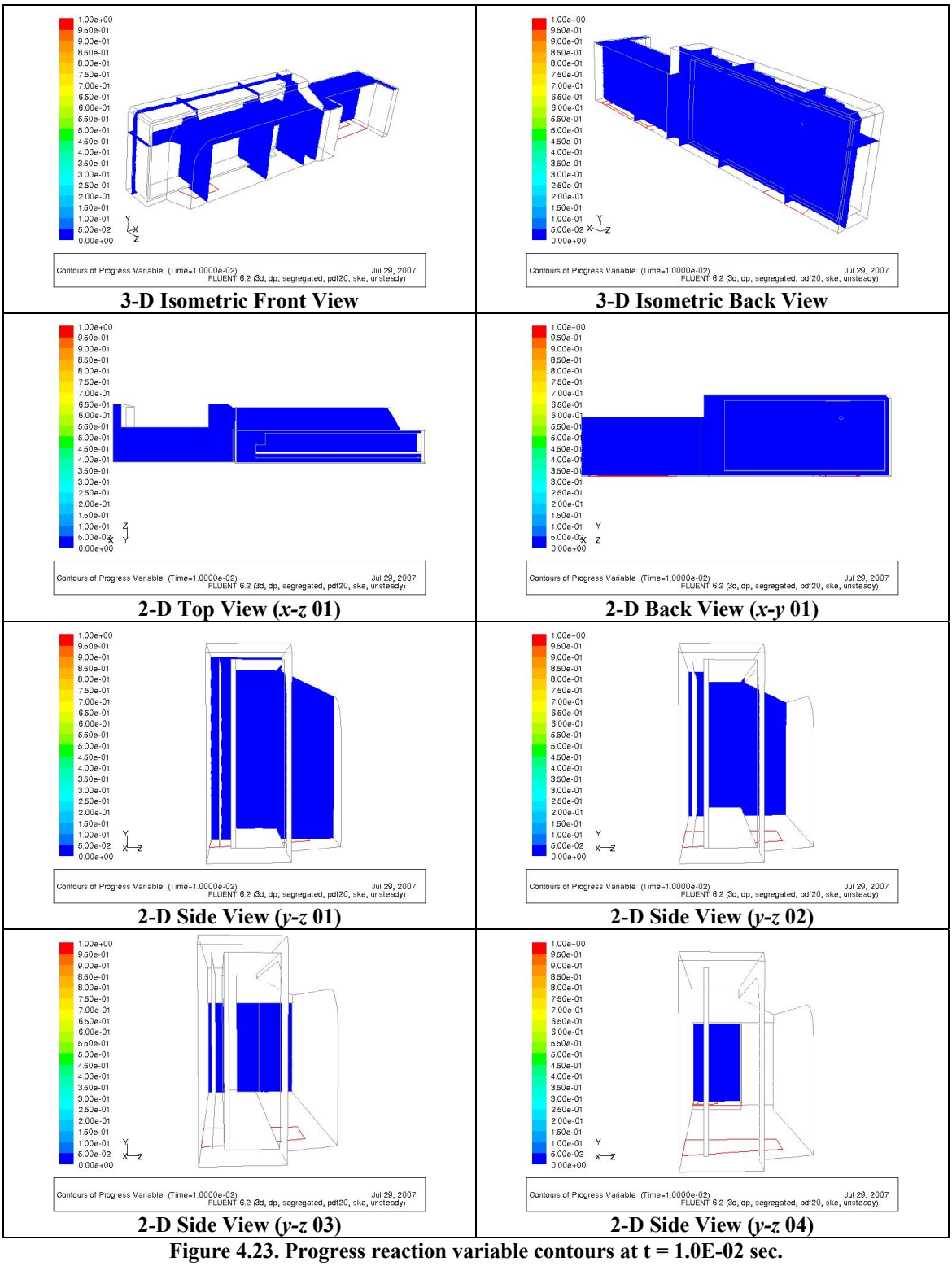

3-D Isometric Front View

3-D Isometric Back View

2-D Top View (*x-z* 01)

2-D Back View (*x-y* 01)

2-D Side View (*y-z* 01)

2-D Side View (*y-z* 02)

2-D Side View (*y-z* 03)

2-D Side View (*y-z* 04)

Figure 4.23. Progress reaction variable contours at t = 1.0E-02 sec.

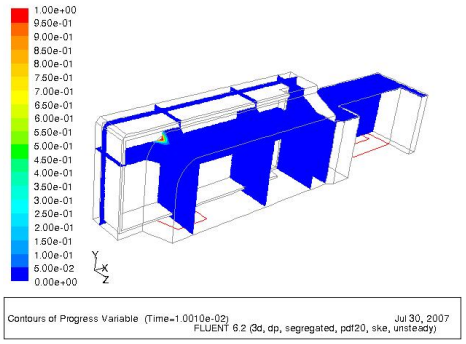

3-D Isometric Front View

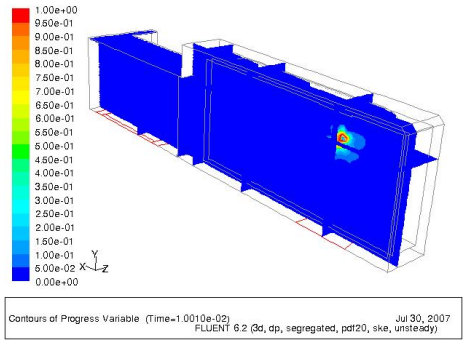

3-D Isometric Back View

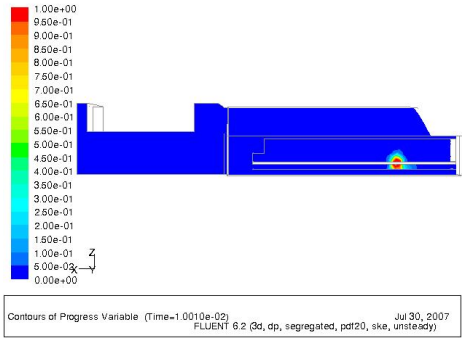

2-D Top View (*x-z* 01)

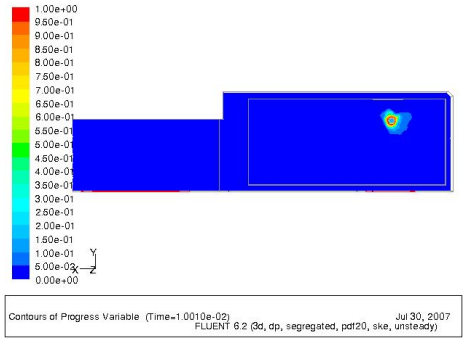

2-D Back View (*x-y* 01)

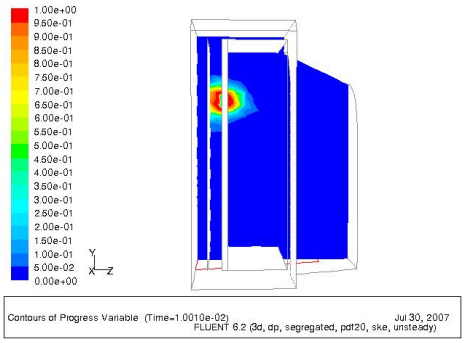

2-D Side View (*y-z* 01)

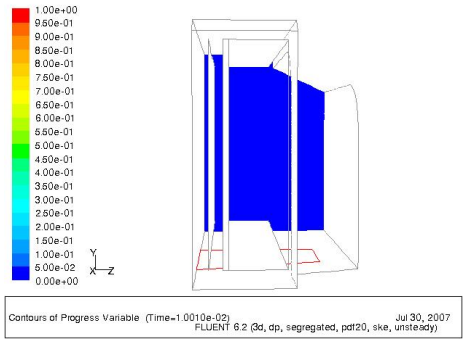

2-D Side View (*y-z* 02)

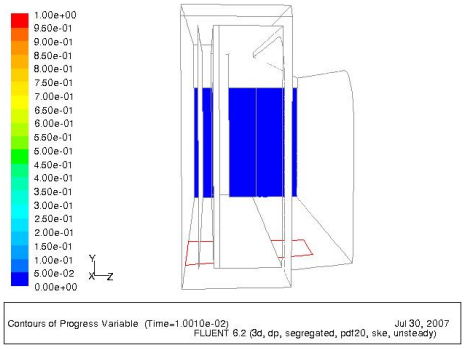

2-D Side View (*y-z* 03)

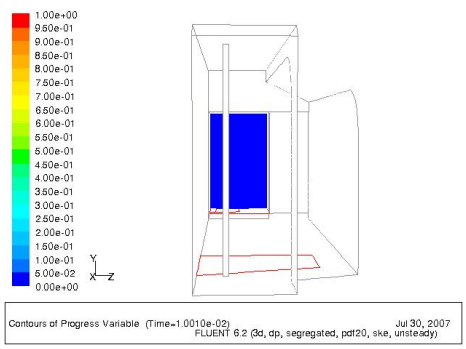

2-D Side View (*y-z* 04)

Figure 4.24. Progress reaction variable contours at t = 1.001E-02 sec.

4.4 Discussion of Results

The data above showed the flame front propagation and general characteristics of the flow at discrete time steps. The contour levels served as a visual aid indicated the range of results, but did not allow for detailed analysis of the data. Further analysis was conducted and is shown as volume-weighted averages. According to [22], this method of data reduction is used to obtain a volume average of mass sources, energy sources or discrete-phase exchange of quantities. Conventional inlet-to-exit approaches used for 2-D or axisymmetric cases will not work for the 3-D nonsymmetric geometry. Additional single point analysis does not offer a broad perspective of the flow characteristics. Therefore, the volume-weighted average was chosen to significantly reduce the number of data points.

In order to establish the validity of the flame propagation, several volume averaged data were used to define the flame front based on chemical reaction products. The data shown in the next section were extracted from the second transient analysis. Molar concentrations of the fuel and char reactants were higher from this simulation than the first, which made for easier analysis of the chemical reactions.

Reference [23] describes a flame as a thin region of rapid exothermic chemical reactions, that is, the flame front is the separation between the products and reactant of the chemical reaction. The control volume used for the simulation initially had a 78.89% nitrogen and 21.01% oxygen mixture to simulate an air atmosphere. The mole fraction of the reactants injected into the control volume did of course increase over

time, however, it is the interaction between all species that was the primary focus for the analysis. As an example, consider the formation of carbon monoxide:

$$C_{(s)} + \frac{1}{2}O_{2(g)} \xrightarrow{298.15\,K} CO_{(g)} - 94.05\ \text{kcal} \tag{4.2}$$

The transient system under consideration is 3-D and could not be analyzed from one specific point. Since the entire system was based on equilibrium reactions a volumetric analysis was used. Referring to Equation (4.2), a decrease in the volume-weighted mole fraction either reactant, would increase the volume-weighted mole fraction of the product. Figure 4.25 validates this statement by showing several reactions over the duration of the spark.

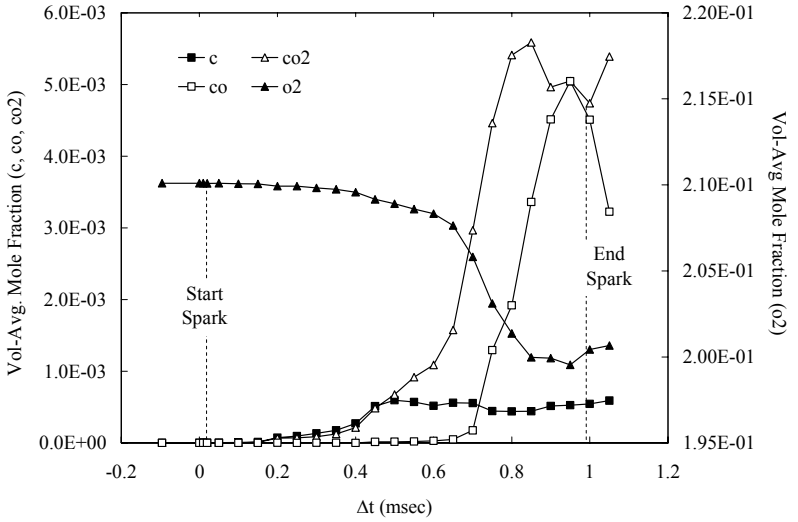

Figure 4.25. Volume-averaged mole fractions of C, CO, CO_2 and O_2 (second transient analysis).

The mole fractions from Figure 4.25 can be added together for each indicated time step to achieve an approximate value of 0.2101 (or 21.01% of total molar species). This indicates that all diatomic oxygen in the system reacted with the gaseous carbon to

form either carbon monoxide or carbon dioxide. However, the number is only approximately equal to 0.2101 and does not account for other reactions that are many orders of magnitude smaller.

According to [23], there are three basic processes for coal combustion. These are as follows.

1) Drying of solid fuel
2) Devolatilization of the solid fuel
3) Char combustion, which comprises of

a. $C_{(s)} + \frac{1}{2} O_{2(g)} \Leftrightarrow CO_{(g)}$

b. $CO_{(g)} + \frac{1}{2} O_{2(g)} \Leftrightarrow CO_{2(g)}$

c. $C_{(s)} + CO_{2(g)} \Leftrightarrow 2CO_{(g)}$

Step 1 was ignored because the coal was assumed to be dry. Step 2 can be ignored because the coal volatilization temperature was set to the same temperature of the injection (350 K). The third step is the most important.

During the third step, namely, char combustion, the products and reactants were traced by the volume-averaged analysis as seen in Figure 4.25. Generally reaction (a) is the most prominent for coal combustion [23]. However, the present results shown in Figure 4.26 indicated that solid carbon did not have a distinguishable connection to the diatomic oxygen reaction. For most of the spark time, the solid carbon mole fraction was between 1E-13 to 1E-11. This was eight to ten orders of magnitude smaller than the rest of the predominant reactions show in Figure 4.25. It is therefore assumed that char

combustion did occur, as was evident by the DPM burnout rate and temperature contour plots, but in was not dominant due to the relatively small amount of solid carbon injected into the control volume.

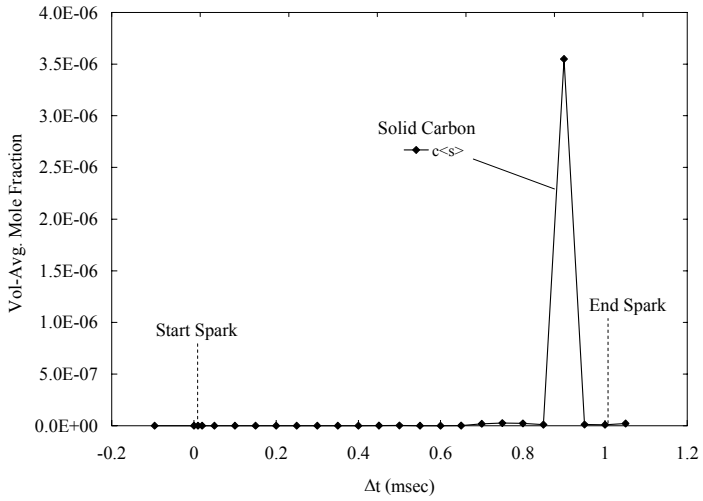

Figure 4.26. Volume-averaged mole fraction of solid carbon during spark duration.

Reaction (a) of the char combustion is also the reaction used to track the discrete phase model (DPM) burnout rate [24]. Figure 4.27 shows the volume-averaged DPM burnout rate with the volume-average mole fraction of the solid carbon over the duration of the spark. With the exception of the data point at 0.9 ms, the two variables have similar behavior. Overall, it was assumed that the DPM was able to track the reactions of solid carbon even though the mass injected was extremely small.

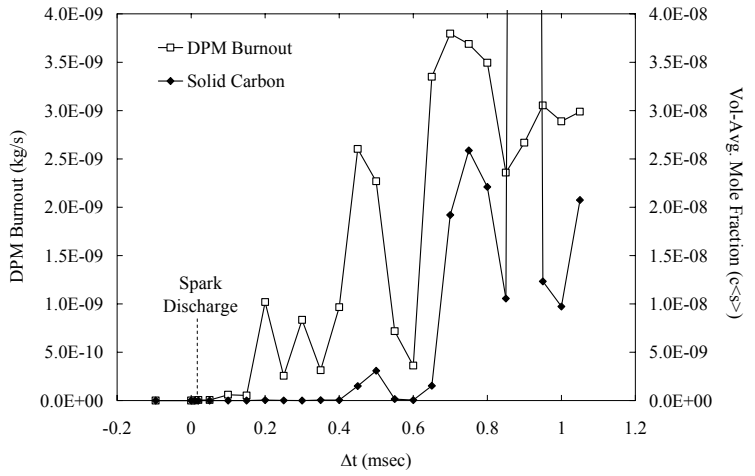

Figure 4.27. DPM burnout rate with vol-avg. mole fraction of solid carbon.

Assuming a constant pressure control volume with predominant reactions in the gas phase, it can be stated the specific heats for the fuel and oxidizer are constant. Using a calorically perfect gas assumption, the enthalpy is a function of specific heat and temperature. Therefore, any reaction that causes a change in temperature will have a direct relationship to the enthalpy. Figure 4.28 verified the relationship between the two variables and also indicates the flow is dominated by gas phase constituents.

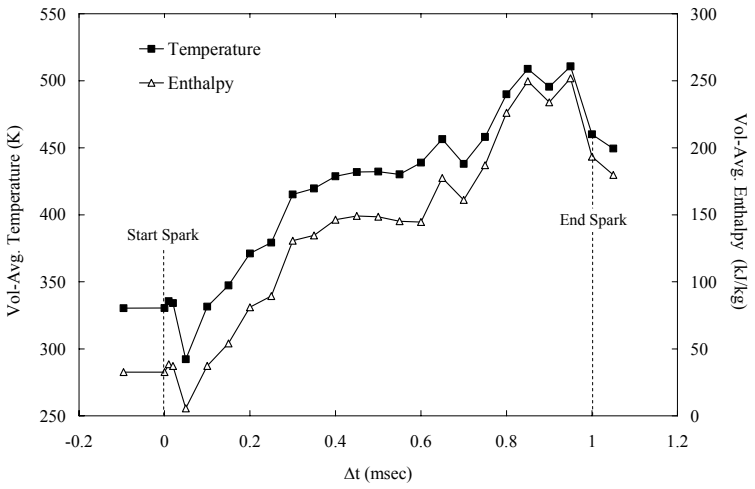

Figure 4.28. Volume-averaged temperature and enthalpy versus Δt.

Another very interesting phenomenon was the progress reaction variable. The basic definition of the progress variable is the combination of the reactants/products to create an unburnt/burnt mixture. Figure 4.29 shows a rapid rise in the volume-averaged progress variable at 0.1 ms after the initiation of the spark. It is assumed, at this time step in sharp rise in the progress variable indicates the chemical energy of the reaction has overcome the input energy of the ignition spark [23]. Additionally, the jump of burnt reactants from Δt=0.01 ms to Δt=0.1 ms is assumed to be further indication a flame. Overall, Figure 4.29 shows the successful ignition of a flame by spark discharge, through the volume-averaged progress variable.

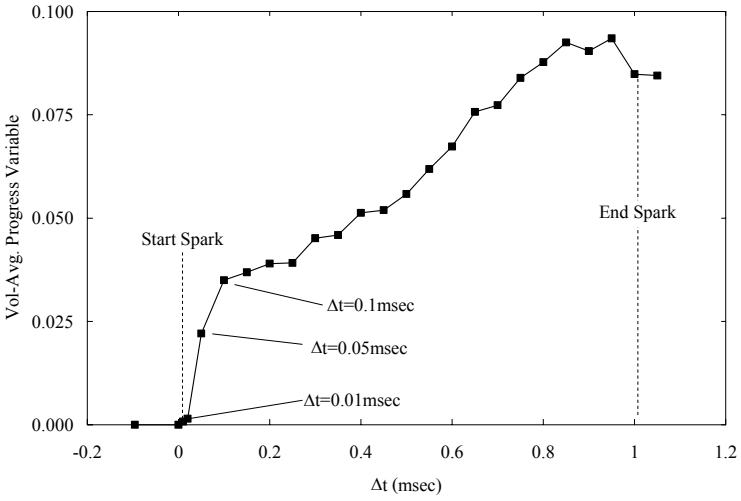

Figure 4.29. Volume-averaged progress variables versus Δt.

Additional visualization of the above results is show in Figure 4.30. Figure 4.30 (a) shows the 2-D back view (*x*-*y* plane) before the spark initiation. Figure 4.30 (b) shows the first time step, 10 μs, after the spark ignition and is denoted in Figure 4.29. A progress reaction variable of one is concentrated around the spark ignition site.

According to previous theory mentioned in [23] this indicates the spark energy is dominating flow reactions. Figure 4.30 (c) shows the progress reaction variable contours at 50 μs after the spark initiation. The time step is also denoted in Figure 4.29 and is first sharp rise in the progress variable indicating the chemical energy of the reaction is overcoming the input energy. Figure 4.30 (d) shows the progress reaction variable of one is no longer concentrated around the spark ignition site and the energy released by the fuel is dominating the progress variable.

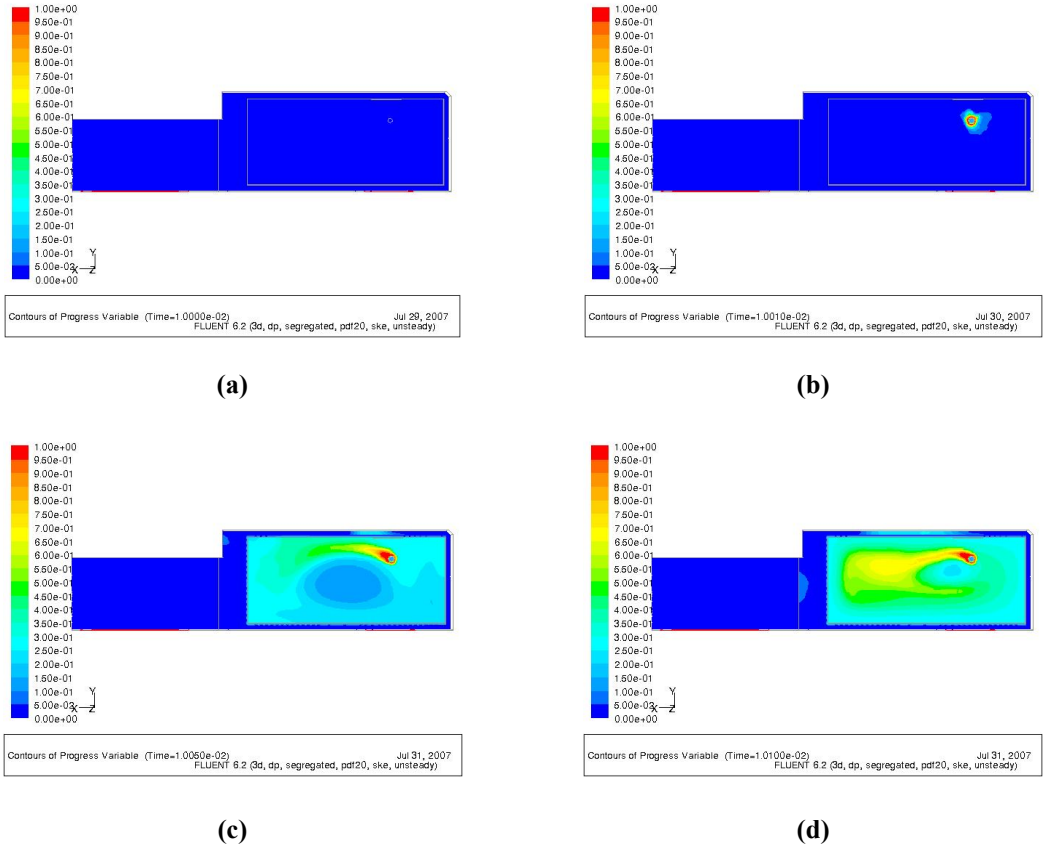

Figure 4.30. *x-y* plane contours of progress variable at (a) Δt=0 msec, (b) Δt=0.01 msec, (c) Δt=0.05 msec and (d) Δt=0.1 msec time steps.

CHAPTER 5

Conclusions and Recommendations

5.1 Conclusions

The demonstration of a partially-premixed combustion model with a spark discharge for an ignition source was effectively demonstrated. The data indicated that the dominant reactions were between the gaseous fuel and oxidizer species. However, reactions did occur between the discrete phase model (DPM) solid fuel and oxidizer.

The benchtop testing data described in Chapter 2 demonstrated that

(i) The solder node spacing on a PCB panel is important in determining if arc discharges can occur and also in sustaining the arcing when contamination is present.

(ii) Flame front propagation in an enclosed package, such as an appliance, can be alleviated with expanded metal foil. Additionally, the test data suggested that sustained arcing causes pyrolization of the surrounding material and possibly the release of combustible gases.

The results in Chapter 4 indicate that a non-adiabatic, single fuel stream, probability density function (PDF) can be successfully implemented for a solid and gas phase fuels of similar chemical composition. Reactions between the discrete solid phase and the gaseous oxidizer were present while the dominant gaseous phase reactions also occurred simultaneously.

5.2 Recommendations and Future Work

As shown in Chapters 4 and 5, through planar and isometric contour plots and volume-averaged analysis, the flame front is predominantly restricted to the inside of the PCB panel and the PCB holder. Further work is suggested for the location of safety features such as the thermistor for shutting down power to the circuit.

Additional simulations are suggested to vary the spark discharge energy. The data provided was obtained on a desktop computer with a Pentium 4-HT 3.2 GHz processor and 4 GB of DDR2 memory with an approximate calculation time of 40 hours for the second transient analysis. The spark discharge energy was discharged over a very short duration to effectively jump-start the reaction. An increase in computing facilities can provide adequate storage and simulation time, thus allowing for a longer duration spark discharge with lower power requirements. As an example, the spark discharge of the current simulation can be extended from 1 ms to 0.5 s with the same energy discharge of 220 J. The resulting simulation will decrease the simulated power consumption from 220 kW to 440 W. However, based on the old simulation convergence, the new simulation will increase number of time steps from 100 to 50,000 and also increase the number of iterations from 13,000 to 3.5 million.

Generally, the benchtop tests and simulations for the exploratory studies of convective flows due to arc tracking were successful. Further investigations may yield a more robust computational model and also optimize the packaging of the simulated dishwasher control panel. The techniques and simulations could also be extended to

investigations into arc tracking and flame front propagation in other domestic or industrial applications.

APPENDIX A

THE CAD MODEL

The initial design was a Pro/ENGINEER™ CAD drawing with full production detail. Only the basic dimensions and contours of the control panel were needed. The figures show the simplification of the model.

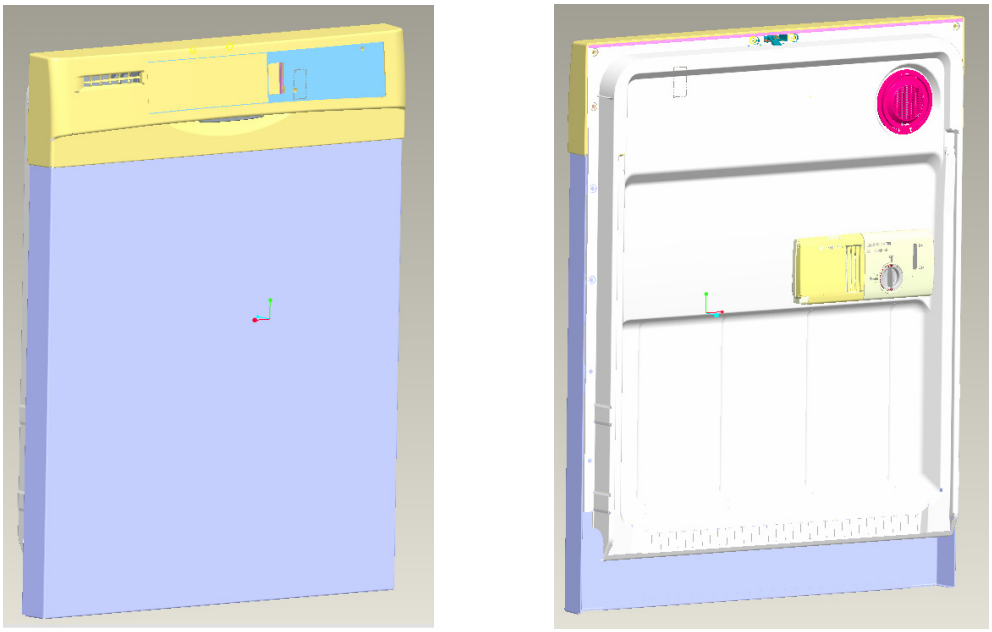

(a) (b)

A 1. (a) Front side and (b) back side of generic door panel assembly.

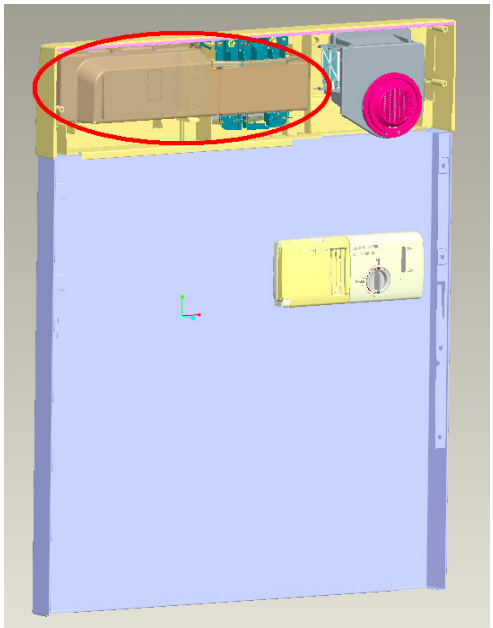

A 2. Back panel removed to shown inside package (circled)

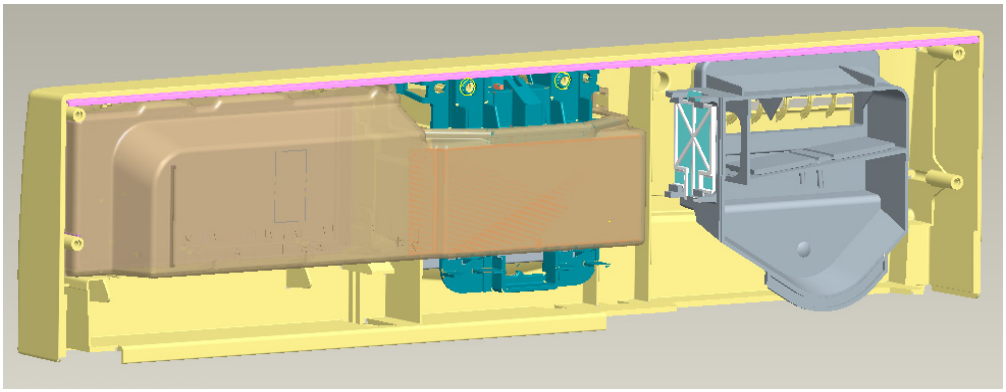

A 3. Close up of package, showing overall geometry

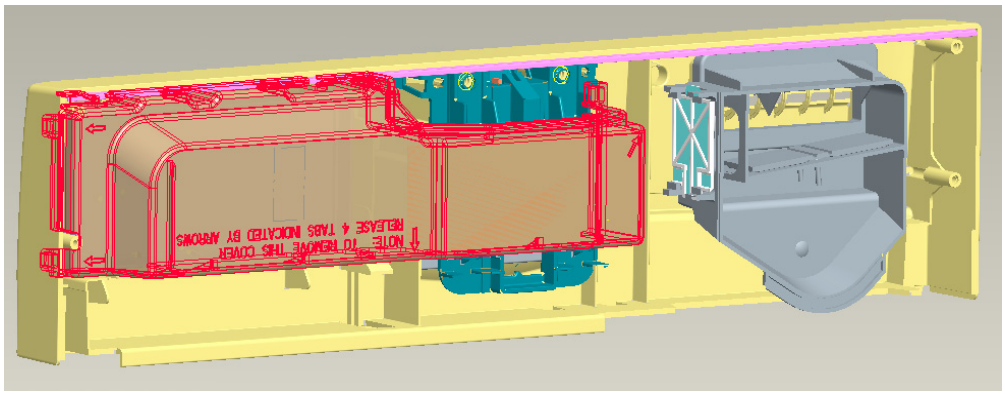

A 4. Highlighting the control volume.

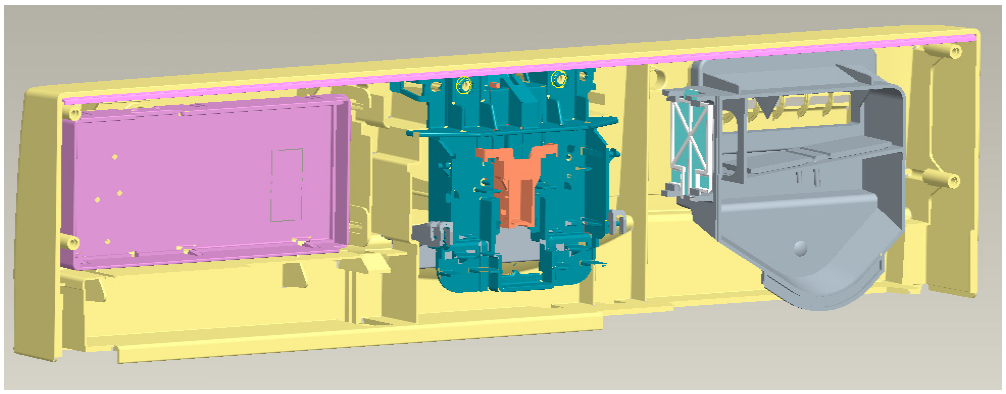

A 5. Showing flow blockages inside control volume

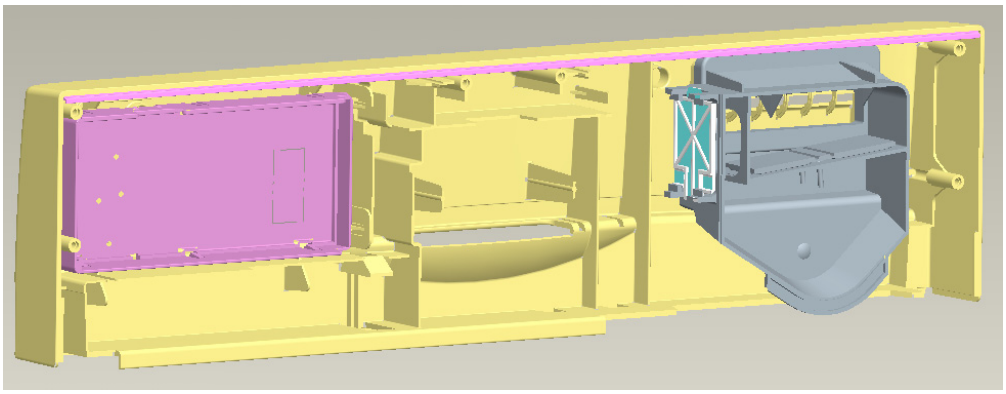

A 6. Removing geometry to show control volume vent in control panel.

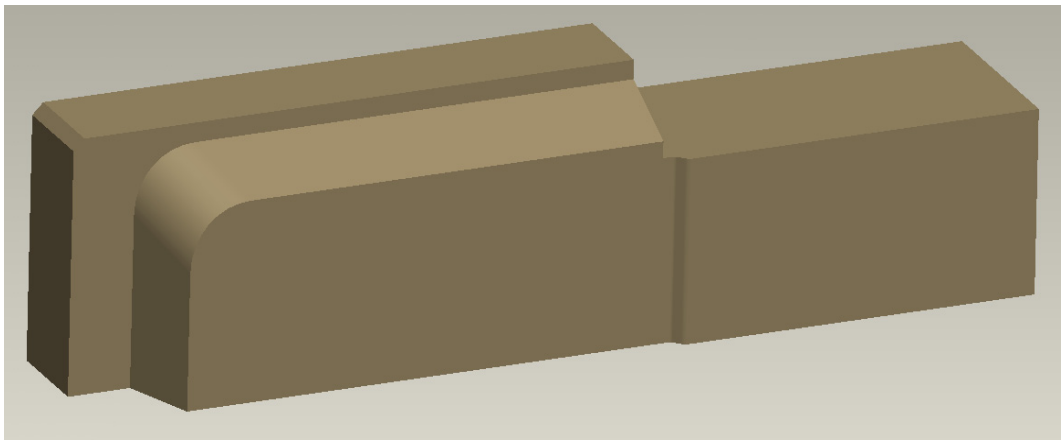

A 7. Front isometric view of simplified model.

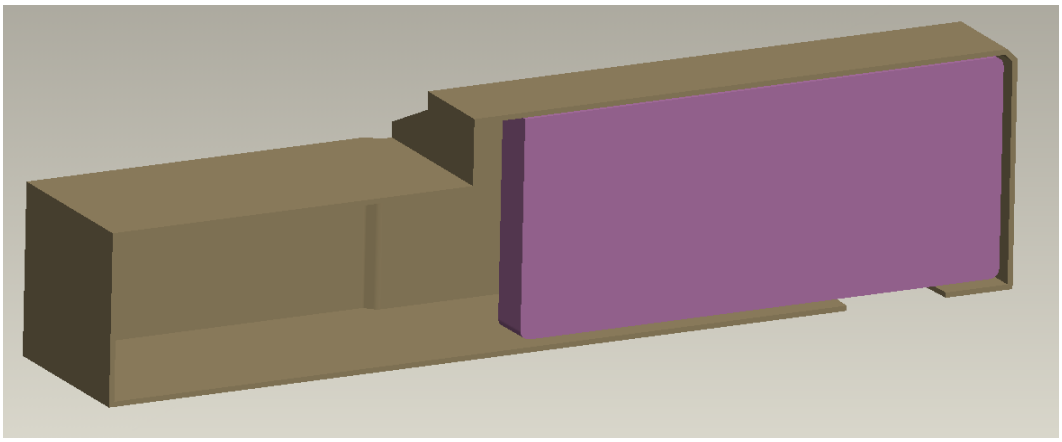

A 8. Back isometric view of simplified model (PCB holder inside).

APPENDIX B

MESH GENERATION

The simplified model was then imported into GAMBIT™. The original import is shown in Figure B.1 with a solid shade.

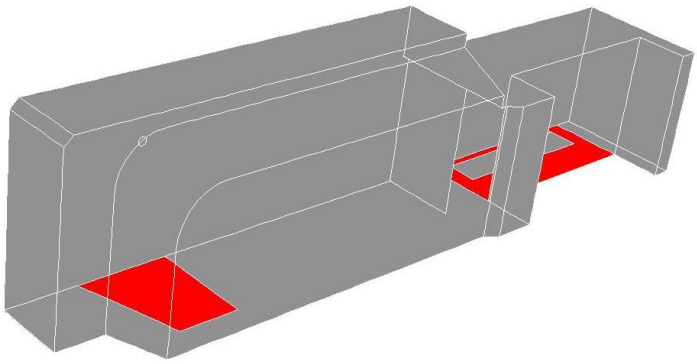

B 1. Solid model import into GAMBIT™, outer air volume.

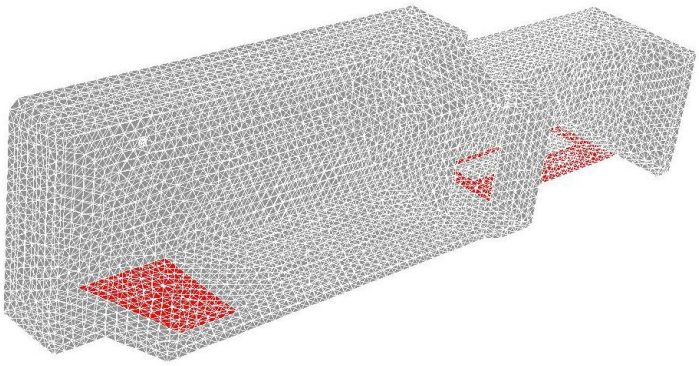

B 2. Outer air volume meshed, tetrahedral hybrid mesh.

Once each of the inside parts were meshed individually to obtain proper element spacing. Working from the inside out will create a fine mesh where the physical geometry is close together and a coarse mesh where the geometry is farther apart.

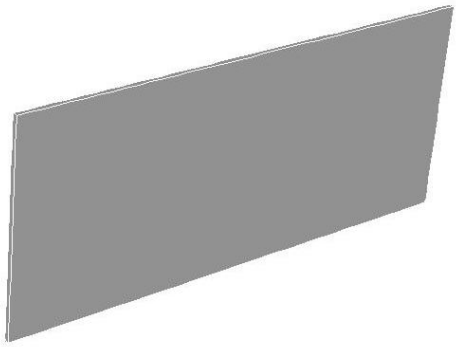

B 3. Inner PCB volume before meshing.

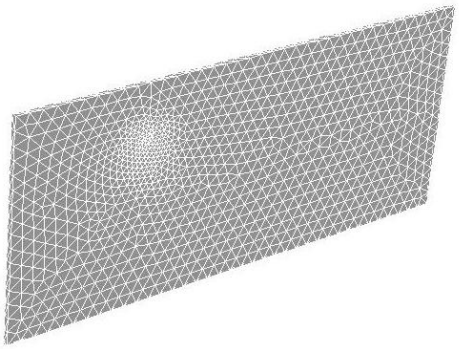

B 4. Inner PCB after volume is meshed with tetrahedral hybrid mesh.

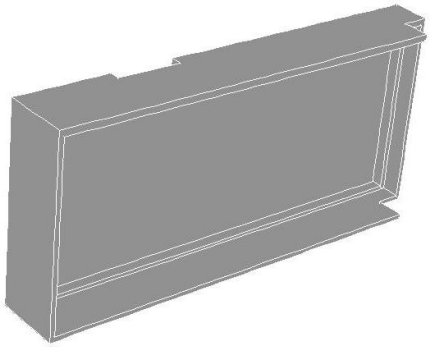

B 5. Inner PCB volume before meshing.

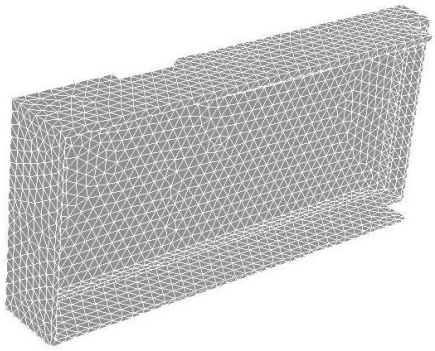

B 6. Inner PCB after volume is meshed with tetrahedral hybrid mesh.

APPENDIX C

BOUNDARY CONDITIONS

After the model is imported into FLUENT®, the geometry was set up for a transient, partially premixed combustion analysis with a spark ignition present.

1. The mesh was imported and checked for skew elements (Figure C1).

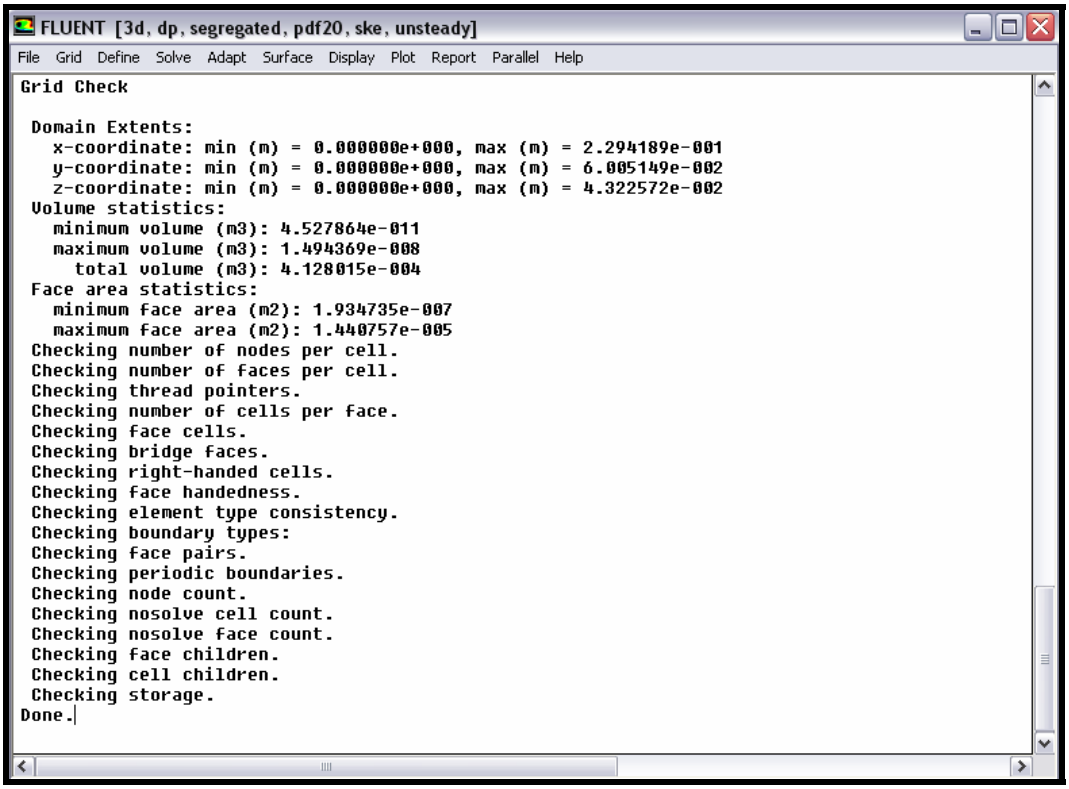

C 1. FLUENT command prompt showing grid checks passed.

2. The domain was reordered to decrease the computing time (Figure C2)

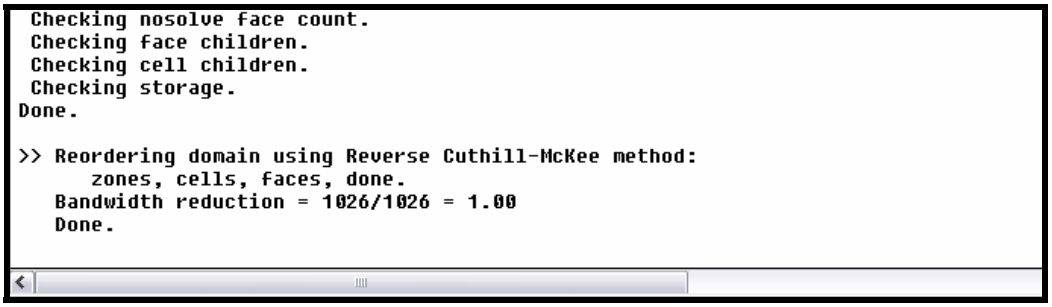

C 2. FLUENT command prompt showing domain reorder.

3. The model was rescaled to fit the specified dimension (Figure C3).

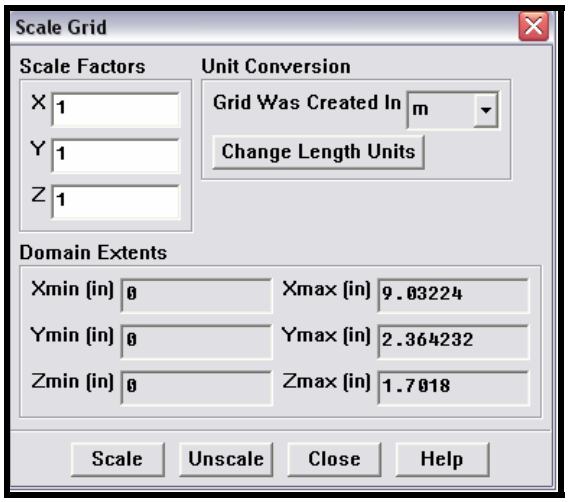

C 3. Scaling the grid to meet geometrical constraints.

4. The solver was set for a segregated, 1st order implicit, unsteady, 3-D analysis (Figure C4).

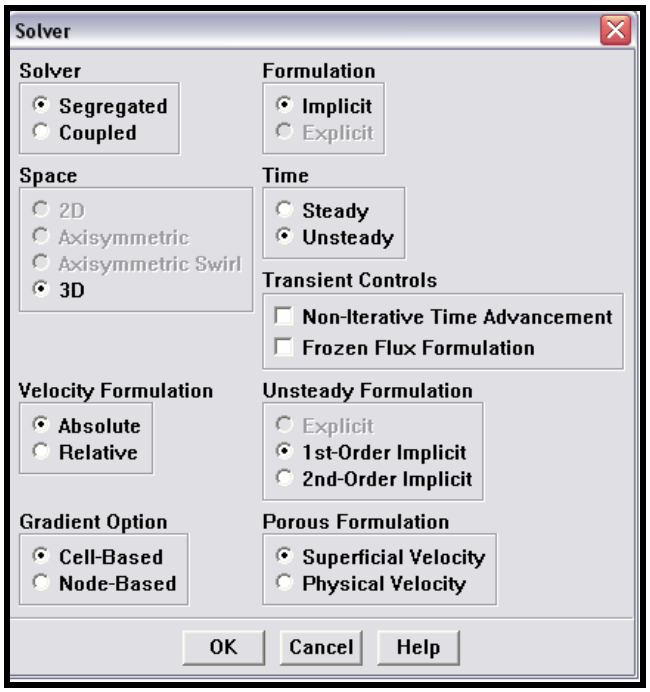

C 4. Setting solver conditions for 3-D transient analysis.

5. The energy equation was selected. (*Define* → *Modes* → *Energy…*)

6. The standard κ–ε turbulence model was selected (*Define* → *Models* → *Viscous…*)

7. A discrete ordinate radiation model was used because the optical thickness was less than one (*Define* → *Models* → *Radiation…*).

8. Next, the partially-premixed combustion solver was selected (*Define* → *Models* → *Species* → *Transport & Reaction…*). See Figure C5 for the model menu.

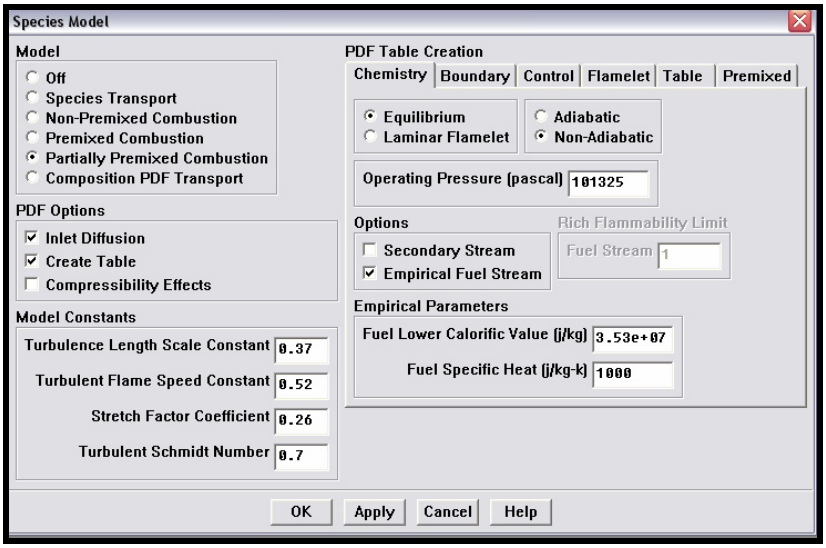

C 5. Species model menu

9. An empirical fuel model was chosen for the PDF table (Figure C6).

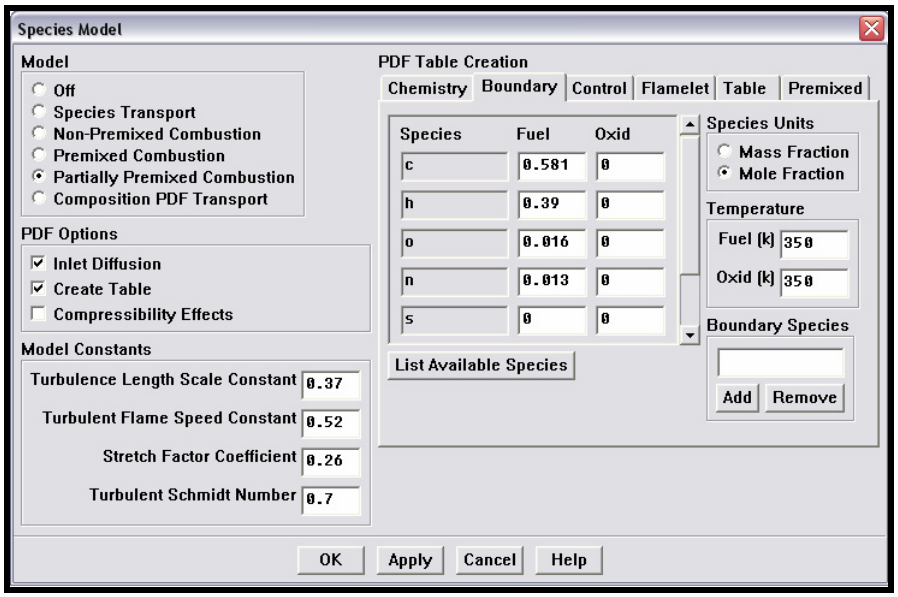

C 6. Species Model

The fuel composition contained the following mole fractions:

C = 0.581; H = 0.390; O = 0.016 and N = 0.013.

The oxidizer composition contained the following mole fractions:

N = 7889 and O = 0.2101.

The inlet temperature for both the fuel and oxidizer was set to 350 K.

10. The next step was to set the "spark discharge" to initiate combustion. A spark energy of 220 J was used for the hybrid model (Figure (C8).

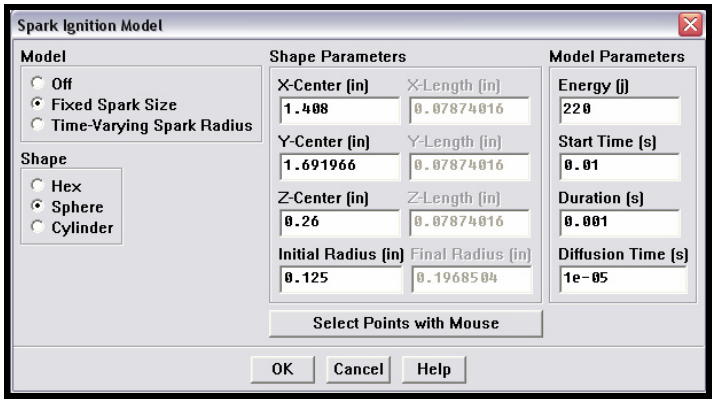

C 7. Spark Ignition menu for initialization of spark in control volume.

11. After the PDF table was generated a DPM model was created (Define → Models → Discrete Phase…). The discrete phase will allow for an interaction with the continuous phase. The fluid of the continuous phase is air…

i) turn on interaction with continuous phase

ii) "Tracking parameters" – 1)max number of steps, 2) step length factor

iii) "number of continuous phase interactions per DPM iteration" = 25 use higher values for this parameter for high grid sizes or higher mass loadings; less frequent trajectory updates can be more beneficial in such problems, in order to converge the gas phase equations more completely before repeating the trajectory calculation

iv) Under "Tracking Parameters" set max number of steps to 10,000 (Figure C9). The limit on the number of trajectory time steps is used to abort trajectories of particles that are trapped in the domain

Create the discrete phase coal injection. The flow of the pulverized coal is defined by the initial conditions that describe coal as it enters the gas. FLUENT® uses these initial conditions as the starting point for the time integration of the particle

equations of motion (trajectory calculations). For this case, the total mass flow is 0.008 kg/s. The particles are assumed to be Rosin-Rammler size distribution between 70 and 200 micron diameter.

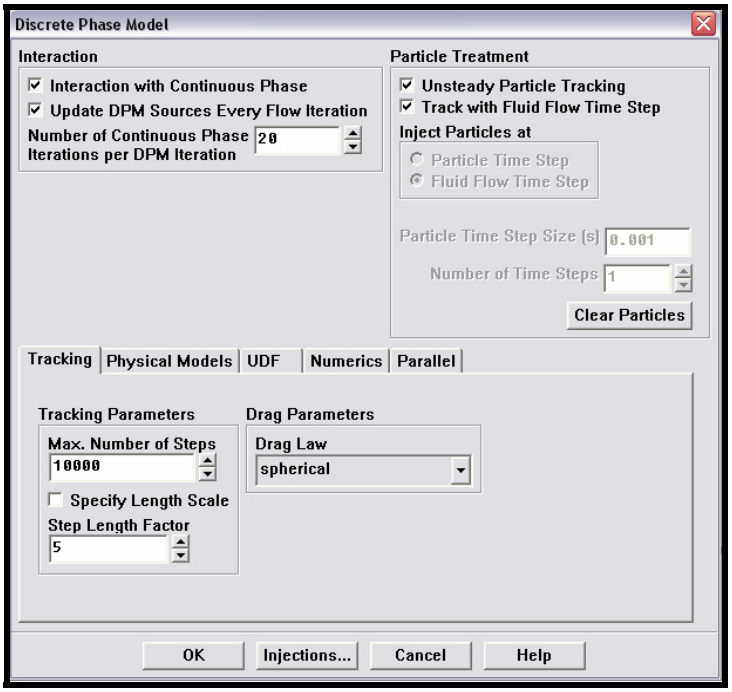

C 8. Discrete Phase Model menu from FLUENT®.

12. Next, the material properties of DPM injection was defined (Define → Materials…). All thermodynamic data for the continuous phase and formation enthalpies were extracted from [24] and are seen Table C1.. See Figure C10 and C11 for examples of the control panels.

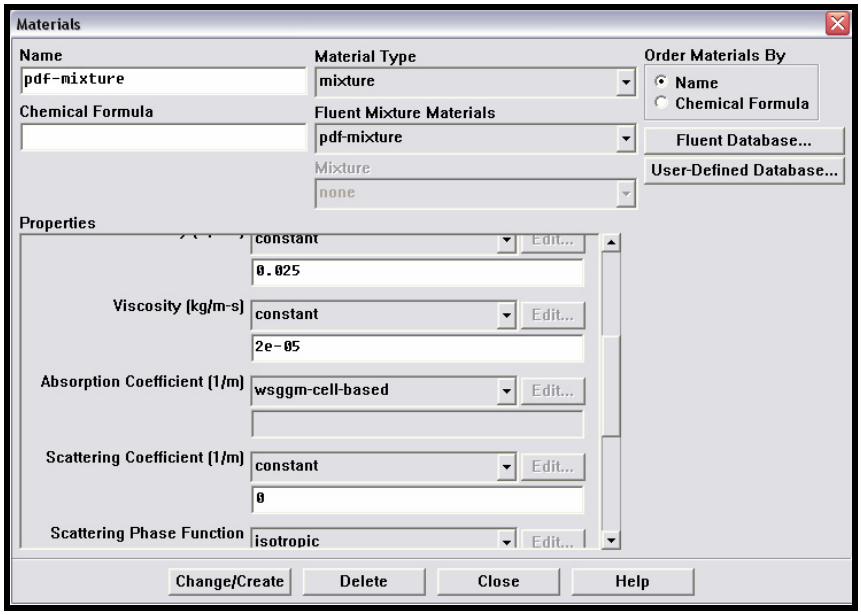

C 9. Material data from FLUENT® for combusting material.

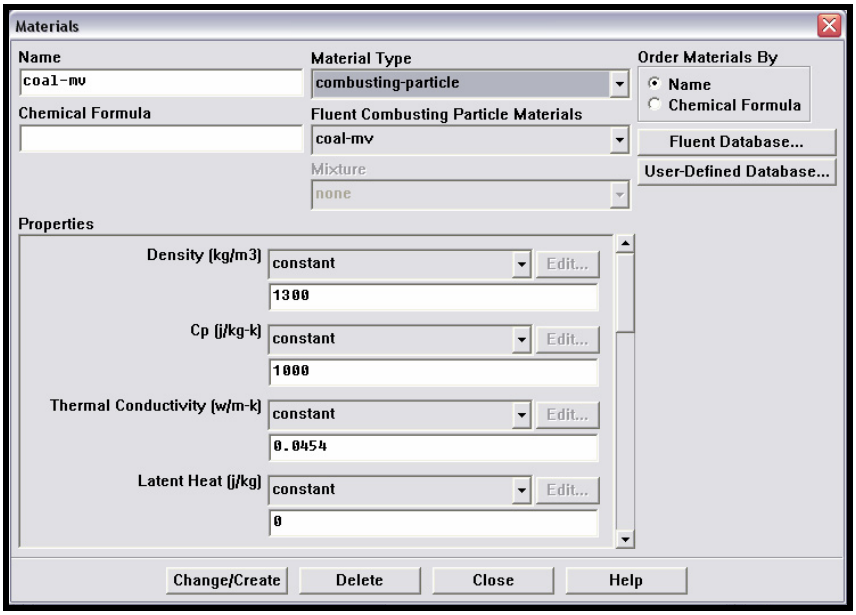

C 10. Materials data

Table C1. Properties of medium-volatile coal model.

Properties	Values
Density , kg/m3	1300
Cp, J/kg-K	1000
Thermal Conductivity, W/m-K	0.0454
Latent Heat	0
Vaporization Temperature, K	400
Volatile Component Fraction, %	28
Binary Diffusivity, W/m-K	5e-4
Particle Emissivity	0.9
Particle Scattering Factor	0.6
Swelling Coefficient	2
Burnout Stoichiometric Ratio	2.67
Combustible Fraction, %	67

Note: The values for the Vaporization Temperature should be the same as the fuel temperature considered previously. The Volatile Component Fraction and Combustible Fraction should be consistent with the volatiles and char ratios in the approximite analysis of the coal shown in the Appendix

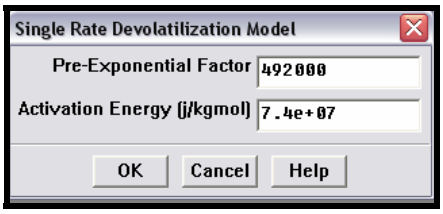

C 11. Devolatilization model.

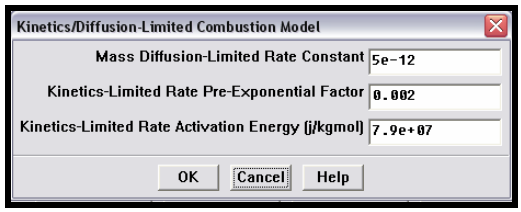

C 12. Diffusion combustion model limits.

13. The combustion was assumed to take place on such a small time scale, so all the walls control volume walls were given an adiabatic boundary condition.

REFERENCES

1. Anon., “Brief of Accident DCA96MA070”, National Transportation Safety Board, 23 Aug. 2000.

2. Anon., “Brief of Accident CHI97IA195”, National Transportation Safety Board, 15 Apr. 1999.

3. Anon., “Brief of Accident LAX01IA066”, National Transportation Safety Board, 25 Nov. 2003.

4. Murphy, R. D., Finn, P. T., Krause, W. R., Wamback, A. R., and Cooper, R. K., “HMCS Chicoutimi Fires and Casualties Board of Inquiry”, National Defence and Canadian Forces, Vice Chief of Defence Staff. 5 July 2005. http://www.vcds.forces.gc.ca/boi_chicoutimi/intro_e.asp

5. Anon., “Arc-Tracking and Wire Insulation Pyrolization,” <http://www.grc.nasa.gov/WWW/epbranch/SpaceEnvSim/arc2.htm>.

6. Stueber, T. J., Hammoud, A., Stavnes, M.W. and Hrovat, K., “Evaluation of Pyrolysis and Arc Tracking on Candidate Wire Insulation Designs for Space Applications”, NASA CR 195332, 1994.

7. Stueber, T. J., “Environmental Influence of Gravity and Pressure on Arc Tracking of Insulated Wires Investigated,” http://www.grc.nasa.gov/WWW/RT1995/5000/5480s.htm, downloaded 16 July 2007.

8. Stueber, T. J., “Evaluation of Kapton Pyrolysis, Arc Tracking, and Arc Propagation on the Space Station Freedom (SSF) Solar Array Flexible Current Carrier (FCC)”, NASA CR 191106, 1993.

9. Ferguson, D.C., “Laboratory Studies of Kapton Degradation in an Oxygen Ion Beam,” AIAA Paper 1983-2658, 1983.

10. Dricot, F., and Reher, H. J., “Survey of Arc Tracking on Aerospace Cables and Wires,” *IEEE Transactions on Dielectrics and Electrical Insulation*, Vol. 1, No. 5, p. 896-903, 1994.

11. Anon., “Brief of Accident DCA88MA054”, National Transportation and Safety Board, 25 June 1990.

12. Slenski, G.A., Kuzniar, J., “Aircraft Wiring System Integrity Initiatives – A Government and Industry Partnership,” *Sixth Joint FAA/DOD/NASA Conference on Aging Aircraft*, September 2002, http://www.wire.nasa.gov/participating_orgs/RTO%20BF%20on%20Aging%20Wiring%20final%20PA%20approved.pdf.

13. NASA Wire Working Group Website, <http://wire.arc.nasa.gov/>.

14. Anon., “Maytag Recalls Dishwashers due to Fire Hazard”, Office of Information and Public Affairs, U.S. Consumer Product Safety Commission, Washington, D.C., 1 February 2007, <http://www.cpsc.gov/CPSCPUB/PREREL/prhtml07/07094.html>.

15. Engel, A., *Ionized Gases*, London: Oxford University Press, 1955, p. 281.

16. Burst, G., “Polyimides,” Polymer Science Learning Center, Department of Polymer Science, University of Southern Mississippi, http://www.pslc.ws/macrog/imide.htm, downloaded 6 June 2007.

17. Walz, M. F., Gomez, C.A. and Cahill, P., “An Analysis of Arc Fault Ignition and Mitigation Techniques”, William J. Hughes Technical Center. Washington, D.C.: Federal Aviation Administration, 2005.

18. Slenski, G.A., Walz, M.F., "Novel Technologies for Improving Wire System Integrity", *Ninth Joint FAA/DOD/NASA Conference on Aging Aircraft*, March 2006, http://www.agingaircraftconference.org/all_files/29/29a/70_ppt.pdf.

19. Park, J., and Leemaster, T., "T-552 Laboratory Test Procedure", Saint Joseph Technology Center, Whirlpool Corporation, 2002.

20. Lu, F. K., Phonharath, L., Mitchell, R. R., and Bigdeli, B., "Flame Suppression Technique in Arc Tracking of Circuit Boards," IMECE2007-41051, 2007.

21. Anon., *GAMBIT 2.2 Modeling Guide*. Lebanon, New Hampshire: Fluent, Incorporated, Sept. 2005 <http://www.fluent.com>.

22. Anon., *FLUENT 6.2 User's Guide*. Lebanon, NH: Fluent Inc., Jan. 2005 <http://www.fluent.com>.

23. Borman, G. L., and Ragland, K. W., *Combustion Engineering,* McGraw-Hill, 1998, p. 613.

24. Anon., "Using the Non-Premixed Combustion Model", Fluent, Incorporated. Lebanon, New Hampshire: Fluent, Incorporated, 2005. 1-13. 01 Jan. 2006 http://www.fluent.com

25. Kuo, K. K., *Principles of Combustion*, 2nd edition*,* Wiley, 2005

BIOGRAPHICAL INFORMATION

Richard Reed Mitchell was born on October 26, 1980 in Tulsa, Oklahoma, the youngest of five children. His family moved to DeSoto, Texas, in the Fall of 1985 where he began his academic career in the DeSoto Independent School District (DISD). After graduating from DeSoto High School in May of 1999, Richard spent one year in the local Dallas County Community College District completing core course work. He then transferred to the University of Texas at Arlington (UTA) in the Fall of 2000. Richard continued at UTA until graduating with his Bachelor of Science in Aerospace Engineering in May 2005. After a brief summer break to get his private pilot license, Richard returned to UTA in Fall 2005 to obtain his Masters of Science in Aerospace Engineering. Richard plans on continuing his education at UTA to obtain a doctorate degree in the same field. His main areas of professional interests have focused on hypersonic technologies including aerodynamics, propulsion and aerothermodynamics. His experimental work has included subsonic and supersonic wind tunnel testing coupled with computational fluid dynamics verification with commercial software such as FLUENT® and CFX™.